AD A093094

SDAC-TR-78-3

LEVEL II

12

RANDOM SCATTERING EFFECTS ON RAYLEIGH-WAVE AMPLITUDES AND PHASES

D.W. Rivers and D.H. von Seggern
Seismic Data Analysis Center
Teledyne Geotech, 314 Montgomery Street, Alexandria Virginia 22314

DTIC
ELECTE
DEC 17 1980
S D
E

01 March 1979

APPROVED FOR PUBLIC RELEASE; DISTRIBUTION UNLIMITED.

Sponsored by
The Defense Advanced Research Projects Agency (DARPA)
DARPA Order No. 2551

Monitored By
AFTAC/VSC
312 Montgomery Street, Alexandria, Virginia 22314

DDC FILE COPY

80 12 17 011

Disclaimer: Neither the Defense Advanced Research Projects Agency nor the Air Force Technical Applications Center will be responsible for information contained herein which has been supplied by other organizations or contractors, and this document is subject to later revision as may be necessary. The views and conclusions presented are those of the authors and should not be interpreted as necessarily representing the official policies, either expressed or implied, of the Defense Advanced Research Projects Agency, the Air Force Technical Applications Center, or the US Government.

Unclassified

SECURITY CLASSIFICATION OF THIS PAGE (When Data Entered)

REPORT DOCUMENTATION PAGE

READ INSTRUCTIONS BEFORE COMPLETING FORM

1. REPORT NUMBER: SDAC-TR-78-3	2. GOVT ACCESSION NO.: AD-A093 094
3. RECIPIENT'S CATALOG NUMBER	
4. TITLE (and Subtitle): RANDOM SCATTERING EFFECTS ON RAYLEIGH-WAVE AMPLITUDES AND PHASES,	5. TYPE OF REPORT & PERIOD COVERED: Technical rept.
	6. PERFORMING ORG. REPORT NUMBER
7. AUTHOR(s): D. W. Rivers, D. H. von Seggern	8. CONTRACT OR GRANT NUMBER(s): F08606-78-C-0007, ARPA Order-2552
9. PERFORMING ORGANIZATION NAME AND ADDRESS: Teledyne Geotech, 314 Montgomery Street, Alexandria, Virginia 22314	10. PROGRAM ELEMENT, PROJECT, TASK AREA & WORK UNIT NUMBERS: VT/8709
11. CONTROLLING OFFICE NAME AND ADDRESS: Defense Advanced Research Projects Agency, Nuclear Monitoring Research Office, 1400 Wilson Blvd. Arlington, Virginia 22209	12. REPORT DATE: 01 March 1979; 13. NUMBER OF PAGES: 137
14. MONITORING AGENCY NAME & ADDRESS (if different from Controlling Office): VELA Seismological Center, 312 Montgomery Street, Alexandria, Virginia 22314	15. SECURITY CLASS. (of this report): Unclassified; 15a. DECLASSIFICATION/DOWNGRADING SCHEDULE

16. DISTRIBUTION STATEMENT (of this Report)

APPROVED FOR PUBLIC RELEASE; DISTRIBUTION UNLIMITED.

17. DISTRIBUTION STATEMENT (of the abstract entered in Block 20, if different from Report)

18. SUPPLEMENTARY NOTES

AUTHOR'S REPORT DATE 02/02/78

19. KEY WORDS (Continue on reverse side if necessary and identify by block number)

Rayleigh Waves
Scattering of Seismic Waves
Surface-Wave Magnitude
Seismic Array

20. ABSTRACT (Continue on reverse side if necessary and identify by block number)

Fluctuations in the amplitudes and phases of 20-sec Rayleigh waves were measured for ten earthquakes recorded at NORSAR and for two earthquakes recorded at an 1100-km long linear array in the Southwestern Unit d States. These measurements were compared with the prediction of Chernov (1962), who analyzed the scattering of elastic waves by random inhomogeneities along the source-to-receiver path. Use of this theory enabled the amplitude and phase fluctuations to be related to a statistical description of the random scattering medium. As predicted, it was found that the fluctuations were correlated over →

DD FORM 1 JAN 73 1473 EDITION OF 1 NOV 65 IS OBSOLETE

Unclassified

SECURITY CLASSIFICATION OF THIS PAGE (When Data Entered)

408258 slt

a longer distance in the direction parallel to the propagation of the wavefront than in the direction perpendicular to it. This implies by reciprocity that relative M_s within a test site would be better determined at a station in line with the vector between two events than by a station perpendicular to the vector. Certain measurements were incompatible with Chernov's theory, however; these discrepancies may be attributable to multipath arrivals and/or large-amplitude scattering for which the Born approximation is not valid.

It was found that narrow-band spectral measurements of Rayleigh wave amplitudes exhibited stronger fluctuations across both arrays than did visual measurements of M_s. The size of the fluctuations was diminished by using broad-band spectra. Fluctuations in M_s are approximately 1/3 those in m_b across equivalent array dimensions. By reciprocity this implies that relative yields within a test site may be determined by using M_s with a standard deviation 1/3 of that obtained from m_b if an equivalent number of station measurements are available.

Random scattering of Rayleigh waves has a large effect upon narrow-band measurements of attenuation than upon measurements of phase velocity. As a result of such scattering, surface-wave spectra may display significant fluctuations at various frequencies, causing source mechanisms inferred from spectral observations at only a few stations to be unreliable.

RANDOM SCATTERING EFFECTS ON RAYLEIGH-WAVE AMPLITUDES AND PHASES

SEISMIC DATA ANALYSIS CENTER REPORT NO.: SDAC-TR-78-3

AFTAC Project Authorization No.:	VELA T/8709/B/ETR
Project Title:	Seismic Data Analysis Center
ARPA Order No.:	2551
Name of Contractor:	TELEDYNE GEOTECH
Contract No.:	F08606-78-C-0007
Date of Contract:	01 October 1977
Amount of Contract:	$2,674,245
Contract Expiration Date:	30 September 1978
Project Manager:	Robert R. Blandford (703) 836-3882

P. O. Box 334, Alexandria, Virginia 22313

APPROVED FOR PUBLIC RELEASE; DISTRIBUTION UNLIMITED.

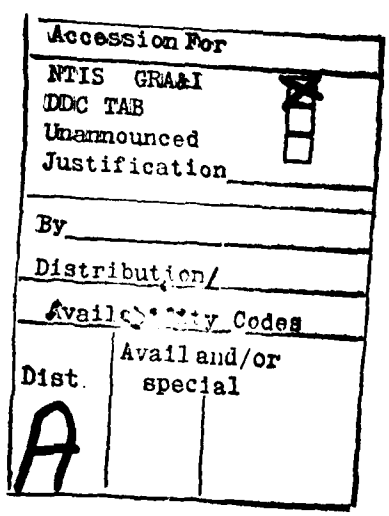

ABSTRACT

Fluctuations in the amplitudes and phases of 20-sec Rayleigh waves were measured for ten earthquakes recorded at NORSAR and for two earthquakes recorded at an 1100-km long linear array in the Southwestern United States. These measurements were compared with the prediction of Chernov (1962), who analyzed the scattering of elastic waves by random inhomogeneities along the source-to-receiver path. Use of this theory enabled the amplitude and phase fluctuations to be related to a statistical description of the random scattering medium. As predicted, it was found that the fluctuations were correlated over a longer distance in the direction parallel to the propagation of the wavefront than in the direction perpendicular to it. This implies by reciprocity that relative M_s within a test site would be better determined at a station in line with the vector between two events than by a station perpendicular to the vector. Certain measurements were incompatible with Chernov's theory, however; these discrepancies may be attributable to multipath arrivals and/or large-amplitude scattering for which the Born approximation is not valid.

It was found that narrow-band spectral measurements of Rayleigh wave amplitudes exhibited stronger fluctuations across both arrays than did visual measurements of M_s. The size of the fluctuations was diminished by using broad-band spectra. Fluctuations in M_s are approximately 1/3 those in m_b across equivalent array dimensions. By reciprocity this implies that relative yields within a test site may be determined by using M_s with a standard deviation 1/3 of that obtained from m_b if an equivalent number of station measurements are available.

Random scattering of Rayleigh waves has a larger effect upon narrow-band measurements of attenuation than upon measurements of phase velocity. As a result of such scattering, surface-wave spectra may display significant fluctuations at various frequencies, causing source mechanisms inferred from spectral observations at only a few stations to be unreliable.

TABLE OF CONTENTS

LIST OF FIGURES

LIST OF FIGURES (Continued)

LIST OF FIGURES (Continued)

LIST OF TABLES

LIST OF TABLES (Continued)

INTRODUCTION

Researchers have long recognized the effects of the earth's lateral inhomogeneity on basic seismological measurements. In fact, systematic variations of wave amplitudes, travel times, and spectral content have been successfully utilized to infer much of the structural variations of the earth's crust and mantle. However, in most cases the structure becomes discernible only when a suitable amount of data is averaged, implying that a significant degree of randomness appears in that data and that single observations are not reliable for making geophysical inferences. For example, the range of P-wave amplitudes over LASA is frequently as large as 10 to 1 (Chang and von Seggern, 1977), with the amplitude pattern changing among events. The random component in data sets, such as travel times or amplitudes, can usually be described with common statistical formulations and a statistical description of the media properties can often be derived from the statistical content of observed seismic data. This observed random scattering is associated with features of the medium having smaller scale than those causing broad regional effects, such as North's (1978) magnitude bias or Herrin and Taggart's (1968) travel time residuals. However, because of its severity, random scattering often obscures broad regional effects and inhibits determining underlying structure and seismic source parameters.

Aki (1973) and Capon (1974) performed scattering analysis on the travel

---

Chang, A. C. and D. H. von Seggern (1977). A study of amplitude variations and m_b bias at LASA subarrays, SDAC-TR-77-11, Teledyne Geotech, Alexandria, Virginia.

North, R. G. (1978). Station bias for ISM-reported magnitudes, Geophys. J., in press.

Herrin, E. and J. Taggart (1968). Regional variations in P travel times, Bull. Seism. Soc. Am., 58, 1325-1337.

Aki, K. (1973). Scattering of P waves under the Montana LASA, J. Geophys. Res., 78, 1334-1347.

Capon, J. (1974). Characterization of crust and upper mantle structure under LASA as a random medium, Bull. Seism. Soc. Am., 64, 235-266.

times and amplitudes of LASA P-wave recordings using Chernov's (1962) theory. This report focusses on whether or not a similar phenomenon exists for Rayleigh waves and how it can be described theoretically; it will not deal with the phenomenon of distinct multipathing of surface waves that Capon (1970) studied because multipathing is a deterministic, not statistical, effect arising from known lateral variations in the gross structure of the crust and upper mantle such as the oceanic/continental boundary. However, such multipathing should grade into random effects on surface-wave amplitudes and phases where the structure is uniform except for small-scale heterogeneities that can be described statistically using Chernov's method. Demonstrable random scattering effects on Rayleigh waves will have important implications for the reliability of surface-wave magnitude estimates, for the accuracy of surface wave phase-velocity and attenuation measurements, and for the character of surface wave spectra.

The first portion of this study examines evidence that suggests random scattering of Rayleigh waves, then modifies Chernov's three-dimensional theory to predict the effects for a two-dimensional propagation problem and presents new results that can be compared with the modified theory and other possible models. Finally, the probable error of various Rayleigh-wave measurements taken from long-period seismograms is investigated. Throughout, waves with periods near 20 sec are stressed because of the practical importance of using surface-wave magnitude (M_s) in estimating yields of underground nuclear explosions.

Chernov, L. A. (1962). Wave propagation in a random medium, New York, Dover Publications, Inc.

Capon, J. (1970). Analysis of Rayleigh-wave multipath propagation at LASA, Bull. Seism. Soc. Am., 60, 1701-1731.

OBSERVATIONS OF SMALL-SCALE SCATTERING OF RAYLEIGH WAVES

Few opportunities exist to observe recorded surface wave signal variations over small spatial dimensions on the order of a few wave-lengths or less with a regularly spaced array. Aside from the large seismic arrays, LASA and NORSAR, there are almost no available data sources. However, during early 1962 one well-placed set of stations existed in the Southwestern United States. These sites, part of the VELA Long Range Seismic Measurements program (Figure 1), were situated to record seismic signals from the GNOME underground nuclear explosion and, all together, composed a 1100 km linear array. During their short recording interval, surface waves from several earthquakes at teleseismic distance were well recorded at most of the 11 sites. For this study, signals arriving perpendicular and parallel to this linear array were needed to verify certain theoretical models; two such events were available. Their epicenter information and great circle paths are indicated on Figure 1; Figure 2 and 3 illustrate the vertical-component recordings of the Rayleigh waves for the two events. Note that the plots preserve the true relative amplitudes. Significantly, the range of amplitude among the seismograms at a period of 20 sec is over a factor of three and it is apparently random. Attenuation along the path or changes in crustal responses at the individual sites cannot alone explain this range and a detailed analysis of these particular recordings will be presented in this report.

Observations of random fluctuation in Rayleigh waves are possible at the NORSAR array of long-period instruments, (shown in Figure 4), but only over a span of 100 km. One example is the recordings made of the Turkish earthquake shown in Figure 5. Comparing the seismograms with those of Figures 2 and 3 reveals less variation in signal amplitudes and shapes, an observation to be expected because the aperture is reduced by an order of magnitude. Yet, among the NORSAR recordings there are significant differences that cannot be explained by varying crustal response or slight calibration errors. For such typical events, the standard deviation of measured M_s over 22 NORSAR sensors will be somewhat less than 0.1. A thorough analysis of these types of recordings will be presented later when we compare theoretical and empirical results for the random scattering of Rayleigh waves.

Figure 1. Locations of a linear array of LRSM sites in the Southwestern United States and arrival directions for two earthquakes studied in this report.

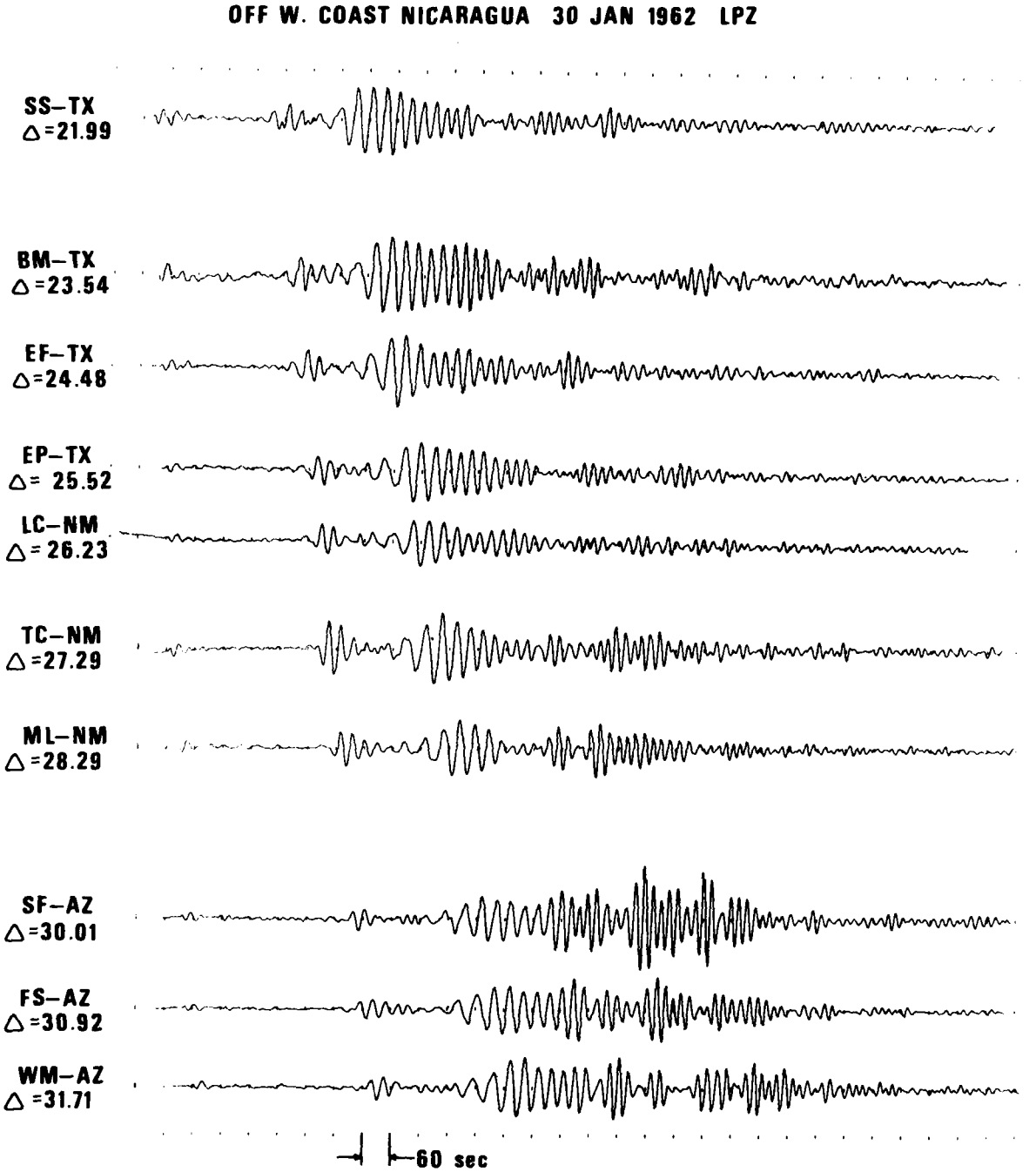

Figure 2. LRSM long-period recordings for the Nicaragua earthquake.

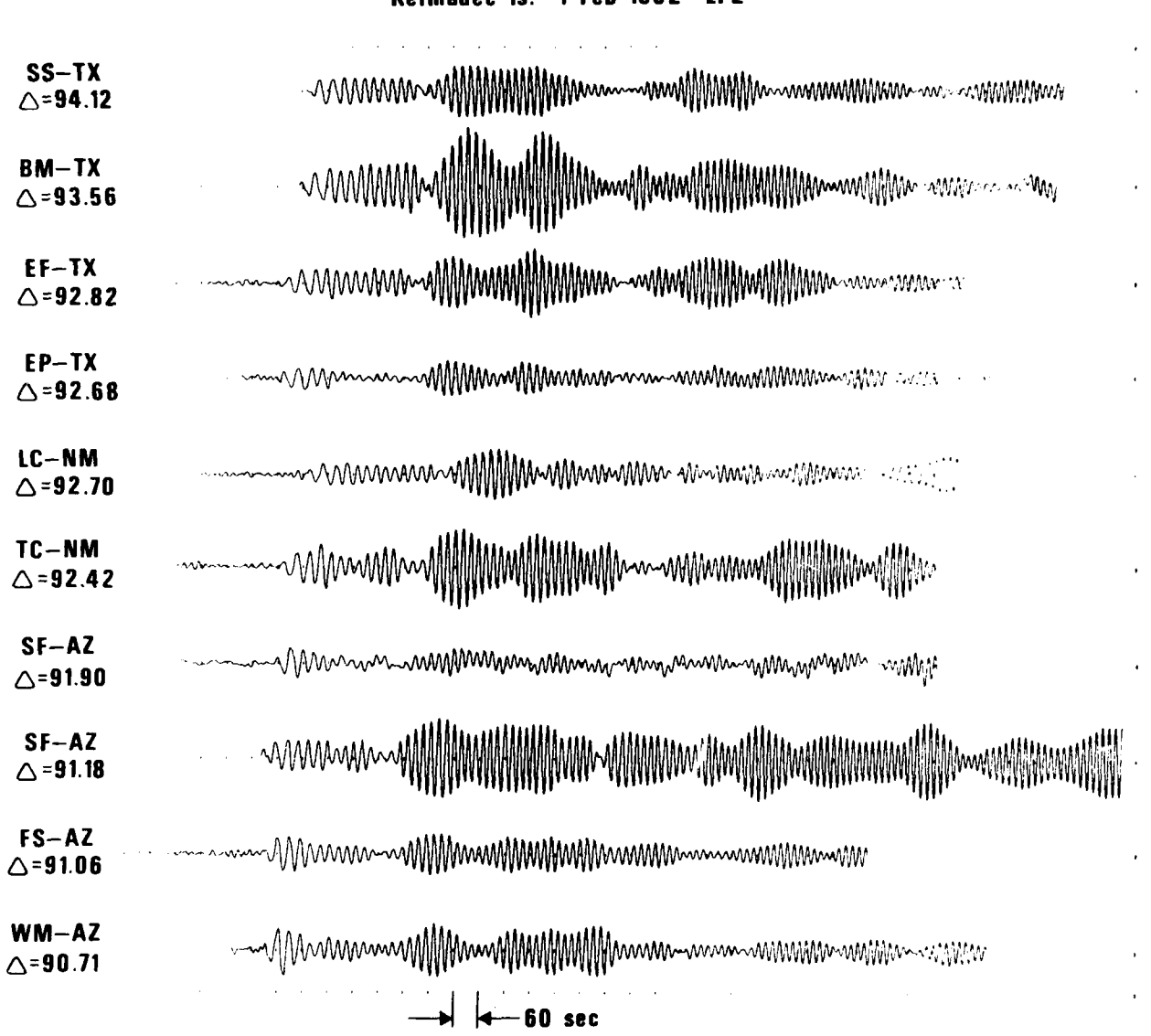

Figure 3. LRSM long-period recordings for the Kermadec earthquake.

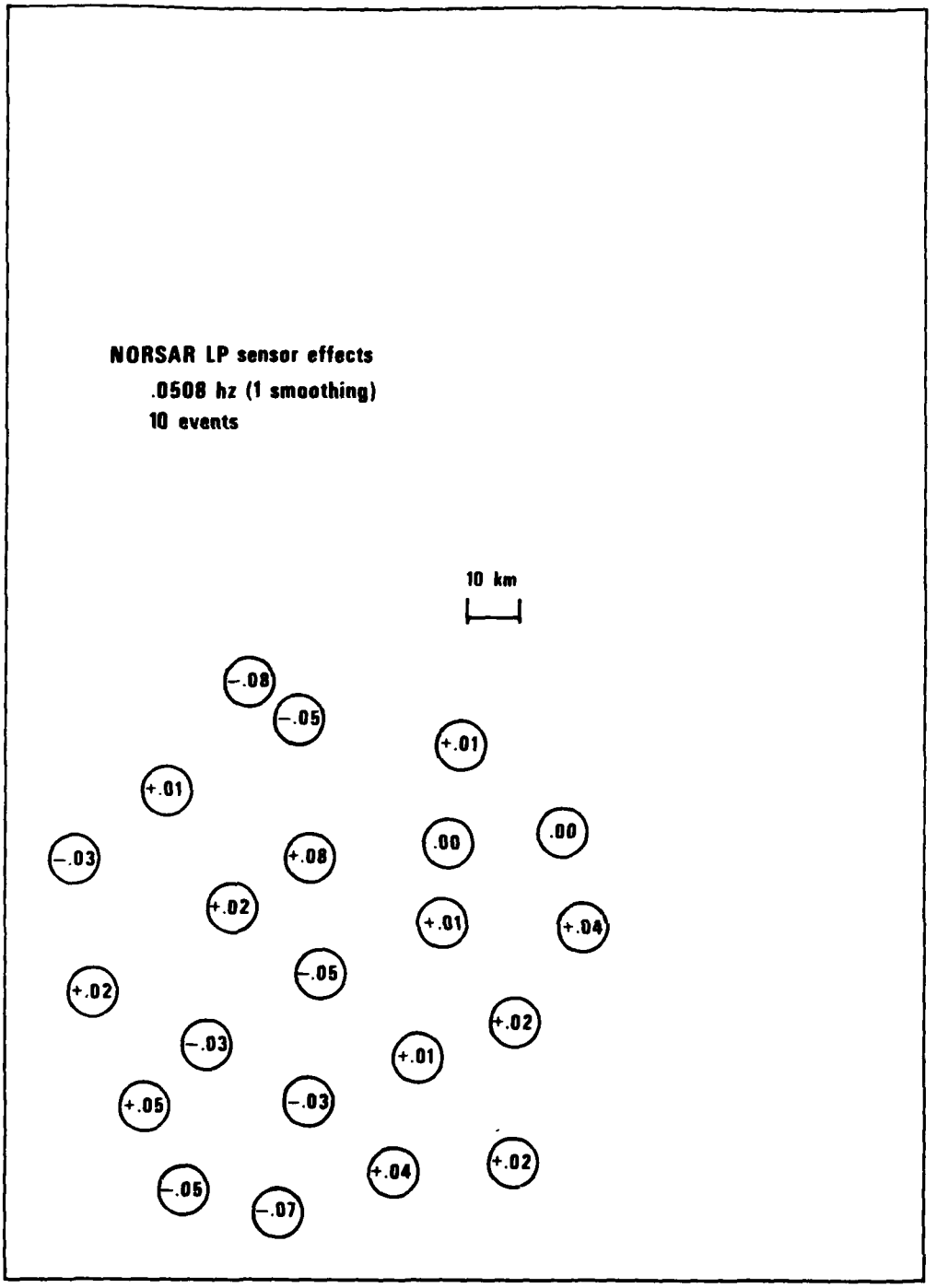

Figure 4. Layout of the NORSAR long-period array. Numbers indicate sensor effects, the difference between the individual spectral amplitudes and the mean spectral amplitude, averaged over 10 events.

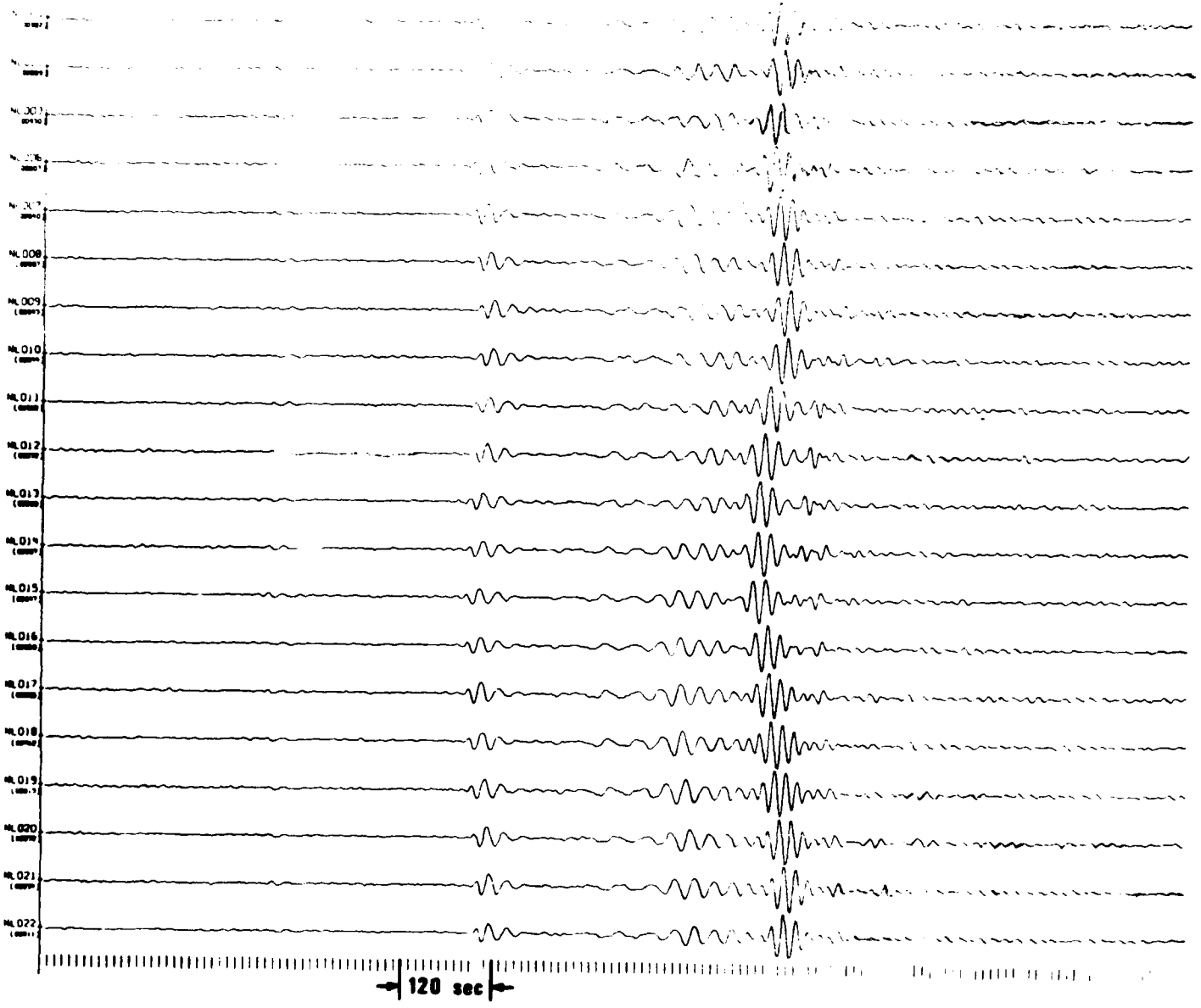

Figure 5. Rayleigh waves recorded at NORSAR from an earthquake in Turkey (06 May 1971, OT = 04:30:04).

Using wavenumber analysis Mack (1972) has already investigated this apparent scattering phenomenon at arrays, suggesting that actual Rayleigh wave signals can be represented in two-dimensional wavenumber space as a distribution rather than as a single discrete point. One of these possible representations is the Gaussian distribution:

$$F(k_x) = \exp(-\alpha^2 k_x^2); \; F(k_y) = \exp[-\beta^2 (k_y - k_o)^2] \tag{1}$$

where the k_x and k_y axes are parallel and normal to the wavefronts, respectively, and k_o is the wavenumber where the power of the signal peaks for a given frequency. From this model, Mack derived the form of the coherence function for spectral amplitudes from two sensors at the frequency corresponding to k_o as

$$\gamma^2(\bar{r}) = \left[\exp - \frac{\pi^2 r_x^2}{\alpha^2} \cdot \exp - \pi^2 r_y^2\right] \tag{2}$$

where r is the vector from one sensor to another within the array of instruments and

$$\begin{aligned} \bar{r} &= (r_x, r_y) \\ r_x &= x_1 - x_2 \\ r_y &= y_1 - y_2 \, . \end{aligned} \tag{3}$$

To simplify, henceforth $r = |\bar{r}|$. At the frequency of .047 Hz, Mack computed coherence between sensor pairs for the signals shown in Figure 5; the results are in Figure 6. Results for sensor pairs nearly normal or parallel to the wavefront are shown as a function of sensor separation r. We have superimposed the relation (2) for various of α (or β). Assuming $r_x = 0$ for sensor pairs aligned normal to the wavefront, we estimate $\beta \sim 1200$; similarly $\alpha \sim 500$ for sensor pairs aligned parallel to it. Clearly, coherence along the raypaths falls off much less rapidly, a fundamental feature of the random forward scattering of waves detailed in Chernov's (1962) theory. However, alternative wavenumber representations or signal models will predict similar coherence patterns; for instance, two discrete multipath arrivals of nearly equal amplitude and equal phase delay at nearby points $\overline{k_1}$ and $\overline{k_2}$ in wavenumber space would result in a theoretical coherence function (Mack, 1972) of

Mack, H. (1972). Spatial coherence of surface waves, Report No. SAAC-8, Teledyne Geotech, Alexandria, Virginia.

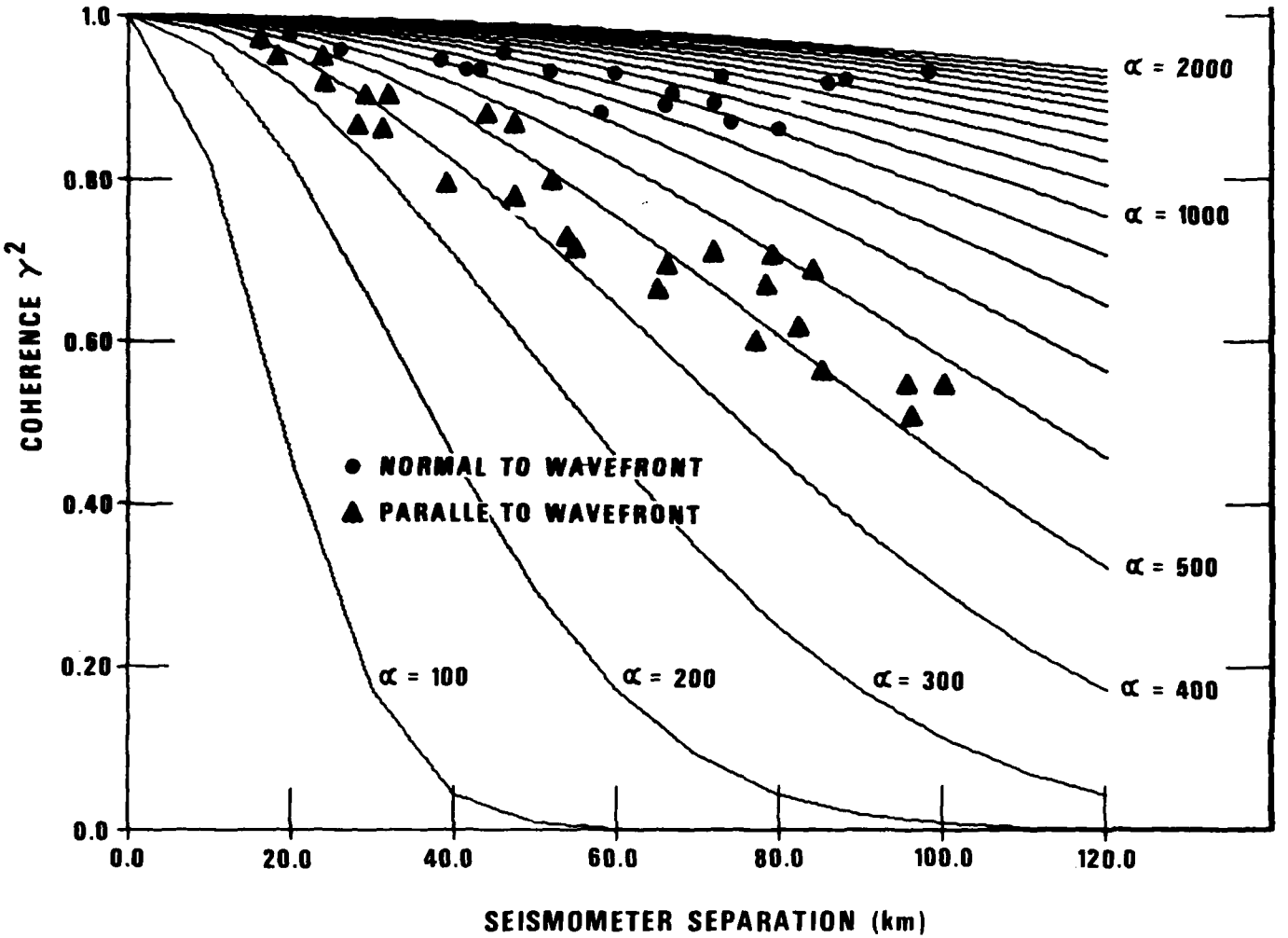

Figure 6. Coherency at a period of 21.3 sec (.0469 Hz) versus seismometer separation for the Rayleigh-wave recordings of Figure 5 (after Mack, 1972).

$$\gamma^2(\bar{r}) = [1 + \cos 2\pi\bar{r} \ (\bar{k}_1 - \bar{k}_2)]/2$$

This equation would fit the actual data of Figure 6 nearly as well as the Gaussian predictions shown there.

In order, then, to define the typical Rayleigh signal wavefield, a more detailed analysis of the observations is required. Information important in determining the best signal model is contained in recording phases at each array sensor; such information is suppressed in the simple coherence computations, but it can be recovered with alternative methods (discussed later). To overcome NORSAR's dimensions, which are inadequate to fully analyze the wavefield nature, signal analysis over a long linear array, such as in Figure 1, will be necessary. Before proceeding to the data analysis, Chernov's work, which is appropriate to a wave propagating in three dimensions, will be modified to obtain predictions for a Rayleigh wave, which essentially propagates in two dimensions near the earth's surface.

CHERNOV'S SCATTERING THEORY MODIFIED FOR RAYLEIGH WAVES

Chernov (1962) derived analytic expressions that statistically described the behavior of monochromatic, acoustic, plane waves as they travelled through a non-turbulent fluid medium characterized by spatial fluctuations of the wave velocity C which are both small and random. Certain simplifying assumptions must be made to apply these results to the problem of waves propagating across the surface of a solid, such as seismic Rayleigh waves. Complications introduced by the elliptical particle motion of Rayleigh waves are ignored, and all displacements are assumed to be along the direction of wave propagation in the plane of the earth's surface. This assumption not only has the effect of replacing Rayleigh waves by acoustic waves, but also eliminates the consideration of effects due to LR-LQ mode conversion when the waves are scattered. Ignoring the dependence of the waves on the depth-varying properties of the medium below the surface further simplifies this problem. The problem is thus considered strictly two-dimensional, and Chernov's theory must be modified. Since our data reduction employs spectral analysis, which allows analysis of waves within only a narrow band of frequencies, the assumption that the waves are monochromatic is acceptable. Our treatment of the spatial variation of phase velocity C(x,y), therefore, does not need to involve dependence upon the frequency C (x,y,ω) characteristic of dispersive waves. In Chernov's fluid medium the velocity fluctuations vary in time as well as in space, and the wave propagation is described in terms of averages over (an infinite) time for a given source and a given receiver. Although in the solid earth the velocity fluctuations are deterministic and permanent, they may be treated in Chernov's manner if averages over the azimuths of incident waves from (all possible) different sources to a given receiver are taken. This method of averaging is discussed more fully in the memorandum of Rivers and von Seggern (1978), which for convenience is reproduced as an appendix to this report.

The scattering properties of an inhomogeneous medium are determined by the spatial fluctuations of the index of refraction, which are defined by

$$\mu(x,y) = \frac{C_o}{C\ (x,y)} - 1$$

Rivers, D. W. and D. H. von Seggern (1978). Theory of wave propagation in a two-dimensional random medium, Technical Memorandum, Teledyne Geotech, Alexandria, Virginia.

where C_o is the average phase velocity of the waves in the medium. Denoting the mean square fluctuation of the index of refraction by $\overline{\mu^2}$, the correlation coefficient of μ is defined to be

$$\nu = \overline{\mu(x_1,y_1)\ \mu(x_2,y_2)} \ / \ \overline{\mu^2} \ . \qquad (6)$$

If the fluctuation $\mu(x,y)$ are truly random, the average denoted by the overbar in (6) depends only upon the distance between the points (x_1, y_1) and (x_2, y_2) and not upon the coordinates of the points themselves; i.e., $\nu = \nu(r)$. In the modification of Chernov's theory presented here, it is assumed throughout that the form of the correlation coefficient is given by the Gaussian function

$$\nu(r) = \exp\ (-r^2/a^2)$$

where the "correlation distance" $\underline{a}$ represents the typical linear dimension of the inhomogeneities which give rise to the scattering. Chernov's theory is a statistical method of describing scattering phenomena within a medium characterized by the parameters $\overline{\mu^2}$ and $\underline{a}$.

Table I gives theoretical expressions derived in Rivers and von Seggern (1978) for seven basic quantities which characterize the scattering process. These seven quantities are:

$\overline{B^2}$, the mean-square fluctuation of the amplitude (in natural logarithmic units) of the wave at a given receiver relative to the average of the amplitudes at all receiver;

$\overline{S^2}$, the mean-square fluctuation of the phase (in radians) of the wave at the same receiver relative to the phase of the (hypothetical) average wavefront;

ρ, the cross-correlation coefficient between the amplitude and phase fluctuations at the same receiver;

$R_b(\Delta L)$ and $R_s(\Delta L)$, the spatial autocorrelation coefficients for amplitude or phase fluctuations measured at two different receivers whose separation distance ΔL lies along the direction of propagation of the incoming wave; and

$R_b(\ell)$ and $R_s(\ell)$ the corresponding autocorrelation coefficients for two receivers whose separation ℓ lies in the direction transverse to the wave propagation.

TABLE I

Comparison of Chernov Scattering Theory for Two- and Three-Dimensional Cases

Fluctuations of Amplitude and Phase for Single-Receiver Case

$$\overline{B^2} = \overline{\mu^2}\,[I_1(0) - I_2(0)]/2$$

$$\overline{S^2} = \overline{\mu^2}\,[I_1(0) + I_2(0)]/2$$

Fluctuations and Correlation Coefficients for Longitudinal Separation of Receivers

$$\overline{B_1 B} \text{ long} = \overline{\mu^2}\,[I_1(\Delta L) - I_2(\Delta L)]/2$$

$$\overline{S_1 S_2} \text{ long} = \overline{\mu^2}\,[I_1(\Delta L) + I_2(\Delta L)]/2$$

$$R_b, \text{ long } (\Delta L) = [I_1(\Delta L) - I_2(\Delta L)]/[I_1(0) - I_2(0)]$$

$$R_s, \text{ long } (\Delta L) = [I_1(\Delta L) + I_2(\Delta L)]/[I_1(0) + I_2(0)]$$

Fluctuations and Correlation Coefficients for Transverse Separation of Receivers

$$\overline{B_1 B_2} \text{ trans} = \overline{\mu^2}\,[I_1(\ell) - I_2(\ell)]/2$$

$$\overline{S_1 S_2} \text{ trans} = \overline{\mu^2}\,[I_1(\ell) + I_2(\ell)]/2$$

$$R_b, \text{ trans } (\ell) = [I_1(\ell) - I_2(\ell)]/[I_1(0) - I_2(0)]$$

$$R_s, \text{ trans } (\ell) = [I_1(\ell) + I_2(\ell)]/[I_1(0) + I_2(0)]$$

where:

	Two Dimensions	Three Dimensions
$I_1(0)$	$\frac{K^3 L a^2}{2} e^{K^2 a^2/8} K_{\frac{1}{4}}(\frac{K^2 a^2}{8}) = \sqrt{\pi} K^2 L a$	$\sqrt{\pi} K^2 L a$
$I_2(0)$	$\frac{\sqrt{2\pi} K^2 L a}{D} [\sqrt{D^2 + 1} - 1]^{1/2}$	$\frac{\sqrt{\pi} K^2 L a}{D} \tan^{-1} D$
$I_1(\Delta L)$	$\frac{K^3 L a^2}{\sqrt{2}} e^{-\Delta L^2/a^2} \int_0^\infty e^{-K^2 a^2 \zeta^2/4} \cosh(K\Delta L \cdot \zeta)\,[\zeta^2 + 1]^{-1/2}\,[\sqrt{\zeta^2 + 1} + 1]^{1/2}\,d\zeta = \sqrt{\pi} K^2 L a$	$\sqrt{\pi} K^2 L a/[1 + (\frac{2L}{Ka^2})^2]$
$I_2(\Delta L)$	$\frac{\sqrt{2\pi} K^3 a^3}{4} ([\sqrt{D_1^2 + 1} - 1]^{1/2} - [\sqrt{D_2^2 + 1} - 1]^{1/2})$	$\frac{\sqrt{\pi} K^2 L a}{D}[\tan^{-1} D - \tan^{-1}(\frac{\Delta L \cdot D}{2L})]$
$I_1(\ell)$	$\frac{K^3 L a^2}{\sqrt{2}} \int_0^\infty [\zeta^2 + 1]^{-1/2} e^{-\ell^2/[a^2(\zeta^2 + 1)]} e^{-K^2 a^2 \zeta^2/4} ((\sqrt{\zeta^2 + 1} - 1)^{1/2} \sin(\frac{\zeta \ell^2/a^2}{\zeta^2 + 1}) + \sqrt{\zeta^2 + 1} + 1)^{1/2} \cos(\frac{\zeta \ell^2/a^2}{\zeta^2 + 1}))\,d\zeta = \sqrt{\pi} K^2 L a e^{-\ell^2/a^2} e^{-\ell^4/(K^2 a^6)}$	$\sqrt{\pi} K^2 L a e^{-\ell^2/a^2} e^{-\ell^4/(K^2 a^6)}$
$I_2(\ell)$	$-\frac{\sqrt{\pi} K^3 L a^2}{4} Im\{\Gamma(-\frac{1}{2}, \frac{-i\ell^2/a^2}{D - i})\}$	$\frac{\sqrt{\pi} K^3 a^3}{8i}[Ei(\frac{i\ell^2/a^2}{D - i}) - Ei(\frac{-i\ell^2/a^2}{D + i})]$

and:

$$D = \frac{4L}{Ka^2}$$

$$D_1 = \frac{2(2L + \Delta L)}{Ka^2}$$

$$D_2 = \frac{4\Delta L}{Ka^2}$$

$K_{\frac{1}{4}}$ = modified Bessel function of order ¼.

Correlation of Amplitude and Phase Fluctuations at a Single Receiver

$$\overline{BS} = \frac{\sqrt{\pi}\,\mu^2 K^3 a^3}{4} ([(\sqrt{D^2 + 1} + 1)/2]^{1/2} - 1) \quad \text{Two Dimensions}$$

$$\frac{\sqrt{\pi}\,\overline{\mu^2} K^3 a^3}{16} \ln(1 + D^2) \quad \text{Three Dimensions}$$

$$c = \overline{BS}/[\sqrt{\overline{B^2} \cdot \overline{S^2}}]$$

As the table shows, these seven quantities can be expressed as functions of the four variables: $\overline{\mu^2}$, $\underline{a}$, the wavenumber k, and L, which is the length of of wave's path through the medium. For a narrow spectral band, k is nearly constant. Rivers and von Seggern (1978) showed that variations in the source to receiver distance L will not strongly effect our analysis. Therefore, this study will determine the values of $\overline{\mu^2}$ and $\underline{a}$ for those inhomogeneities in the earth's crust causing the random scattering of Rayleigh waves (near 20 sec period). This study will also determine the applicability of Chernov's theory to the quantitative prediction of fluctuations due to that scattering, particularly $R_b(\Delta L)$ and $R_b(\ell)$.

Note the conditions that govern the validity of the result in Table I. The two-dimensional, longitudinal-wave model of Rayleigh waves, which is employed in our modification of Chernov's theory, has already been described; also the assumptions that permit replacement of equation (6) with (7) were stated. One other set of Chernov's key assumptions pertained to the smallness of fluctuations in density, phase velocity, and refractive index:

$$\Delta\rho << P_o, \ \Delta c << c_o, \text{ and hence } \overline{\mu^2} << 1. \tag{8}$$

The validity of these assumptions must be tested after the value of $\overline{\mu^2}$ is determined. Further, we assume that the scattering caused by density fluctuation can be neglected when compared with scattering caused by fluctuations in phase velocity. This assumption is valid if, for a wave travelling along the x-axis,

$$\left| \frac{1}{2k\rho_o} \quad \frac{\partial(\Delta\rho)}{\partial x} \right| << \left| \frac{\Delta c}{c_o} \right|.$$

For a fairly uniform crustal structure, $\partial(\Delta\rho)/\partial x \sim 01.01$/gm/cc/km would be a liberal value while $\Delta c/c_0 \sim 0.05$ would be a reasonable value. Using $\rho_0 \sim 3$ gm/cc and $k \sim 0.1$ for 20 sec periods, the relation is satisfied.

Another assumption, reflected in Table I, that Chernov used was that the Born approximation was valid for the Rayleigh waves. This first-order approximation, which Chernov referred to as the method of small perturbations, consists of substituting, within the integrand of an integral equation, the

expression for the composite wave field after scattering in place of the expression for the unscattered incident wave. The Born approximation is, therefore, essentially the assumption that the scattering process results in a small perturbation, i.e., that the amplitude and phase fluctuations are both small:

$$\left|\frac{\Delta A}{A_o}\right| \ll 1 \text{ and } |\Delta\Phi| \ll 1.$$

Chernov claimed that his formulas were valid under conditions less restrictive than those imposed by (10); i.e., that the amplitude and phase fluctuations be small over the distance of a wavelength λ rather than over the entire source-to-receiver path length L. This claim, based upon Rytov's method, was disputed by Aki (1973) who claimed that incident wave field attenuation due to energy lost by scattering throughout the path length L must be small. Thus, determining whether the Rayleigh-wave data is consistent with the assumption of small fluctuations (10) is important.

Chernov also assumed that the source-to-receiver path length L is large when compared to the correlation distance, which, in turn, is assumed to be large when compared with the wavelength:

$$L \gg a \gg \frac{1}{k}.$$

Chernov defined the "wave parameter" as

$$D = \frac{4L}{ka^2}.$$

If $D \ll 1$, the ray equation may be used to approximate the equations of motion; if $D \gg 1$, Fraunhofer diffraction theory is appropriate. In either case the condition of small wavelength (known as the Fresnel approximation), $ka \gg 1$, must be obeyed. Since for Rayleigh waves with periods of 20 sec and phase velocities of 3.6 km/sec, $k \sim .1\ \text{km}^{-1}$, this condition implies that a should be much larger than 10 km. Because this condition may not be met, there are listed in Table I, wherever appropriate, two expressions for the given functions. The more precise (and more cumbersome) of the expressions is less sensitive to the restriction $ka \gg 1$ than the other. Note, however, that even the more exact expressions are of questionable validity where the size of the scatterers is approximately equal to a wavelength, that is, $ka \simeq 1$.

The Fresnel approximation implies that most scattering deflects the waves forward into a cone of aperture angle $\frac{1}{ka}$, suggesting that the direction of the scattered wave deviates little from the incident wave. Our justification for the validity of this approximation is based upon Capon's (1970) observations that most of the energy in a typical incident wave is concentrated in a small range of azimuths. Finally, note that even if $ka >> 1$, the transition to geometrical acoustics ($k \to \infty$) is not allowed by the Chernov theory.

RAYLEIGH-WAVE SCATTERING AT NORSAR

Data

Measurements were made of the amplitude and phase of 20-sec Rayleigh waves recorded at NORSAR for a selected suite of ten events (listed in Table II) to provide a quantitative description of fluctuation magnitudes and of the correlation among the fluctuation at different locations within a seismic sensors array. Rivers and von Seggern (1978) explained that the present adaptation of Chernov's theory utilizes averages over source-to-receiver paths of the full 360° range of incident azimuths. However, this procedure could not be fully implemented because of the location of suitable seismic regions. Still, the events chosen for analysis in this study were selected to attain as wide a range as possible and yield even spacing in incident azimuths. Nevertheless, the range of (geometrical) azimuths, shown in Table II, is only about 135°. The range is limited because of the need to include only events for which the great-circle paths to NORSAR did not cross any major source of non-random scattering, such as an ocean-continent boundary. Also, selection was restricted because we wanted events that took place within as short a time period as possible to minimize the effects of potential long-term instabilities in the response of the instruments at NORSAR. To check measurement repeatability, one event was chosen that was an aftershock of another; thus, two events in the chosen data set occurred at approximately the same epicenter within three days of each other. Finally, an effort was made to pick events with as large a Rayleigh-wave magnitude as possible so that most of the measured fluctuations would stem from wave scattering and not from background noise.

Computational Methods

The data for each event consisted of seismograms from twenty-two long-period vertical instruments within the array. These twenty-two seismograms were analyzed in frequency-wavenumber space using the program that Smart (1972) developed, indicating the time window (chosen to be 256 sec long) where the signal power was greatest, the phase velocity, and the incident azimuth, all as a function of frequency. The FKCOMB results confirmed that no strong

---

Smart, E. (1972). FKCOMB, a fast general-purpose array processor, Report No. SAAC-9, Teledyne Geotech, Alexandria, Virginia.

TABLE II

Events Used in NORSAR Study

Event	Date	Time	Latitude	Longitude	m_b	M_s	Epicenter to NORSAR Distance (km)	Geometrical NORSAR to Epicenter Azimuth (degrees)	Azimuth From FKCOMB (degrees)	Geographic Region
200	3 Nov 72	23:57:59.4	34.232N	69.658E	5.4	5.4	5081.88	99.0	106.9	Afghanistan
300	26 May 71	02:41:46.0	35.509N	58.220E	5.4	5.4	4360.57	108.7	106.7	Iran
400	19 Jun 71	17:23:02.7	41.502N	79.307E	5.2	5.3	4971.47	81.8	80.9	Kirgiz-Sinkiang border
500	8 Sep 71	03:17:25.4	46.734N	141.344E	5.0	5.2	7286.60	34.9	16.0	Sakhalin Island
600	27 Sep 72	00:08:29.9	30.308N	101.672E	5.0	5.5	7163.16	73.1	73.0	Szechwan Province China
700	29 Sep 72	20:24:42.0	30.275N	101.673E	5.1	5.4	7166.28	73.1	73.9	Szechwan Province China
800	22 Apr 74	00:29:19.8	31.649N	119.171E	5.2	5.5	7905.09	58.6	62.8	Eastern China
900	5 Nov 72	19:25:42.4	35.063N	24.852E	5.2	5.4	3038.70	154.4	152.4	Crete
1000	9 Jan 74	02:49:46.2	51.645N	159.639E	5.4	5.4	7238.81	20.8	6.0	Off Eastern Coast Kamchatka
1100	11 Aug 74	07:02:08.5	39.351N	73.854E	5.2	5.4	4858.87	85.5	85.4	Tadzhik-Sinkiang border

multipath arrivals contaminated the data for the selected events. The time windows chosen with the aid of FKCOMB as the best for waves of 19.7 sec period were then used to compute the amplitude and phase spectra for each of the twenty-two seismograms; for any of the events, this time window was identical for all 22 sensors. We then determined the amplitude at each instrument by smoothing the natural logarithms of the spectral amplitudes for the periods 21.3, 19.7, and 18.3 sec, using Hanning weights of 1/4, 1/2, 1/4, respectively. The phase of the wave at each intrument was assumed to be the spectral phase for the period 19.7 sec.

Amplitude fluctuations for each event at each instrument were then calculated from the values found for each instrument. Also for each event a grid search of azimuths and a linear least-squares fit to the phase yielded the azimuth and phase velocity of the plane wave best fitting the spectral phase data. The azimuths and phase velocities of the best-fitting wave found with this procedure were consistent with values calculated by FKCOMB. These phase fluctuations were assumed to be the advance or the delay of the spectral phase at each instrument relative to the phase of the hypothetical plane wave as it passes through that point in the array. Thus, we have

$$B_{ij} = \ell nA_{ij} - \ell nA_i \qquad i = 1,2, \ldots, 10 \quad j = 1,2, \ldots, 22 \qquad (13)$$

$$S_{ij} = \Phi_i(j) - \Phi_{ij} \qquad i = 1,2, \ldots, 10 \quad j = 1,2, \ldots, 22 \qquad (14)$$

where $\phi_i(j)$ denotes the phases of the (hypothetical) coherent incident wave as measured at the jth instrument. Note that $\phi_i(j)$ is, of course, dependent upon values assumed for the phase velocity and azimuth of the incident wave. The phase velocities computed for the best-fitting plane waves were not the same for each event; in fact, they varied from 3.503 to 3.976 km/sec (see Figure 7). Since theoretical models of the crustal structure underneath NORSAR (Massé and Alexander, 1974) yield a phase velocity (for waves of 19.7 sec period) of 3.64 km/sec and since this value should presumably be constant for all events, we decided to proceed with the analysis in two different ways.

Massé, R. P., and S. S. Alexander (1974). Compressional velocity distribution beneath Scandinavia and western Russia, Geophys. J., 39, 587-602.

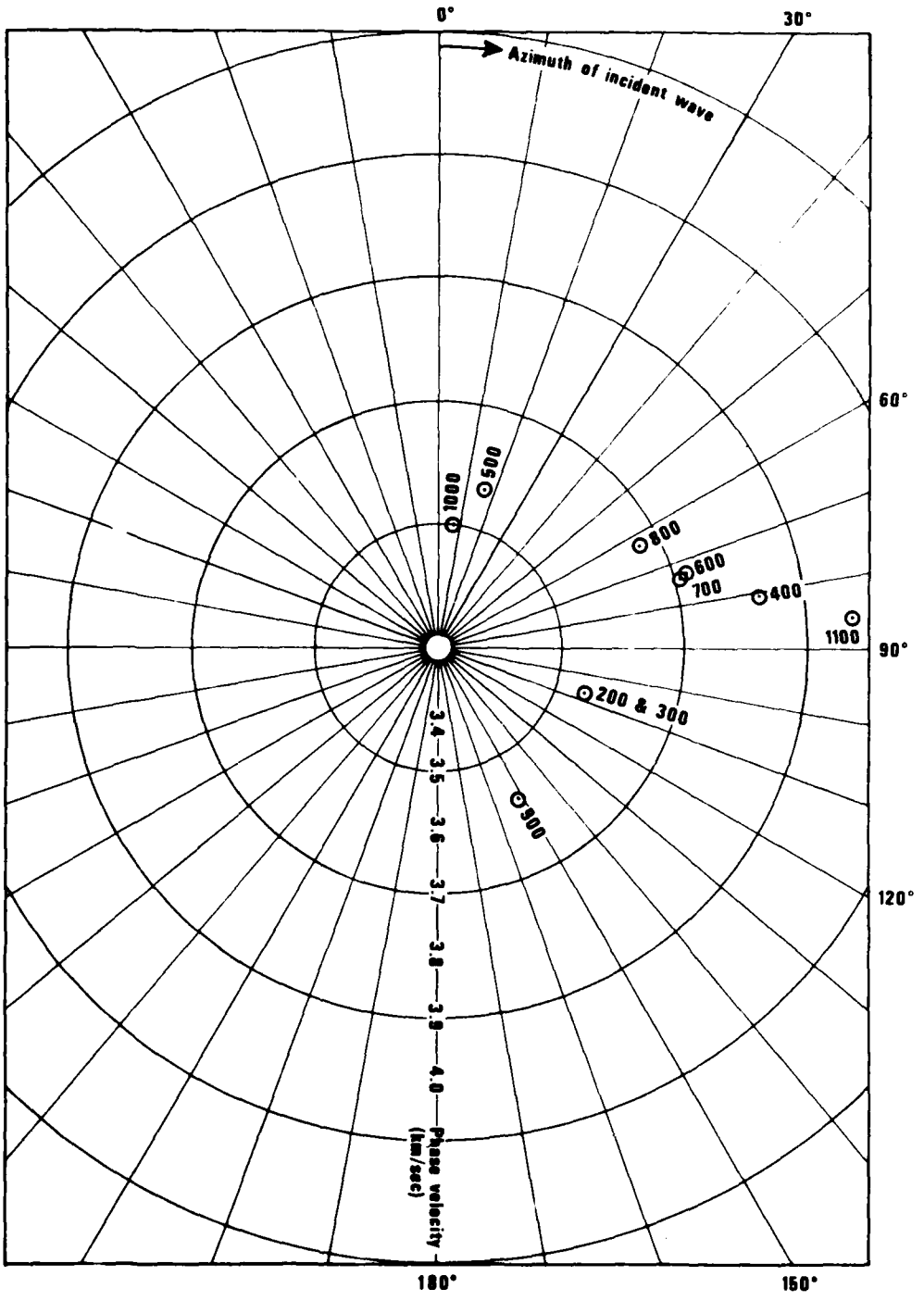

Figure 7. Phase velocities and azimuths measured at 19.7 sec period for ten earthquakes recorded at NORSAR.

One mode of analysis calculated $\bar{\phi}_i(j)$ on the basis of a constant phase velocity of 3.64 km/sec for each event; the other mode used the phase velocity C_i which best fit the data for the ith event. Our data base thus consisted of the set of amplitude residuals B_{ij} and two sets of phase residuals S_{ij}.

Results

These three sets of residuals are listed in Tables III, IV, and V. In Table III, for the amplitude fluctuations, the extreme right-hand column contains for each instrument the mean fluctuation and its standard deviation over all events. (Note that not every instrument was operative during each of the ten events.) For every instrument the 95% confidence limits (±2 standard deviation/number of events) on the mean overlaps zero demonstrating that no significant net amplitude biases existed that had to be removed from the data for each instrument. At the bottom of each event column in Table III the standard deviation of the amplitude fluctuations for that event over all the instruments is listed. (The mean of the fluctuations is zero by definition in equation (13).) This value is equal to $(\overline{B^2}_i)^{\frac{1}{2}}$ for the ith event. The average of this quantity for all ten events is 0.249, corresponding to a standard deviation in surface-wave magnitude of $(0.249)/\ell n\ (10) = 0.108$. A typical value of $\overline{B^2}$ is thus $(0.249)^2 = 0.062$. The rms fluctuation of 0.249 is only in fair agreement with our hypothesis of small fluctuation in amplitude. Similar results hold for Tables IV and V, which list the two sets of phase residuals S_{ij}. The mean fluctuation over all events and all instruments had a standard deviation of about 13 degrees for both data sets, which corresponds to a value of $\overline{S^2} = 0.051$ in radian measure. The rms $(\overline{S^2})^{\frac{1}{2}} = 0.227$, which again is somewhat larger than the fluctuations considered in Chernov's theory.

The repeatability, and to a certain extent the reliability, of the measurements can be determined by comparing the fluctuations for the two events in the same aftershock sequence, events 600 and 700. Since the epicenter-to-NORSAR path for these two events is nearly identical, the residuals at each instrument should also be identical, an observation supported in an examination of Tables III, IV, and V. (One glaring exception, however, is instrument number 16, whose amplitude residual for event 600 suggests a malfunction.) Although most other residuals for the two events are nearly the same, they are not exactly so. This difference is thought to stem from slight differences in

TABLE III

Amplitude Fluctuations at NORSAR
(natural log of amplitudes, with event mean removed)

Complete Data Set

	Event Number										Fluctuation (for given seismometer)
Seismometer	200	300	400	500	600	700	800	900	1000	1100	mean stn. dev.
1	.136	.036	-.006	.019			-.062	.021	-.989	.367	-.060 ± .398
2	.073	.495*	.021	.284	.219	.248	.112	-.186	-.397	.073	.094 ± .250
3	.059	-.011	.074	.019	.201	.242	.096	.291	-.378	-.013	.058 ± .186
4	-.004	.045	-.042	-.201	.079	.145	.143	-.077		.108	.022 ± .155
5	.010		.091	-.059	-.034	.066	-.058	-.168		.313	.020 ± .143
6	-.026	-.076	-.021	-.114	-.186	-.083	.124	-.101	-.745	.162	-.107 ± .248
7	-.105	-.057	-.233	-.028	.110	.163	-.004	-.109	-.312	-.027	-.059 ± .141
8	-.055	.024	.006	.203	.098	.140	-.155	-.367	-.169	.037	-.024 ± .169
9	-.067	-.123	-.064		-.415	-.538*	-.081	.168	.505	-.905*	-.169 ± .409
10		-.192	-.071	.274	-.134	-.191	-.120	.181	.010	-.756*	-.111 ± .291
11	-.066	-.166	.127	.073	.179	.180	.039	.410	-.363	-.143	.027 ± .219
12	-.045	-.237		-.275	.141	.155	.060	.453*	.251	.079	.065 ± .229
13	-.012	.147	.196	-.210	.004	.068	.043	.137	.468	.159	.100 ± .174
14	.099	.240	.148	-.082	-.099	-.007	.048	.137	.312	.154	.095 ± .132
15	.154*	-.117	.220	-.091	-.121	-.039	.039	-.177	.607	.190	.067 ± .237
16	.079	-.083	.188	.021	.632*	-.009	.132	-.142	.232	.304	.135 ± .223
17	-.001		-.035	-.131			-.081	-.186	-.424	.017	-.120 ± .152
18	-.046	.344	-.069		-.327	-.274	-.039	.091	-.572		-.112 ± .279
19	-.001	-.145		.130	.248	.310	.064	-.069	.034	.121	.007 ± .144
20	-.115	-.116	-.058		.108	.198	.014	-.195	.518	.039	.044 ± .216
21	-.064	.114	-.211	.002	-.378	-.388	-.370*	-.195	.742	-.271	-.102 ± .342
22	.002	-.112	-.272	.168	-.321	-.381	.052	.084	.667		-.013 ± .319
Fluctuation (for given event)											
mean + stn. dev.	0.0 ±.075	0.0 ±.188	0.0 ±.138	0.0 ±.160	0.0 ±.256	0.0 ±.240	0.0 ±.118	0.0 ±.214	0.0 ±.509	0.0 ±.321	

Average fluctuation for all seismometers and all events: 0.00 ± .249

* Absolute value of the fluctuation at this seismometer is greater than twice the standard deviation of this event

\+ Method of computing fluctuations for given event requires that mean = 0.0

TABLE IV

Phase Fluctuations at NORSAR Assuming Phase Velocity = 3.641 km/sec
(fluctuation = calculated - observed residual in degrees)

Complete Data Set

	Event Number										Average Fluctuation (for given seismometer)
Seismometer	200	300	400	500	600	700	800	900	1000	1100	mean stn. dev.
1	-2	3	1	-10			-4	-4	-18	-6	-5.0 ± 6.6
2	-2	24	-2	-14	4	7	-7	-13	-25	-2	-3.0 ± 13.3
3	2	5	-6	-19	4	2	5	1	14	-2	0.6 ± 8.6
4	-4	-7	-1	-4	-6	-7	6	5		5	-1.4 ± 5.4
5	-10		0	-4	-4	-6	9	-15		9	-2.6 ± 8.5
6	-2	-6	-17	-6	-6	-7	-8	11	53*	-12	0.0 ± 20.0
7	-3	-10	-44*	-2	9	10	1	-15	-1	-18	-7.3 ± 15.8
8	1	20	1	-9	-2	-2	-6	-7	-22	-16	-4.2 ± 11.3
9	11	-22	11		-10	-18	1	11	-4	25	0.6 ± 15.5
10		-14	3	1	2	-3	1	12	-27	0	-2.8 ± 11.3
11	4	-5	24	-26	14	16	-9	-1	1	5	2.3 ± 14.1
12	-1	8		5	19*	20	3	7	6	22	9.9 ± 8.3
13	-12	-22	5	20	5	4	7	14	-32	21	1.0 ± 17.6
14	-8	-10	11	15	2	4	5	-9	-13	11	0.8 ± 10.1
15	-6	1	19	21	-2	-2	5	-39*	-40	16	-2.7 ± 21.5
16	-1	8	8	1	-5	-3	-9	-17	4	7	-0.7 ± 8.1
18	9	-5	12		3	1	-1	29	15		7.9 ± 10.9
19	8	-15		2	6	8	-2	-6	-9	-20	-3.1 ± 10.2
20	4	6	-15		-12	-10	5	-9	16	-27	-4.7 ± 13.3
21	2	21	1	20	4	8	11	-14	32	-22	6.3 ± 16.2
22	0	19	-16	11	-23*	-24*	-4	22	9		-0.7 ± 17.4
Fluctuations (for given event)											
mean +	0.0	0.0	0.0	0.0	0.0	0.0	0.0	0.0	0.0	0.0	
stn. dev.	±6.4	±14.0	±15.0	±13.1	±9.3	±10.5	±6.3	±17.2	±24.6	±15.4	

average fluctuation for all seismometers and all events: 0.0 ± 13.6

* absolute value of the fluctuation at this seismometer is greater than twice the standard deviation for this event

\+ method of computing fluctuations for a given event requires that mean = 0.0

TABLE V

Phase fluctuations at NORSAR assuming different phase velocities for each event
(fluctuation = calculated - observed residual in degrees)

Complete Data Set

	Event Number										Fluctuation (for given seismometer)
Seismometer	200	300	400	500	600	700	800	900	1000	1100	mean stn. dev.
1	-2	3	1	-10			-4	-4	-18	-6	-5.0 ± 6.6
2	-4	23	-1	-13	4	7	-8	-14	-22	0	-2.8 ± 12.7
3	4	7	-13	-16	1	0	4	0	18	-11	-0.6 ± 10.3
4	-1	-4	-7	-3	-9	-9	5	5		-4	-3.0 ± 5.3
5	-7		-3	-5	-6	-7	9	-12		4	-3.4 ± 6.7
6	-1	-6	-15	-9	-5	-6	-7	13	47	-8	0.3 ± 17.9
7	-6	-12	-38*	-4	12	13	2	-15	-5	-6	-5.9 ± 14.5
8	-2	18	5	-9	0	0	-5	-9	-20	-7	-2.9 ± 10.0
9	7	-26	13		-10	-18	0	7	6	30*	1.0 ± 16.9
10		-16	2	5	1	-4	0	8	-18	2	-2.2 ± 9.0
11	6	-3	16	-21	10	13	-11	-3	10	-7	1.0 ± 11.9
12	3	13		8	13	15	1	7	12	4	8.4 ± 5.1
13	-6	-16	-7	22	0	-1	5	15	-30	1	-1.7 ± 14.7
14	-3	-5	2	15	-2	1	4	-7	-15	-3	-1.3 ± 7.8
15	0	7	12	18	-4	-4	4	-35*	-47	3	-4.6 ± 20.5
16	2	11	6	-3	-5	-2	-9	-13	-4	5	-1.2 ± 7.3
17	11*		9	-6			-7	40*	32	10	12.7 ± 17.7
18	8	-7	21		7	5	0	32	6		9.0 ± 12.2
19	5	-18		-2	11	12	0	-5	-16	-2	-1.7 ± 10.5
20	-2	1	-4		-7	-5	7	-10	14	-6	-1.3 ± 7.6
21	-5	14	12	20	8	12	13*	-18	35	0	9.1 ± 14.4
22	-5	14	-10	13	-21*	-22*	-4	18	15		-0.2 ± 15.7
Fluctuation (for given event)											
mean +	0.0	0.0	0.0	0.0	0.0	0.0	0.0	0.0	0.0	0.0	
stn. dev.	±5.1	±13.4	±13.3	±12.8	±8.7	±10.2	±6.2	±17.0	±23.7	±8.9	

average fluctuation for all seismometers and all events: 0.0 ± 13.0

* absolute value of the fluctuation at this seismometer is greater than twice the standard deviation for this event

\+ method of computing fluctuation for a given event requires that mean = 0.0

the paths of the incident waves and not from variations within a three-day period of the instrument responses. If this were the case it would strongly suggest that instrument responses, at least for some instruments, were subject to significant random fluctuations during the period the data set represents.

Rivers and von Seggern (1978) explained that important parameters in the Chernov theory are the ratio of $\overline{B^2}$ to $\overline{S^2}$ and the correlation coefficient ρ between the amplitude and phase fluctuations. Capon (1974) derived expressions for the confidence limits about the theoretical values of $\overline{B^2}/\overline{S^2}$ and ρ within which estimates of those quantities should fall based upon N observations. The confidence limits R about ρ are given by

$$R = \tanh (\overline{Z} \pm 2\sigma) \tag{15}$$

where

$$\overline{Z} = 1/2 \ \ell n \left(\frac{1 + \rho}{1 - \rho}\right) \tag{16}$$

and

$$\sigma = (N - 3)^{-1/2} \tag{17}$$

We surround our observed values of ρ with error bars by substituting the observed value in place of the theoretical value in (16). Error bars about $\overline{B^2}/\overline{S^2}$ are obtained by noting that this quantity has the F distribution. The values of $\overline{B^2}/\overline{S^2}$, ρ, and their 95% confidence limits are given in Table VI. For every event the ratio $\overline{B^2}/\overline{S^2}$ is greater for the data set where the phase velocity of the best-fitting incident wave rather than the constant C = 3.64 km/sec was used, because the best-fitting phase velocity is defined to be the one for which $\overline{S^2}$ is a minimum for that event. The difference between the values of ρ found by using the two different sets of phase residuals is impossible to predict.

The phase residuals and, therefore, the quantities $\overline{B^2}/\overline{S^2}$ and ρ are dependent not only upon the assumed phase velocity of the incident wave but also upon the value assumed for its azimuth. Table II shows that the azimuths found by FKCOMB, which minimized the residuals $\overline{S^2}$ for a given event, did not always agree with the geometrical NORSAR-to-epicenter azimuth for that event. The sensitivity of $\overline{S^2}$ and ρ to variations in the assumed azimuth of the incident wave should be examined. This is done for event 200 in Table VII, which

TABLE VI

Ratios and correlations of single-receiver amplitude and phase fluctuations at NORSAR

Complete Data Set

Event	Azimuth (degrees)	Phase velocity (km/sec)	$\frac{\overline{B^2}}{\overline{S^2}}$	Confidence interval		ρ	Confidence interval	
200	106.9	3.641	0.448	0.185 to	1.084	-0.385	-0.700 to	0.056
		3.550	0.701	0.290	1.696	-0.081	-0.495	0.363
300	106.7	3.641	0.591	0.240	1.454	0.227	-0.240	0.608
		3.550	0.641	0.261	1.577	0.246	-0.220	0.621
400	80.9	3.641	0.280	0.114	0.689	0.616	0.238	0.832
		3.829	0.355	0.144	0.873	0.290	-0.174	0.650
500	16.0	3.641	0.490	0.194	1.240	-0.339	-0.687	0.136
		3.575	0.512	0.202	1.295	-0.306	-0.668	0.172
600	73.0	3.641	2.473	1.005	6.084	0.323	-0.139	0.670
		3.720	2.835	1.152	6.974	0.267	-0.199	0.634
700	73.9	3.641	1.702	0.692	4.187	0.538	0.125	0.792
		3.707	1.832	0.745	4.507	0.492	0.064	0.768
800	62.8	3.641	1.156	0.484	2.763	-0.283	-0.630	0.157
		3.668	1.196	0.500	2.853	-0.348	-0.671	0.086
900	152.4	3.641	0.507	0.212	1.212	0.349	-0.085	0.672
		3.579	0.519	0.217	1.240	0.312	-0.126	0.648
1000	6.0	3.641	1.405	0.571	3.456	-0.192	-0.585	0.274
		3.503	1.510	0.614	3.715	-0.135	-0.545	0.327
1100	85.4	3.641	1.432	0.582	3.523	-0.100	-0.519	0.358
		3.976	4.262	1.733	10.485	-0.529	-0.787	-0.113

TABLE VII

Effect of varying the assumed NORSAR-to-epicenter azimuth for event 200

Phase velocity assumed to be 3.641 km/sec.

Complete Data Set

Assumed azimuth (degrees)	20 $\overline{S^2}$ = sum of squares of phase residuals (degrees^2)	$\frac{\overline{B^2}}{\overline{S^2}}$	ρ
96.9	14,740	0.025	-0.259
97.9	12,030	0.031	-0.264
98.9	9,611	0.038	-0.270
99.9	7,482	0.049	-0.280
100.9	5,644	0.065	-0.293
101.9	4,099	0.090	-0.311
102.9	2,849	0.129	-0.336
103.9	1,895	0.194	-0.368
104.9	1,238	0.297	-0.405
105.9	880	0.418	-0.424
106.9	821	0.448	-0.385
107.9	1,061	0.347	-0.294
108.9	1,603	0.230	-0.206
109.9	2,446	0.150	-0.142
110.9	3,591	0.102	-0.098
111.9	5,038	0.073	-0.069
112.9	6,788	0.054	-0.048
113.9	8,841	0.042	-0.034
114.9	11,200	0.033	-0.024
115.9	13,860	0.027	-0.016
116.9	16,820	0.022	-0.011

assumes the phase velocity of the incident wave to be 3.64 km/sec and in Table VIII, which uses the best-fitting phase velocity for each value assumed for the incident azimuth. Clearly $\overline{S^2}$ and $\overline{B^2}/\overline{S^2}$ change markedly for azimuths only a few degrees from the values for which S^2 is a minimum. The correlation ρ also exhibits a strong, but less dramatic, dependence upon azimuth. The values $\overline{B^2}/\overline{S^2}$ and ρ for event 200 would have been significantly different if the geometrical azimuth (99.0°) rather than the value found by FKCOMB (106.9°) were used.

Table III, IV, and V show several amplitude and phase fluctuations whose magnitude exceeds twice the standard deviation of fluctuations for that event. That is, for certain events i and certain instruments j,

$$|B_{ij}| > 2(\overline{B_i^2})\ 1/2 \qquad (18)$$

and similarly for S_{ij}. Because these large (and possibly spurious) fluctuations have a signicant effect upon $\overline{B^2}$, $\overline{S^2}$, and ρ, another data set, the "edited" set, was formed by omitting these anomalous values from the complete data set. As already noted, we also wanted the data set to reflect as wide and as well-spaced a range of azimuths as possible so the statistical average over source-to-receiver paths in the Chernov theory would be valid; for this reason one of the events in the aftershock sequence (event 600) was not included in the edited data set. Ths omission prevents excess emphasis on a particular path in the averaging process. (Athough event 200 and 300 had almost the same FKCOMB azimuths for the incident wave, their geometrical NORSAR-to-epicenter azimuths are different.)

For the edited data set (Tables IX, X, and XI), the rms amplitude fluctuation is 0.147 natural log unit, a figure equivalent to a standard deviation of 0.064 in the measurement of the Rayleigh-wave magnitude M_s from 20 sec waves. The rms phase fluctuation, calculated by assuming a phase velocity of 3.64 km/sec, is 11.2 degrees, or 0.195 radians; the fluctuation calculated on the basis of the best-fitting phase velocity is 9.7 degrees, or 0.169 radians. The amplitude fluctuations, therefore, are much smaller, and the phase fluctuations somewhat smaller, for the edited data set than for the complete data set. The values of $\overline{B^2/S^2}$ and ρ calculated for the edited data set are listed in Table XII.

TABLE VIII

Effect of varying the assumed NORSAR-to-epicenter azimuth for event 200

Best-fitting phase velocity used for each azimuth

Complete Data Set

Assumed azimuth (degrees)	$20\ \overline{S^2}$ = sum of squares of phase residuals (degrees^2)	$\frac{\overline{B^2}}{\overline{S^2}}$	ρ	phase velocity (km/sec)
96.9	14,740	0.025	-0.261	3.644
97.9	12,030	0.031	-0.254	3.629
98.9	9,589	0.038	-0.246	3.616
99.9	7,432	0.050	-0.239	3.603
100.9	5,559	0.066	-0.232	3.592
101.9	3,976	0.093	-0.225	3.582
102.9	2,686	0.137	-0.217	3.573
103.9	1.693	0.217	-0.208	3.565
104.9	1,000	0.368	-0.193	3.559
105.9	610	0.604	-0.156	3.554
106.9	525	0.701	-0.081	3.550
107.9	748	0.492	-0.003	3.547
108.9	1,280	0.287	0.040	3.546
109.9	2,122	0.173	0.059	3.545
110.9	3,275	0.112	0.066	3.546
111.9	4,739	0.078	0.066	3.549
112.9	6,513	0.056	0.063	3.552
113.9	8,597	0.043	0.058	3.557
114.9	10,990	0.033	0.052	3.564
115.9	13,690	0.029	0.044	3.571
116.9	16,690	0.022	0.037	3.580

TABLE IX

Amplitude fluctuations at NORSAR (natural log of amplitudes, with event mean removed)

Edited Data Set

	Event Number								
Seismometer	200	300	400	500	700	800	900	1000	1100
1	.144	.062	-.018	.019		-.079	.026	-.989	.274
2	.081		.009	.284	.197	.095	-.181	-.397	-.020
3	.067	.015	.062	.019	.191	.079	.296	-.378	-.106
4	.004	.071	-.054	-.201	.094	.126	-.072		.015
5	.018		.079	-.059	.015	-.075	-.163		.220
6	-.018	-.050	-.033	-.114	-.134	.107	-.096	-.745	.069
7	-.097	-.031		-.028	.112	-.021	-.104	-.312	-.120
8	-.047	.050	-.006	.203	.089	-.172	-.362	-.169	-.056
9	-.059	-.097	-.076			-.098	.173	.505	
10		-.166	-.083	.274	-.242	-.137	.186	.010	
11	-.058	-.140	.115	.073	.129	.022	.415	-.363	-.236
12	-.037	-.211		-.275	.104	.043		.251	-.014
13	-.004	.168	.184	-.210	.017	.026	.142	.468	.066
14	.107	.266	.136	-.082	-.058	.031	.142	.312	.061
15		-.091	.208	-.091	-.090	.022		.607	.097
16	.087	-.057	.176	.021	-.060	.115	-.137	.232	.211
17			.047	-.131		-.098		-.424	-.076
18	-.038	.370	-.081		-.325	-.056	.096	-.572	
19	.007	-.119		.130	.259	.047	-.064	.034	.028
20	-.107	-.090	-.070		.147	-.003	-.190	.518	-.054
21	-.056	.140	-.223	.002	-.439		-.190	.742	-.364
22	.010	-.086	-.284	.168		.035	.089	.667	
Stn. dev.	±.070	±.151	±.131	±.160	±.190	±.086	±.196	±.509	±.157

Average fluctuation for all seismometers and all event:
0.00 ± .147

TABLE X

Phase fluctuations at NORSAR assuming phase velocity = 3.641 km/sec
(fluctuation = calculated-observed residual in degrees)

Edited Data Set

	Event Number								
Seismometer	200	300	400	500	700	800	900	1000	1100
1	-2	4	-1	-10		-4	-4	-18	-5
2	-2		-4	-14	5	-7	-12	-25	-1
3	2	6	-9	-19	0	6	1	14	0
4	-4	-6	-3	-4	-9	6	5		7
5	-10		-2	-4	-9	10	-14		10
6	-2	-5	-19	-6	-9	-7	12	53	-10
7	-3	-8		-2	8	2	-15	-1	-17
8	1	22	-2	-9	-4	-5	-7	-22	-14
9	11	-21	9			1	12	-4	
10		-13	1	1	-6	1	12	-27	
11	5	-4	22	-26	14	-8	-1	1	6
12	-1	9		5	18	4		6	24
13	-12	-21	3	20	2	7	14	-32	23
14	-8	-8	8	15	2	6	-9	-13	12
15		3	17	21	-5	5		-40	17
16	0	9	5	1	-5	-9	-16	4	9
17			3	-1		-8		42	5
18	10	-4	10		-1	-1	30	15	
19	8	-14		2	6	-1	-5	-9	-18
20	4	8	-18		-12	6	-9	16	-25
21	2	22	-2	20	6		-14	32	-21
22	1	20	-18	11		-4	22	9	
Stn. dev.	± 6.1	±13.1	±11.0	±13.1	± 8.2	± 5.9	±13.5	±24.6	±15.1

Average fluctuations for all seismometers and all events:
0.00 ± 11.2

TABLE XI

Phase fluctuations at NORSAR assuming different phase velocities for each event
(fluctuation = calculated-observed residual in degrees)

Edited Data Set

Seismometer	Event Number 200	300	400	500	700	800	900	1000	1100
1	-2	5	-1	-10		-4	-3	-18	-4
2	-3		-4	-13	5	-7	-14	-22	2
3	5	8	-13	-16	-1	4	1	18	-10
4	-1	-3	-8	-3	-10	5	6		-3
5	-7		-4	-5	-9	9	-12		5
6	-1	-5	-18	-9	-8	-6	14	47	-5
7	-5	-10		-4	10	4	-14	-5	-4
8	-1	19	2	-9	-3	-4	-8	-20	-5
9	7	-24	10			1	8	6	
10		-15	0	5	-6	1	9	-18	
11	7	-2	16	-21	12	-11	-2	10	-5
12	4	13		8	15	1		12	4
13	-6	-15	-6	22	-1	4	15	-30	2
14	-2	-4	3	15	0	4	-6	-15	-2
15		8	12	18	-6	5		-47	4
16	3	12	5	-3	-5	-8	-13	-4	7
17			6	-6		-6		32	13
18	8	-5	16		1	2	32	6	
19	5	-17		-2	9	2	-4	-16	1
20	-1	3	-10		-9	9	-10	14	-3
21	-5	16	6	20	9		-17	35	3
22	-4	16	-14	13		-3	19	15	
Stn. dev.	± 4.7	±12.6	± 9.9	±12.8	± 8.0	± 5.6	±13.4	±23.7	± 5.5

Average flucutuation for all seismometers and all event:
0.00 ± 9.7

TABLE XII

Ratios and correlations of single-receiver amplitude and phase fluctuations at NORSAR

Edited Data Set

Event	Azimuth (degrees)	Phase velocity (km/sec)	$\frac{\overline{B^2}}{\overline{S^2}}$	Confidence interval	ρ	Confidence interval
200	106.9	3.641	0.425	0.168 to 1.075	-0.359	-0.699 to 0.113
		3.548	0.715	0.283 1.809	-0.096	-0.527 0.375
300	106.7	3.641	0.437	0.173 1.106	-0.038	-0.484 0.424
		3.559	0.473	0.187 1.197	-0.011	-0.463 0.445
400	80.9	3.641	0.465	0.184 1.176	0.530	0.100 0.793
		3.772	0.576	0.228 1.457	0.213	-0.267 0.608
500	16.0	3.641	0.490	0.194 1.240	-0.339	-0.687 0.136
		3.575	0.512	0.202 1.295	-0.306	-0.668 0.172
700	73.9	3.641	1.754	0.675 4.560	0.196	-0.298 0.608
		3.686	1.864	0.717 4.846	0.144	-0.346 0.573
800	62.8	3.641	0.695	0.287 1.682	-0.003	-0.434 0.429
		3.687	0.776	0.321 1.878	-0.075	-0.491 0.369
900	152.4	3.641	0.689	0.272 1.743	0.499	0.058 0.777
		3.587	0.707	0.279 1.789	0.477	0.029 0.765
1000	6.0	3.641	1.405	0.571 3.456	-0.192	-0.585 0.274
		3.503	1.510	0.614 3.715	-0.135	-0.545 0.327
1100	85.4	3.641	0.355	0.137 0.923	0.379	-0.106 0.719
		4.000	2.705	1.040 7.033	0.180	-0.313 0.597

While the logarithmic amplitude fluctuation mentioned above was calculated by smoothing the spectral amplitudes for the three distinct periods 21.3, 19.7, and 18.3 sec, the phase fluctuation was calculated upon the basis of spectral phases for the distinct period 19.7 sec alone. A third data set was created that treated each of these three periods separately by calculating unsmoothed logarithmic amplitudes and phase delays on the basis of each period's data alone. As before, two sets of phase residuals were calculated; for one set the phase velocities were assumed constant for all events. For the other set, the phase velocity used for each event was the best-fitting value for that event. However, it was assumed that the incident azimuth was the same for each period, namely the value which was found for the waves of period 19.7 sec. Only events and instruments which were included in the "edited" data set were included in the third data set. The amplitude and phase fluctuation for this data set are typified by event 200, shown in Table XIII. The phase residuals are smaller for the 19.7 sec waves than for the other two periods, since the chosen azimuth minimizes the residuals for this period. A fourth data set was created like the third except for each period the azimuth of the incident wave was assumed to be the value that minimized the phase residuals for that period alone. The fluctuations in this fourth data set (not tabulated) were the same size as those in the third, save that the phase residuals for periods of 21.3 and 18.3 sec were now about the same size as those for 19.7 sec. The third data set thus represents the same assumption as the "complete" and "edited" sets, i.e., that the "true" azimuth of the waves within the spectral band under consideration is given by the value that minimizes the phase residuals for the period in the middle of that band, an assumption not made in calculating the fourth data set. The best-fitting azimuths and phase velocities (Table XIV and Figure 8) vary significantly within the chosen spectral band for several events.

The quantities $\overline{B^2}/\overline{S^2}$ and ρ were not evaluated for each event and each frequency using the third and fourth data sets. Instead, these data sets, as well as the first two, are now used in a different form of analysis. Chernov's theory involves taking averages over all possible incident azimuths; so, average values of $\overline{B^2}$, $\overline{S^2}$, and ρ were found for each of the four data sets using the combined data from all events. Thus, instead of ten values of $\overline{B^2}$

TABLE XIII

Amplitude and phase fluctuations at NORSAR for event 200.

Three frequencies considered separately (i.e., amplitudes not smoothed)
Azimuth specified to be 106.9°.

	Logarithmic Amplitude Fluctuation			Phase Fluctuation (degrees)					
				Period (sec)			Period (sec)		
	Period (Sec)			21.3	19.7	18.3	21.3	19.7	18.3
				Phase velocity Specified to be (km/sec)			Phase velocity found to be (km/sec)		
Seismometer	21.3	19.7	18.3	3.705	3.641	3.587	3.606	3.545	3.566
1	0.178	0.158	0.106	1	-2	6	1	-2	7
2	0.084	0.061	0.106	-11	-2	-9	-12	-3	-9
3	0.025	0.009	0.162	-7	2	-9	-5	4	-9
4	0.012	-0.041	0.052	-6	-4	-1	-3	-1	0
5	0.015	0.040	0.000	1	-10	0	4	-7	1
6	0.012	0.009	-0.068	9	11	12	10	-1	12
7	-0.037	-0.069	-0.171	10	-3	8	8	-6	8
8	-0.002	-0.046	-0.076	2	1	4	-1	-1	4
9	-0.204	0.035	-0.068	-17	11	-24	-21	7	-24
11	-0.238	-0.041	0.045	-16	5	-27	-14	7	-27
12	-0.162	-0.094	0.106	-17	-1	-14	-12	4	-13
13	-0.005	-0.009	0.005	-11	-12	-1	-5	-6	0
14	0.103	0.130	0.085	-1	-8	5	4	-2	6
16	0.052	0.061	0.140	14	-1	15	17	3	16
18	-0.023	-0.004	-0.084	25	10	20	24	8	19
19	0.121	0.044	-0.132	21	9	15	18	5	14
20	0.032	-0.144	-0.171	11	4	14	6	-1	12
21	0.045	-0.109	-0.068	2	2	-1	-4	-5	-3
22	-0.009	0.009	0.030	-9	1	-14	-14	-4	-15

TABLE XIV

Azimuths and phase velocities yielding best fit to data for each of three frequencies

	Period = 21.3 sec		Period = 19.7 sec		Period = 18.3 sec	
Event	θ (degrees)	c(km/sec)	θ (degrees)	c(km/sec)	θ (degrees)	c(km/sec)
200	102.0	3.643	107.0	3.543	102.4	3.601
300	129.4	3.649	106.4	3.561	110.3	3.603
400	83.9	3.618	80.5	3.770	83.6	3.431
500	20.4	3.752	15.5	3.576	14.0	3.487
700	71.9	3.631	75.0	3.679	71.2	3.553
800	66.0	3.670	62.5	3.693	61.4	3.403
900	155.5	3.489	152.9	3.593	170.8	3.543
1000	353.0	3.337	9.1	3.504	18.4	3.369
1100	78.7	3.751	84.1	4.012	83.2	3.658

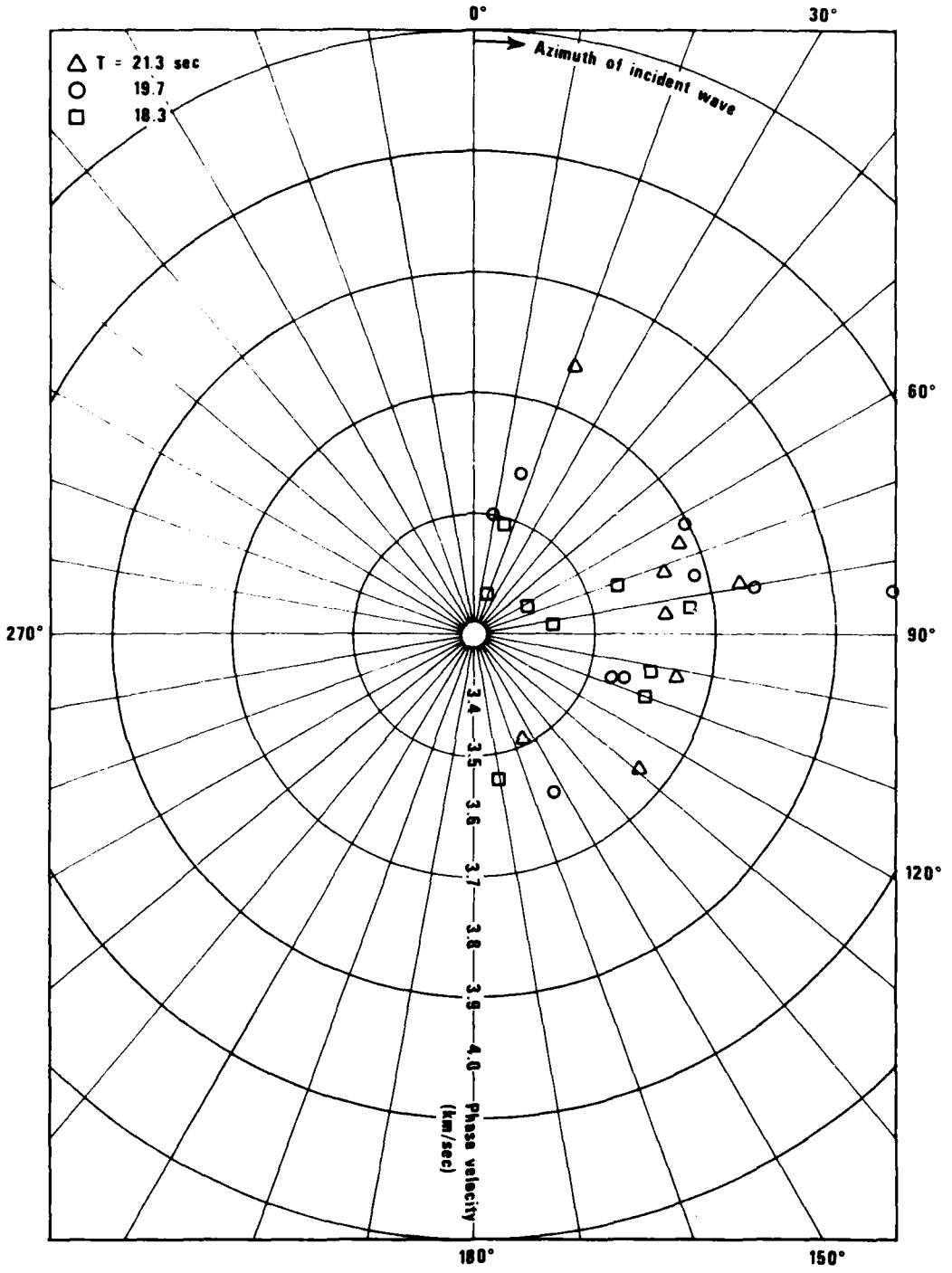

Figure 8. Phase velocities and azimuths measured at three periods for earthquakes in the edited data set.

being computed on the basis of as many as twenty-two observations each, one value is computed on the basis of 204 observations. (Raw data from different events must not be used together. Rather, use the fluctuations, i.e., data from which had been removed the mean of the amplitude and the phase delays of the incident wave for each event.)

Table II indicates that the azimuth determined by FKCOMB differs markedly from the geometrical NORSAR-to-epicenter azimuth for events 500 and 1000. Their geometrical azimuths and source regions suggest that the eastern and, especially, the northern edges of the Asian continent scatter rays from these events. Possibly as a result of this scattering, the amplitude and phase residuals for event 1000 are significantly greater than those for the other events. To avoid the possible systematic (non-random) scattering phenomena that created these fluctuations, $\overline{B^2}$, $\overline{S^2}$, and ρ have been redetermined from the second and third data sets by deleting the data from these two events. Therefore, six data sets were used to determine the average over several events of $\overline{B^2}$, $\overline{S^2}$, and ρ; in addition, each of these data sets has, in turn, two sets of phase residuals, one set assuming the constant phase velocity and the other set using a different value of C for each event. These results are summarized in Table XV.

Wave Parameter D

The wave parameter D is an important quantity in the Chernov theory. Rivers and von Seggern (1978) showed that D can be determined from either $\overline{B^2}/\overline{S^2}$ or from ρ by means of the formula listed in Table I. Also, the wave parameter can be eliminated between the expressions for $\overline{B^2}/\overline{S^2}$ and for ρ, thereby determining one of these quantities as a function of the other. Following Aki's (1973) approach, D is calculated from $\overline{B^2}/\overline{S^2}$ and also independently from ρ. A value which lies between these two independent values is found by determining the point on the theoretical $\overline{B^2}/\overline{S^2}$ versus ρ curve (shown in Rivers and von Seggern (1978)) closest to the observed point (ρ, $\overline{B^2}/\overline{S^2}$); this value is designated D_{curve}. Tables XVI and XVII list these three values of D for each event for the complete and edited data sets. Another value of D was also calculated using these three methods for each of the six data sets that are composites of all events; it was from composite data that Capon (1974) found his value of D_{curve}. These results are shown in Table XVIII.

TABLE XV

Ratios and correlations of single-receiver amplitude and phase fluctuations at NORSAR

Average over all events

Data Set	Phase Velocity (km/sec)	$\frac{\overline{B^2}}{\overline{S^2}}$	ρ	Number of Detections
Complete	3.641	1.028	0.039	204
	variable	1.211	0.006	
Edited	3.641	0.894	-0.009	172
	variable	1.100	-0.020	
Edited, 7 events	3.641	0.586	0.267	133
	variable	0.838	0.196	
Edited, 3 separate frequencies	3.705, 3.641, 3.587	0.646	0.010	172
	variable	0.683	0.025	
Edited, 3 separate frequencies, 7 events	3.705, 3.641, 3.587	0.569	0.107	133
	variable	0.608	0.104	
Edited, 3 separate frequencies, different azimuth for each frequency	3.705, 3.641, 3.587	1.353	0.009	172
	variable	1.536	0.060	

TABLE XVI

Values of the wave parameter D

Complete Data Set

Event	Phase velocity (km/sec)	$\frac{D}{\overline{B^2}/\overline{S^2}}$	D_ρ	D_{curve}
200	3.641	12.8	——	——
	3.550	69	——	——
300	3.641	29	22	28
	3.550	41	18	34
400	3.641	5.2	——	——
	3.829	7.6	11.0	8.5
500	3.641	16	——	——
	3.575	18	——	——
600	3.641	——	7.7	——
	3.720	——	14.0	——
700	3.641	——	——	——
	3.707	——	0.6	——
800	3.641	——	——	——
	3.668	——	——	——
900	3.641	18	5.9	14
	3.579	19	8.8	16
1000	3.641	——	——	——
	3.503	——	——	——
1100	3.641	——	——	——

TABLE XVII

Values of the wave parameter D

Edited Data Set

Event	Phase velocity (km/sec)	$D_{\overline{B^2}/\overline{S^2}}$	D_ρ	D_{curve}
200	3.641	11.2	——	——
	3.548	76	——	——
300	3.641	12.0	——	——
	3.559	14.4	——	——
400	3.641	14.0	——	——
	3.772	26	27	27
500	3.641	16	——	——
	3.575	18	——	——
700	3.641	——	33	——
	3.686	——	74	——
800	3.641	68	——	——
	3.687	130	——	——
900	3.641	63	0	——
	3.587	71	0.97	——
1000	3.641	——	——	——
	3.503	——	——	——
1100	3.641	7.8	4.1	6.9
	4.000	——	40	——

TABLE XVIII

Values of the wave parameter D

Average over all events

Data Set	Phase velocity (km/sec)	$D_{\overline{B^2}/\overline{S^2}}$	D_ρ	D_{curve}
Complete	3.641	——	——	——
	variable	——	——	——
Edited	3.641	830	——	——
	variable	——	——	——
Edited, 7 events	3.641	28	14	25
	variable	310	32	140
Edited, 3 separate frequencies	3.705, 3.641, 3.587	44	——	——
	variable	61	——	——
Edited, 3 separate frequencies, 7 events	3.705, 3.641, 3.587	25	150	34
	variable	32	160	43
Edited, 3 separate frequencies, different azimuth for each frequency	3.705, 3.641, 3.587	——	——	——
	variable	——	700	——

Discussion of Experimental Observation

Note that about half the data consists of values with D undefined because the observed values of ρ, or $\overline{B^2}/\overline{S^2}$, lie outside the range of permissable values useful in calculating D. The Chernov theory predicts that

$$0 < \rho < 0.5 \tag{19}$$

$$\overline{B^2} \quad < \overline{S^2} \tag{20}$$

but frequently our data did not meet these conditions. Perhaps, the inequality (20), and also indirectly (19), should not always be expected to hold because for several of the data sets efforts were made to minimize the phase residuals by selecting the best value of the incident azimuth and phase velocity. This procedure indicates the need to determine the proper average values to use when calculating amplitude and phase residuals. (So far we have assumed that these values were: for amplitude, the average of the logarithmic amplitudes for all the instruments; and, for phase, the plane wave with azimuth and velocity that best fits the phase data.) The values calculated for the fluctuations would have been different if these mean values were chosen differently. One reason that they perhaps should have been different is that the mean values themselves may reflect the random scattering process. For example, if the data set had consisted of magnitudes measured not only at NORSAR, but also at other stations nearby the array, the average of the amplitudes probably would have been different from the value determined by NORSAR data alone. Because we think that some of this difference stems from random scattering, the question arises of the applicability of Chernov's theory to random fluctuations about a value which is itself a random fluctuation. Again, note that the fluctuations are assumed small, but the difference between the average magnitude at NORSAR and the average magnitude at a point several hundred kilometers away can be considerably greater than the average magnitude difference within the hundred kilometer-wide array. The fluctuations measured across NORSAR, then, may represent scattering on a smaller scale than that for which Chernov's theory is valid, given the true size of the inhomogeneities which are the most efficient scatters of waves of 70 km wavelength. These points will be further discussed following analysis of data from the linear array in the Southwestern United States.

Another problem in analyzing the data is that the azimuth and phase velocity for the best-fitting plane wave can vary significantly within a narrow spectral band, further demonstrating the difficulty of choosing the mean value about which fluctuations should be measured. This variation of azimuth with frequency suggests that Rayleigh-wave scattering may differ from the model that Aki (1973) and Capon (1974) assumed for P-wave scattering. In their model, amplitude and phase fluctuations measured at LASA stemmed from scattering within the crust of a single coherent wave incident from the mantle. However, because of the Rayleigh waves' much longer path through the scattering medium, the fluctuation measured at NORSAR results from scattering through the array of several different rays incident at different angles, and these rays themselves might have been scattered from other rays rather than from the same wavefront. If this multiple scattering occurs, then the Born approximation, which separates the wave field into an incident wave carrying most of the energy and a diffracted wave of small amplitude, breaks down. In any case, our data is frequently inconsistent with inequalities (19) and (20) predicted by the Chernov theory; however, note that values measured for $\overline{B^2}/\overline{S^2}$ and for ρ lie within large confidence limits.

Spatial Correlations

The spatial correlation among fluctuations measured at different receivers for the same event is another characteristic of the scattering studied here using the "edited" data set. In order that Chernov's theory be applicable, the separation between any given pair of instruments is projected along two directions: the "longitudinal" direction which is parallel to the direction of propagation of the incident wave and the "transverse" direction which runs perpendicular to the longitudinal. The separation between any two given receivers measured with this coordinate system will depend upon the azimuth assumed for the incident wave and, therefore, will differ among events. Now consider these separations to be measured on a grid consisting of overlapping squares of side 20 km in the longitudinal and transverse directions, i.e., a grid made up of blocks defined by

$$x_{1i} \leq \text{longitudinal separation} \leq x_{2i} \qquad (21)$$

x_{1i} = o, 5, 10, ..., 90 km x_{2i} = 20, 25, 30, ..., 110 km

$$y_{1i} \leq \text{transverse separation} \leq y_{2i} \qquad (22)$$

y_{1i} = o, 5, 10, ..., 90 km y_{2i} = 20, 25, 30, ..., 110 km

The blocks are defined by (21) and (22) to overlap in order to smooth the data. For the nine events of the edited data set, the number of pairs of instruments with separations that fall into each of the blocks defined by (21) and (22) are shown in Figure 9. If $(i,j)_k$ denotes the indices of a pair of instruments which for the kth event have a separation which lies within a given block and if S_k denotes the set of all such pairs, then the correlation coefficient of amplitude fluctuation for the block is given by

$$R_b = \sum_{k=1}^{9} \sum_{S_k} B_i B_j / \left(\sum_{k-1}^{9} \left(\sum_{\text{all } i} B_i^2 \cdot \sum_{\text{all } j} B_j^2 \right) \right)^{1/2} . \qquad (23)$$

A similar expression holds for the correlation coefficient of phase fluctuations R_s.

The results of evaluating R_b and R_s, using the edited data set (with its two sets of phase residuals), are shown in Figures 10, 11, and 12. The extreme left-hand column and the uppermost row in these figures, corresponding to pure transverse and pure longitudinal separation of the instruments, should be compared to theoretical results derived in Rivers and von Seggern (1978). An idea of the reliability of the correlation found for each block is found in Figure 9, which shows the number of observations used for each measurement.

Figure 10 shows that distinct regions of positive and negative amplitude correlation exist. The nodal curves separating these regions are roughly linear and parallel to the longitudinal and transverse axes. There are nodes at transverse separations of 25 and 75 km and at a longitudinal separation of 70 km. The amplitude fluctuations are correlated over a longer distance (by a factor of almost three) in the longitudinal direction than in the transverse direction, a fact at least in qualitative agreement both with Chernov's theory and with the empirical results of Mack's (1972) study of Rayleigh-wave coherence.

The correlation coefficient for phase fluctuations calculated for phase residuals determined on the basis of an assumed constant C for all events (Figure 11) does not reflect so clear a spatial pattern as does the amplitdue correlation coefficient. However, the pattern becomes clearer when the residuals used are those which were calculated using a different value of C for

TRANSVERSE SEPARATION (km)		0	5	10	15	20	25	30	35	40	45	50	55	60	65	70	75	80	85	90	95	100	(±10)
0		1	7	18	63	85	92	90	72	65	68	66	50	45	40	39	36	28	20	19	12	9	
5		8	21	47	106	134	139	132	109	100	100	95	72	63	60	57	52	39	30	28	19	16	
10		26	57	99	157	186	180	163	141	133	133	123	96	83	80	80	75	55	40	34	23	20	
15		60	112	163	192	190	165	146	132	136	130	118	93	80	81	78	76	53	39	30	21	19	
20		88	146	197	190	178	147	134	129	130	123	106	89	71	71	69	67	53	40	28	21	17	
25		94	150	188	169	154	131	125	121	119	112	103	92	79	72	64	60	47	34	25	20	15	
30		87	129	157	148	136	129	136	119	113	103	92	82	72	61	51	47	42	34	26	22	12	
35		81	111	136	133	127	133	133	117	99	84	77	71	68	60	56	46	44	38	28	33	11	
40		67	95	122	132	128	136	129	109	99	79	77	75	75	65	55	40	31	25	20	16	8	
45		65	92	122	123	116	119	111	101	93	78	66	61	58	51	48	36	31	27	20	13	4	
50		65	97	125	119	105	99	88	89	83	68	62	61	56	54	50	34	27	21	14	7	3	
55		48	78	99	91	80	72	70	74	76	68	59	56	48	42	36	26	22	15	11	4	1	
60		39	66	8	78	69	63	65	70	70	62	52	44	39	32	27	22	20	15	10	4	1	
65		37	64	79	80	71	67	69	66	59	48	44	41	39	33	26	19	16	10	4	1	0	
70		30	52	66	65	61	60	61	60	49	38	33	29	32	25	19	14	10	7	3	1	0	
75		27	43	56	52	54	54	51	51	39	32	32	26	29	20	13	9	4	4	1	0	0	
80		26	36	44	37	38	39	38	41	30	26	25	20	22	15	11	6	2	2	0	0	0	
85		22	29	38	32	30	28	23	27	22	24	22	15	14	7	6	4	1	1	0	0	0	
90		19	23	32	25	25	24	17	20	16	20	20	13	10	3	1	1	0	0	0	0	0	
95		12	15	22	19	18	18	14	16	13	12	9	4	2	0	0	0	0	0	0	0	0	
100		8	11	18	16	17	16	10	9	6	5	4	3	1	0	0	0	0	0	0	0	0	
(±10)																							

LONGITUDINAL SEPARATION (km)

Figure 9. Number of pairs of receivers at NORSAR which were used in the edited data set and which have a given separation (within overlapping separation intervals of size 20 km X 20 km). Note that the interval size is actually smaller than 20 km X 20 km for transverse and/or longitudinal separations of less than 20 km.

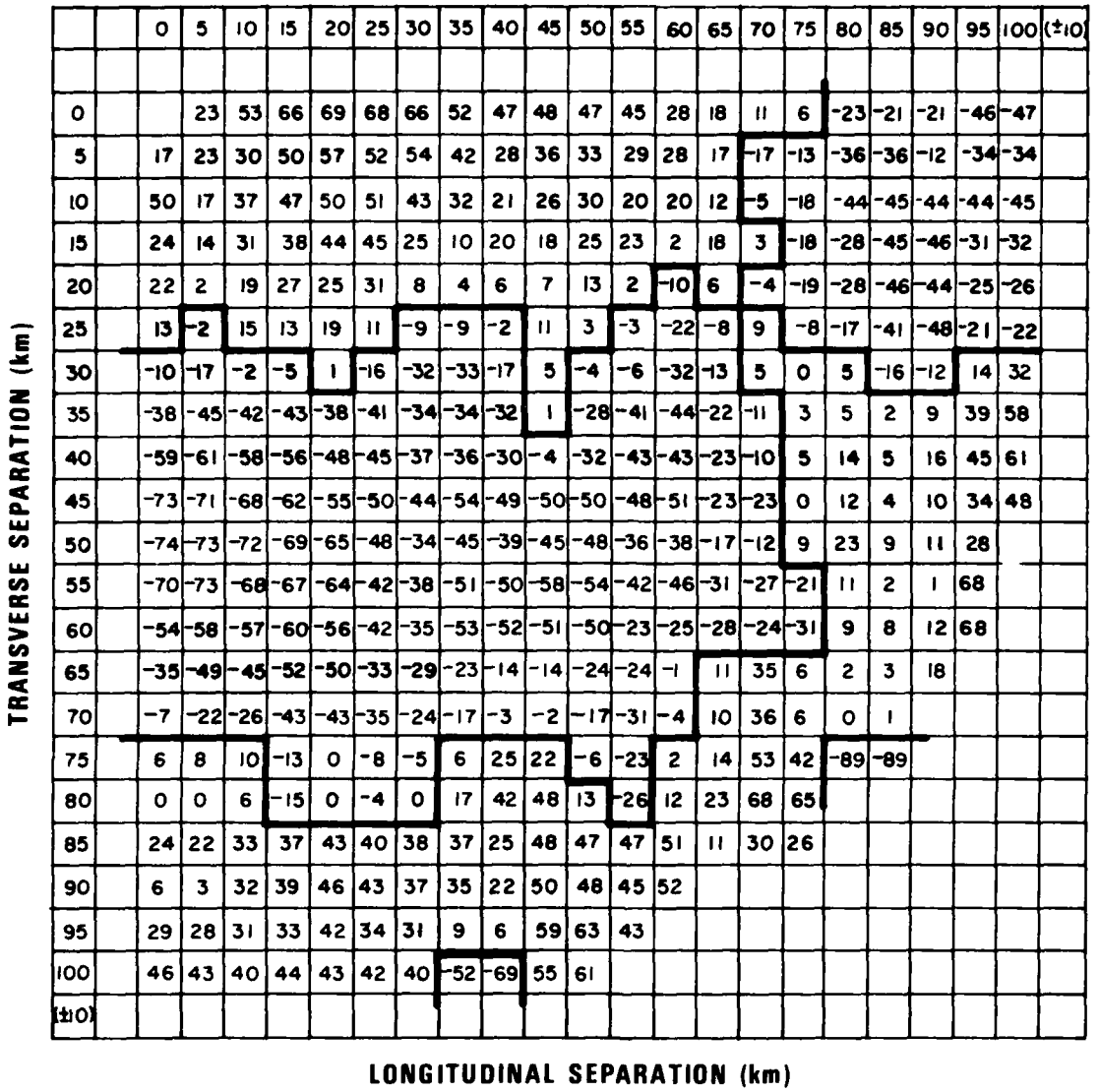

		0	5	10	15	20	25	30	35	40	45	50	55	60	65	70	75	80	85	90	95	100	(±10)
0			23	53	66	69	68	66	52	47	48	47	45	28	18	11	6	-23	-21	-21	-46	-47	
5		17	23	30	50	57	52	54	42	28	36	33	29	28	17	-17	-13	-36	-36	-12	-34	-34	
10		50	17	37	47	50	51	43	32	21	26	30	20	20	12	-5	-18	-44	-45	-44	-44	-45	
15		24	14	31	38	44	45	25	10	20	18	25	23	2	18	3	-18	-28	-45	-46	-31	-32	
20		22	2	19	27	25	31	8	4	6	7	13	2	-10	6	-4	-19	-28	-46	-44	-25	-26	
25		13	-2	15	13	19	11	-9	-9	-2	11	3	-3	-22	-8	9	-8	-17	-41	-48	-21	-22	
30		-10	-17	-2	-5	1	-16	-32	-33	-17	5	-4	-6	-32	-13	5	0	5	-16	-12	14	32	
35		-38	-45	-42	-43	-38	-41	-34	-34	-32	1	-28	-41	-44	-22	-11	3	5	2	9	39	58	
40		-59	-61	-58	-56	-48	-45	-37	-36	-30	-4	-32	-43	-43	-23	-10	5	14	5	16	45	61	
45		-73	-71	-68	-62	-55	-50	-44	-54	-49	-50	-50	-48	-51	-23	-23	0	12	4	10	34	48	
50		-74	-73	-72	-69	-65	-48	-34	-45	-39	-45	-48	-36	-38	-17	-12	9	23	9	11	28		
55		-70	-73	-68	-67	-64	-42	-38	-51	-50	-58	-54	-42	-46	-31	-27	-21	11	2	1	68		
60		-54	-58	-57	-60	-56	-42	-35	-53	-52	-51	-50	-23	-25	-28	-24	-31	9	8	12	68		
65		-35	-49	-45	-52	-50	-33	-29	-23	-14	-14	-24	-24	-1	11	35	6	2	3	18			
70		-7	-22	-26	-43	-43	-35	-24	-17	-3	-2	-17	-31	-4	10	36	6	0	1				
75		6	8	10	-13	0	-8	-5	6	25	22	-6	-23	2	14	53	42	-89	-89				
80		0	0	6	-15	0	-4	0	17	42	48	13	-26	12	23	68	65						
85		24	22	33	37	43	40	38	37	25	48	47	47	51	11	30	26						
90		6	3	32	39	46	43	37	35	22	50	48	45	52									
95		29	28	31	33	42	34	31	9	6	59	63	43										
100		46	43	40	44	43	42	40	-52	-69	55	61											
(±10)																							

Figure 10. Correlation (in percent) of logarithmic amplitude fluctuations at NORSAR as a function of the separation between the receivers. The amplitude fluctuations were calculated using the edited data set.

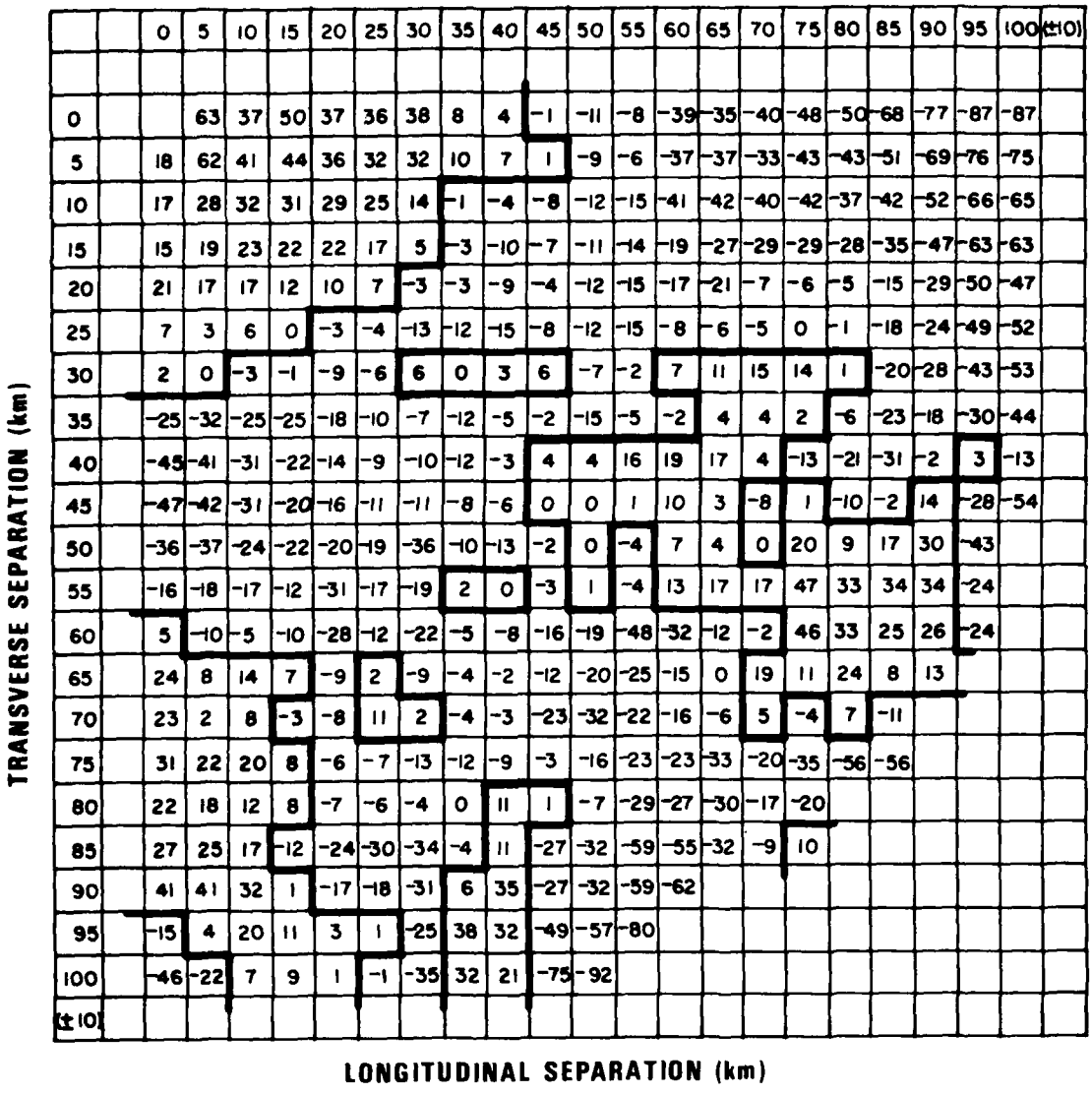

	0	5	10	15	20	25	30	35	40	45	50	55	60	65	70	75	80	85	90	95	100	(±10)
0		63	37	50	37	36	38	8	4	-1	-11	-8	-39	-35	-40	-48	-50	-68	-77	-87	-87	
5	18	62	41	44	36	32	32	10	7	1	-9	-6	-37	-37	-33	-43	-43	-51	-69	-76	-75	
10	17	28	32	31	29	25	14	-1	-4	-8	-12	-15	-41	-42	-40	-42	-37	-42	-52	-66	-65	
15	15	19	23	22	22	17	5	-3	-10	-7	-11	-14	-19	-27	-29	-29	-28	-35	-47	-63	-63	
20	21	17	17	12	10	7	-3	-3	-9	-4	-12	-15	-17	-21	-7	-6	-5	-15	-29	-50	-47	
25	7	3	6	0	-3	-4	-13	-12	-15	-8	-12	-15	-8	-6	-5	0	-1	-18	-24	-49	-52	
30	2	0	-3	-1	-9	-6	6	0	3	6	-7	-2	7	11	15	14	1	-20	-28	-43	-53	
35	-25	-32	-25	-25	-18	-10	-7	-12	-5	-2	-15	-5	-2	4	4	2	-6	-23	-18	-30	-44	
40	-45	-41	-31	-22	-14	-9	-10	-12	-3	4	4	16	19	17	4	-13	-21	-31	-2	3	-13	
45	-47	-42	-31	-20	-16	-11	-11	-8	-6	0	0	1	10	3	-8	1	-10	-2	14	-28	-54	
50	-36	-37	-24	-22	-20	-19	-36	-10	-13	-2	0	-4	7	4	0	20	9	17	30	-43		
55	-16	-18	-17	-12	-31	-17	-19	2	0	-3	1	-4	13	17	17	47	33	34	34	-24		
60	5	-10	-5	-10	-28	-12	-22	-5	-8	-16	-19	-48	-32	-12	-2	46	33	25	26	-24		
65	24	8	14	7	-9	2	-9	-4	-2	-12	-20	-25	-15	0	19	11	24	8	13			
70	23	2	8	-3	-8	11	2	-4	-3	-23	-32	-22	-16	-6	5	-4	7	-11				
75	31	22	20	8	-6	-7	-13	-12	-9	-3	-16	-23	-23	-33	-20	-35	-56	-56				
80	22	18	12	8	-7	-6	-4	0	11	1	-7	-29	-27	-30	-17	-20						
85	27	25	17	-12	-24	-30	-34	-4	11	-27	-32	-59	-55	-32	-9	10						
90	41	41	32	1	-17	-18	-31	6	35	-27	-32	-59	-62									
95	-15	4	20	11	3	1	-25	38	32	-49	-57	-80										
100	-46	-22	7	9	1	-1	-35	32	21	-75	-92											
(±10)																						

Figure 11. Correlation (in percent) of spectral phase delays at NORSAR as a function of the separation between the receivers. The phase delays calculated using the edited data set and an assumed phase velocity of 3.641 km/sec.

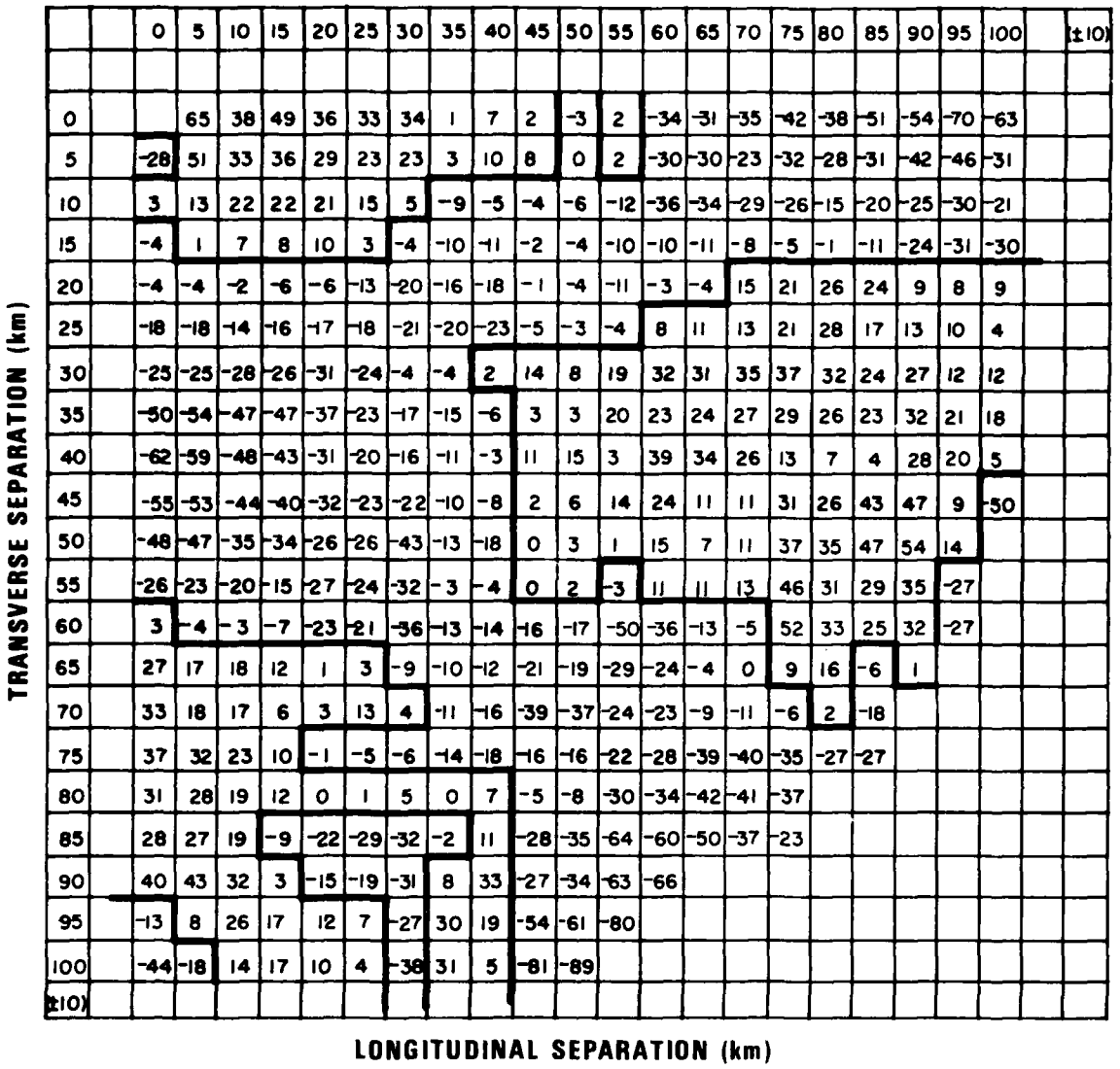

		0	5	10	15	20	25	30	35	40	45	50	55	60	65	70	75	80	85	90	95	100		±10
0			65	38	49	36	33	34	1	7	2	-3	2	-34	-31	-35	-42	-38	-51	-54	-70	-63		
5		-28	51	33	36	29	23	23	3	10	8	0	2	-30	-30	-23	-32	-28	-31	-42	-46	-31		
10		3	13	22	22	21	15	5	-9	-5	-4	-6	-12	-36	-34	-29	-26	-15	-20	-25	-30	-21		
15		-4	1	7	8	10	3	-4	-10	-11	-2	-4	-10	-10	-11	-8	-5	-1	-11	-24	-31	-30		
20		-4	-4	-2	-6	-6	-13	-20	-16	-18	-1	-4	-11	-3	-4	15	21	26	24	9	8	9		
25		-18	-18	-14	-16	-17	-18	-21	-20	-23	-5	-3	-4	8	11	13	21	28	17	13	10	4		
30		-25	-25	-28	-26	-31	-24	-4	-4	2	14	8	19	32	31	35	37	32	24	27	12	12		
35		-50	-54	-47	-47	-37	-23	-17	-15	-6	3	3	20	23	24	27	29	26	23	32	21	18		
40		-62	-59	-48	-43	-31	-20	-16	-11	-3	11	15	3	39	34	26	13	7	4	28	20	5		
45		-55	-53	-44	-40	-32	-23	-22	-10	-8	2	6	14	24	11	11	31	26	43	47	9	-50		
50		-48	-47	-35	-34	-26	-26	-43	-13	-18	0	3	1	15	7	11	37	35	47	54	14			
55		-26	-23	-20	-15	-27	-24	-32	-3	-4	0	2	-3	11	11	13	46	31	29	35	-27			
60		3	-4	-3	-7	-23	-21	-36	-13	-14	-16	-17	-50	-36	-13	-5	52	33	25	32	-27			
65		27	17	18	12	1	3	-9	-10	-12	-21	-19	-29	-24	-4	0	9	16	-6	1				
70		33	18	17	6	3	13	4	-11	-16	-39	-37	-24	-23	-9	-11	-6	2	-18					
75		37	32	23	10	-1	-5	-6	-14	-18	-16	-16	-22	-28	-39	-40	-35	-27	-27					
80		31	28	19	12	0	1	5	0	7	-5	-8	-30	-34	-42	-41	-37							
85		28	27	19	-9	-22	-29	-32	-2	11	-28	-35	-64	-60	-50	-37	-23							
90		40	43	32	3	-15	-19	-31	8	33	-27	-34	-63	-66										
95		-13	8	26	17	12	7	-27	30	19	-54	-61	-80											
100		-44	-18	14	17	10	4	-38	31	5	-81	-89												
±10																								

Figure 12. Correlation (in percent) of spectral phase delays at NORSAR as a function of the separation between the receivers. The phase delays were calculated using the edited data set and a different value of the phase velocity for each event.

each event (Figure 12). For this second set of phase residuals, R_s has nodes at transverse separations of 15 and 55 km and at a longitudinal separation of 40 km. Thus, the phase fluctuations, as well as the amplitude fluctuations, are correlated over nearly three times as great a distance in the longitudinal direction as in the transverse direction. However, the nodes for R_b and R_s occur at different distances.

Comparing these results with predictions of the modified Chernov theory (Rivers and von Seggern (1978), Tables I-IV; Figures 6-13) reveals certain important results and discrepancies. First, the theoretical amplitude correlation in the transverse direction is less oscillatory than is the observed R_b, and the theoretical value does not oscillate at all in the longitudinal direction. Second, the theoretical R_s takes on no negative values for separation in either direction while the observations do. Reasons for these discrepancies may lie, at least in part, in the fact that the values of R_b and R_s for large separations in either direction are not particularly reliable, because they are based on few observations. Further discrepancy may be due to the constraint that, on account of the methods used in calculating them, about half of the residuals must be positive and about half must be negative. This result again reveals the problems in determining the correct average amplitude (or phase) from which the fluctuations are to be calculated. For example, if an event's average amplitude were significantly lower in the vicinity of NORSAR than was the average of the values measured at NORSAR alone, then all twenty-two amplitude residuals would actually be positive, and R_b would be positive for all blocks in the grid. In general, then, these discrepancies restrict the comparison with the theoretical results to a broad discussion of the amplitude correlation coefficient R_b in the transverse direction.

Figures 10 and 13 of Rivers and von Seggern (1978) reveal that for large values of the wave parameter D, R_b has a node in the transverse direction at $\ell/a \simeq 1$, where ℓ is the transverse separation between instruments and where a is the correlation distance. Specifically, Figure 13 of that report shows a node at $\ell = 1.15a$ for $D = 24.4$ and at $\ell = 1.30a$ for $D = 85.6$. (The difficulty in calculating D from our data sets was explained above.) Temporarily consider the value $D_{curve} = 43$, determined using seven events from edited data sets

that were analyzed by considering three distinct periods, a common azimuth for the waves of each period, and a different phase velocity for each event (Table XVIII). For $D \simeq 40$, the node occurs at about $\ell \simeq 1.2a$, so $a \simeq (25\text{km})/1.2 \simeq 21$ km. For waves of period 19.7 sec and phase velocity 3.64 km/sec, the wavenumber $k = 0.0876$, so $ka \simeq 1.8$. The condition that $ka \gg 1$, an assumption made in the Chernov theory, is, therefore, not valid. Since $D = 4L/ka^2$, the length L of the path through the scattering medium is found to be roughly 380 km, a value that is much less than the actual epicenter-to-NORSAR distance for any of the events. This result indicates that all the waves incident at NORSAR have been scattered once within 380 km of the array. Since details of the propagation along the previous 2600 km of the path are lost by this scattering, we cannot say whether all the scattered waves were part of the same wavefront at a distance of 380 km, as in the P-wave model of Aki (1973) and Capon (1974) or whether the wavefield at NORSAR is the final result of the multiple scattering of several different rays which diverge over a longer distance, possibly even back to the source. Had the opposite approach been adopted of assuming values of about 21 km for the correlation distance and 3000 km for the path length, a value of about 310 would have been obtained for the wave parameter. Note that the many disallowed values of $\overline{B^2}/\overline{S^2} > 1$ and $\rho < 0$ suggest a large value of D since many of these disallowed values at least lie within the confidence limits surrounding the tail end of the $\overline{B^2}/\overline{S^2}$ versus ρ curve, for which $D \to \infty$. It is unlikely, however, that the Born approximation could hold for a distance L of 3000 km, since it is strictly valid only for single, not multiple, scattering. Inability to solve for accurate values of D and L renders it impossible to solve accurately for the remaining parameter in the Chernov theory, the mean-square fluctuation in refractive index $\overline{\mu^2}$. It is possible, however, to calculate an approximate value of $\overline{\mu^2}$ by using the data set mentioned above, for which $D_{curve} = 43$. For this data set the mean-square amplitude and phase fluctuation are $\overline{B^2} = 0.0848$ and $\overline{S^2} = 0.140$. The value of $\overline{\mu^2}$ may be calculated by using either of these values and the formulas for $\overline{B^2}$ or $\overline{S^2}$ given in Table I. It is assumed that $D = 43$, $k = 0.0876$, $a = 21$ km, and $L = 380$ km. Substitution of the assumed values into the formulas for $\overline{B^2}$ yields an rms fluctuation of $\sqrt{\overline{\mu^2}} = 4.46\%$ and substitution into the formulas for $\overline{S^2}$ yields $\sqrt{\overline{\mu^2}} = 4.60\%$. Although these two values of the refractive index fluctuation are in good agreement, their derivation is hardly convincing, so they should be regarded only as rough estimates.

RAYLEIGH-WAVE SCATTERING OVER A LINEAR ARRAY IN THE SOUTHWESTERN UNITED STATES

Data

In January and February 1962 eleven LRSM stations, set up to monitor GNOME, an explosion in southern New Mexico, (Figure 1), were operative in the Southwestern United States. These eleven stations were selected to form an approximately linear array extending over a distance of almost 1100 km from northern Arizona to the Big Bend region of Texas. Analysis of the amplitude and phase fluctuations for events recorded by this array will provide insights into the effects of Rayleigh-wave scattering over long distances.

The two events chosen for this study were an earthquake near Nicaragua and one in the Kermadec Islands region (Table XIX). These events were selected so that incident waves would be both longitudinal and transverse to the separation between the stations in the array. It would of course have been helpful to have had a larger data base than two events, but during the period of operation of the array no other suitably large events occurred for which the array-to-epicenter azimuth was either nearly longitudinal or transverse. Although the ray path for waves from the Kermadec event crosses an oceanic-continental boundary and although the path for the Nicaragua event runs along the margin of the Pacific Ocean and through the Sierra Madre mountain range, results of a ray-tracing program (Sobel and von Seggern, 1978), shown in Figure 13 and 14, reveal no significant effects at the array due to systematic multipathing (i.e., non-random scattering).

Computational Methods

Spectra were calculated for both events with the method used for the NORSAR data: the logarithmic amplitudes were smoothed over the band of periods 18.3 to 21.3 sec, and the phase delays measured at the distinct period 19.7 sec. However, unlike the NORSAR study, where the same time window was analyzed for each instrument, the large dimensions of the array required choosing a time window for analysis that was different for each station, so at each station the maximum amplitude for 20-sec Rayleigh waves would arrive centered

---

Sobel, P. A. and D. H. von Seggern (1978). Applications of surface-wave ray tracing, Bull. Seism. Soc. Am., in press.

TABLE XIX

Events used in Southwestern US study and events used to determine station effects

Date	Time	Lat.	Long.	array-to-epicenter azimuth (degrees)	angle between azimuth and array (degrees)	Δ° (to center of array)	Geographic Region
30 Jan 62	08:34:26.8	12.7N	87.7W	134	11	27	Off W. Coast Nicaragua
1 Feb 62	00:39:54.6	31.7S	177.3W	233	70	92	Kermadec Is. Region
25 Jan 62	01:50:11.4	10.7S	161.8E	261	42	97	Solomon Islands
26 Jan 62	08:17:37.0	35.1N	22.7S	39	84	98	Mediterranean Sea
28 Jan 62	05:40:08.2	17.2S	172.0W	241	62	79	Tonga Islands
31 Jan 62	00:05:57.0	38.5N	70.3E	2	59	109	Tadzhik S. S. R.
3 Feb 62 (A)	00:37:53.6	1.2S	137.8E	283	20	111	North of New Guinea
3 Feb 62 (B)	11:36:19.2	17.4S	66.9E	160	37	164	Mascarene Is. Region
4 Feb 62	21:29:33.2	0.5S	20.2W	92	31	88	South Atlantic Ocean
8 Feb 62	11:49:13.9	3.2S	141.3E	279	24	110	New Guinea
10 Feb 62	19:31:56.2	17.9N	62.2W	99	24	43	Leeward Islands
11 Feb 62	18:55:32.0	4.5S	153.5E	271	32	100	New Ireland Region

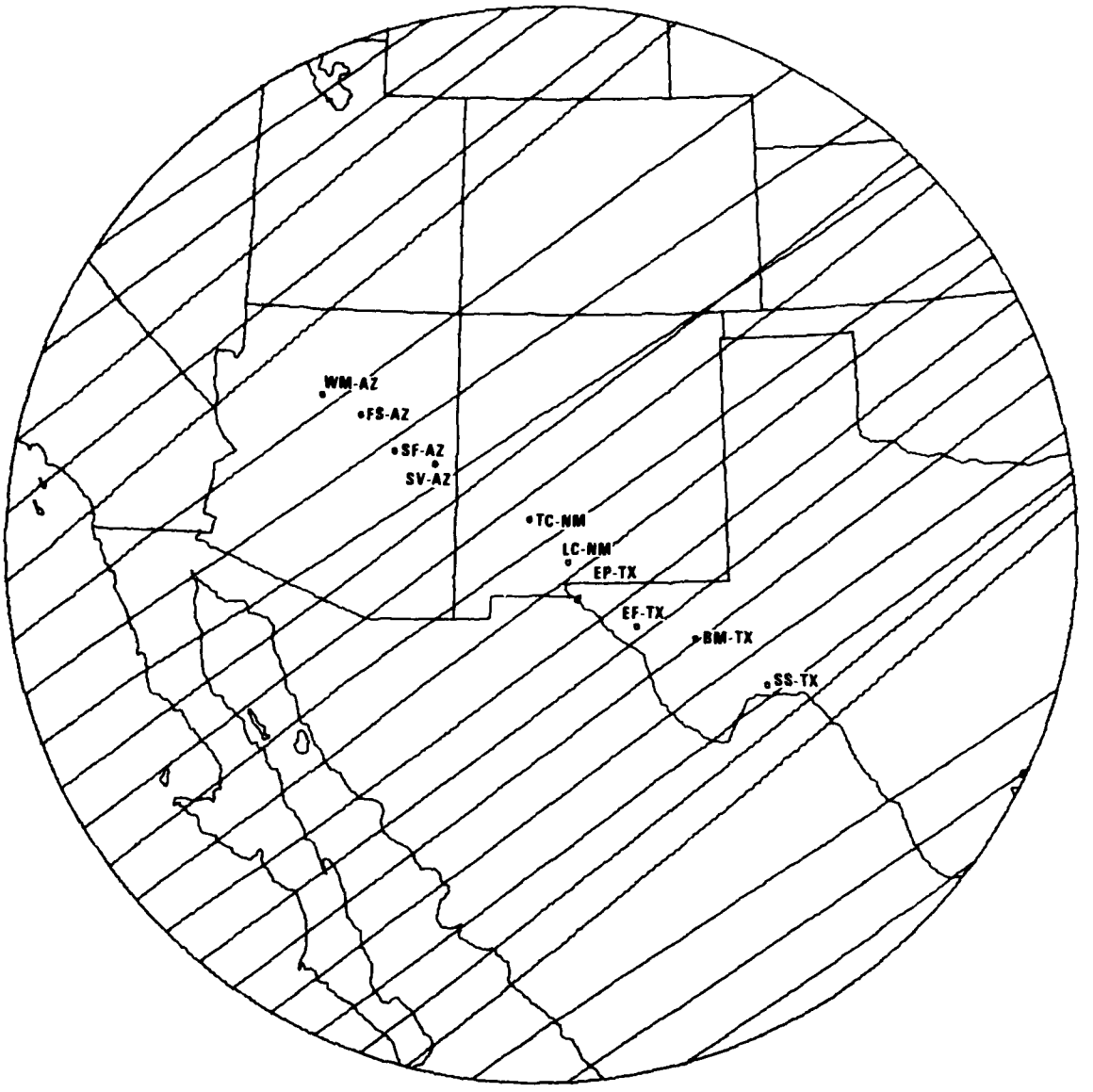

Figure 13. Raypaths for LR20 from the Kermadec earthquake to a linear array of LRSM sites in the Southwestern United States.

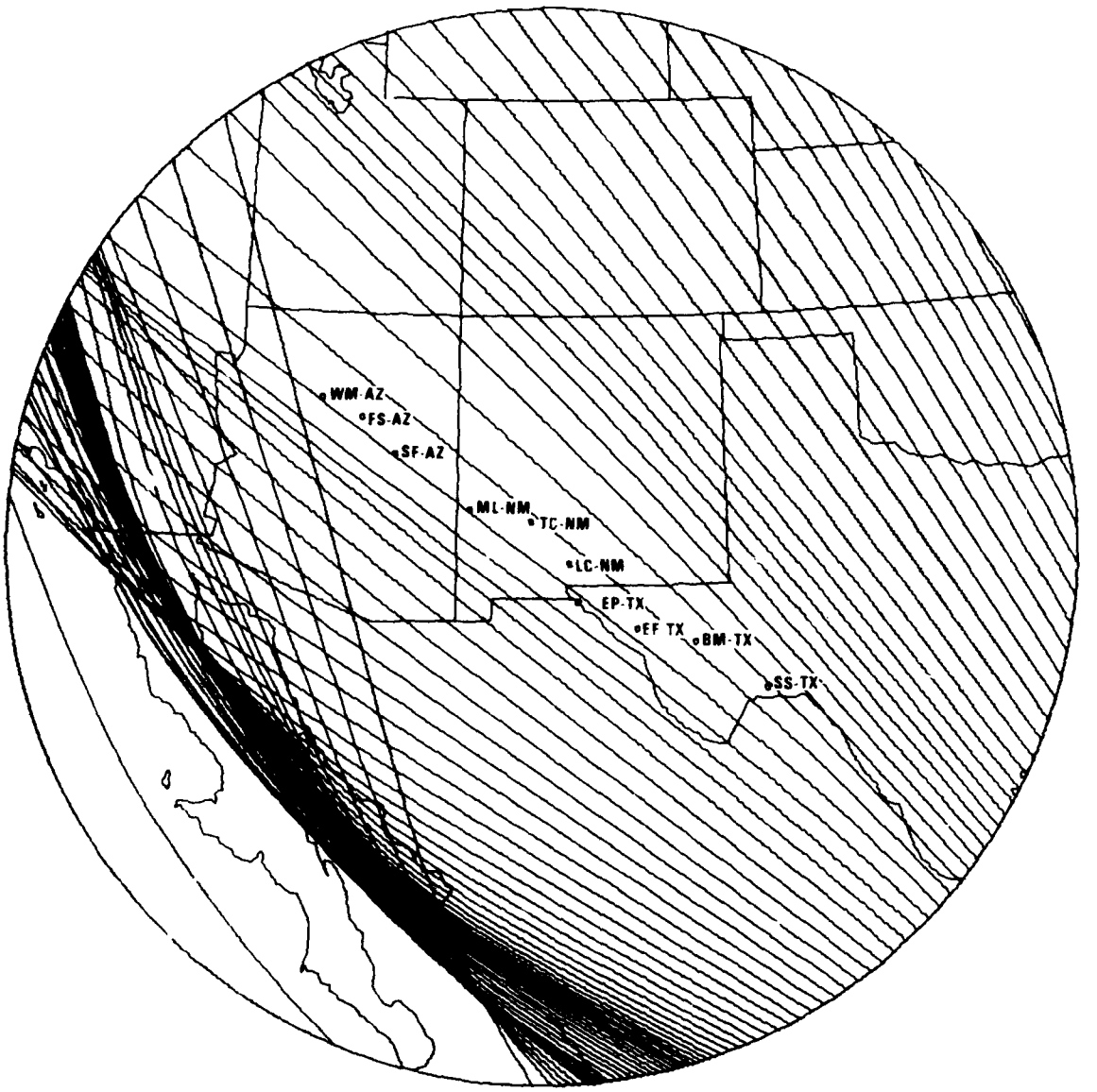

Figure 14. Raypaths for LR20 from the Nicaragua earthquake to a linear array of LRSM sites in the Southwestern United States.

TABLE XX

Spectral amplitudes and phases measured by Southwestern U.S. array

Amplitudes smoothed over 0.0469 - 0.0547 Hz band.

Kermadec Eq. (256 seconds of signal)

Station	Δ°	Sep. along array (km)	Spectral ampl. (mμ)	ℓn ampl.	Fluctuation	Phase (deg)	Corrected	Fluctuation
SSTX	94.12	0	125.5	4.832	0.163	54	-306	78
BMTX	93.56	167	255.6	5.544	0.875	121	-239	55
EFTX	92.82	260	141.7	4.954	0.285	161	-199	73
EPTX	92.68	375	34.3	3.535	-1.135	47	47	-163
LCNM	92.70	452	71.5	4.270	-0.400	-54	-54	-63
TCNM	92.42	570	178.5	5.185	0.516	-68	-68	-27
SVAZ	91.90	753	63.4	4.149	-0.521	34	34	-89
SFAZ	91.18	853	114.0	4.736	0.067	-95	-95	96
FSAZ	91.06	954	102.1	4.626	-0.044	77	77	-67
WMAZ	90.71	1037	129.5	4.864	0.195	-69	-69	107

Nicaragua Eq. (512 seconds of signal)

Station	Δ°	Sep. along array (km)	Spectral ampl. (mμ)	ℓn ampl.	Fluctuation	Phase (deg)	Corrected	Fluctuation
SSTX	21.99	0	132.3	4.885	-0.065	-20	340	-20
BMTX	23.54	175	161.7	5.086	0.137	-171	189	-15
EFTX	24.48	280	146.4	4.986	0.037	78	78	7
EPTX	25.52	395	97.9	4.584	-0.366	13	13	-26
LCNM	26.23	474	44.9	3.804	-1.146	-129	-129	49
TCNM	27.29	593	135.9	4.912	-0.038	-162	-162	-19
MLNM	28.29	703	171.4	5.144	0.195	28	-332	57
SFAZ	30.01	894	357.1	5.878	0.929	-103	-463	25
FSAZ	30.92	995	195.3	5.275	0.326	-170	-530	6
WMAZ	31.71	1083	139.9	4.941	-0.009	-174	-534	-64

within the chosen window. After visually inspecting the seismograms, we decided to select a time window that propagated, along with the wave train, across the array at a velocity of 3.87 km/sec. If the true phase velocity had been equal to this value, the phase delays calculated by the spectral analysis would have been random (as it was, the phase delays exhibited a slight linear trend). The phase fluctuations were assumed equal to the difference between the value corresponding to this linear trend, as determined by a least-squares fit, and the observed spectral phases. The slope of the trend removed was then used to calculate a correction to the assumed value of the phase velocity.

Results

The amplitude and phase fluctuations for the two events are shown in Table XX. The column headed "corrected" contains spectral phases with multiples of 360 degrees added or subtracted, as necessary, to minimize phase fluctuations while at the same time yielding a physically realistic value of the phase velocity. Note that other choices of the "corrected" phase would have resulted in different values of C, $\overline{B^2}/\overline{S^2}$, and ρ. While for the Kermadec earthquake certain of these other choices cannot be completely ruled out, for the Nicaragua earthquake the choice shown in Table XX appears valid.

For the Kermadec earthquake, the phase velocity C = 3.37 km/sec, the mean-square amplitude and phase fluctuations are $\overline{B^2} = 0.323$ and $\overline{S^2} = 2.666$, and the correlation between amplitude and phase fluctuations is $\rho = 0.740$. For the Nicaragua earthquake, C = 3.29 km/sec, $\overline{B^2} = 0.275$, $\overline{S^2} = 0.410$, and $\rho = 0.056$. For fluctuations this large, particularly the case of $\overline{S^2}$ for the Kermadec earthquake, Chernov's assumption of small perturbations is clearly violated. The ratio $\overline{B^2}/\overline{S^2} < 1$ for both events, but for the Kermadec earthquake $\rho > 0.5$ and for the Nicaragua earthquake $\rho<0$, so the wave parameter D is undefined in both cases. However, again note that the error bars are quite large for values of $\overline{B^2}/\overline{S^2}$ and ρ determined from only ten observations. (On the day of each event only ten of the eleven stations were operative.)

For the spatial autocorrelation of amplitude fluctuation R_b, note that each event has $\binom{10}{2} = 45$ different pairs of receivers and that the longitudinal or transverse separation represented by each pair is an erratically

distributed function because the instruments were not spaced evenly along the array. Therefore, calculating results by dividing the separations into segments, like for the NORSAR study, will fail because too few pairs of receivers exist whose separation falls within a given segment and because a given segment would need to encompass too great a range of separations. One ad hoc solution to this dilemma was a procedure where the data were smoothed before computing the correlation. An expanded "data set" was formed by interpolating the values of the logarithmic amplitudes at 10 km increments along the length of the array. The spatial correlation coefficient R_b was then calculated for the even spacing of receiver separations this expanded data set represented. The validity of this interpolation process can be questioned, however, because in practice the amplitudes that would have been observed at the evenly-spaced points would not equal the interpolated values. Justification for this procedure, admittedly questionable, is based upon the NORSAR study which showed that the rms amplitude fluctuation over the separation of 100 km is typically 0.25 natural log unit while the amplitude fluctuations for the linear array are more than twice as great. Thus, the fluctuations about the values interpolated between consecutive stations typically 100 km apart are small when compared to the fluctuations measured between stations in the array that are several hundred km apart. Note that when examining the results of this procedure the linear interpolation imposes a priori the constraint of strong correlation over small separations. Therefore, values found for separations of less than about 100 km, which represents the true resolution of the linear array, are rather tenuous.

Figures 15 and 16 illustrate the amplitudes measured at the different stations for the two events. The value of R_b, determined for the interpolated (dashed) curves, is shown in Figures 17 and 18. Again, assuming that the correlation distance a of the scattering medium is roughly equal to the distance where $R_b(\ell)$ falls to zero, this value is estimated to be about 125 km. These figures also show that the correlation extends in the longitudinal direction about 1.8 times farther than in the transverse direction. The effect of attenuation, previously ignored, can be accounted for by adding a correction factor of 1.66 log Δ to the logarithmic amplitudes, where Δ is the epicenter-to-station distance in degrees (Figure 19). This term is nearly the same for all

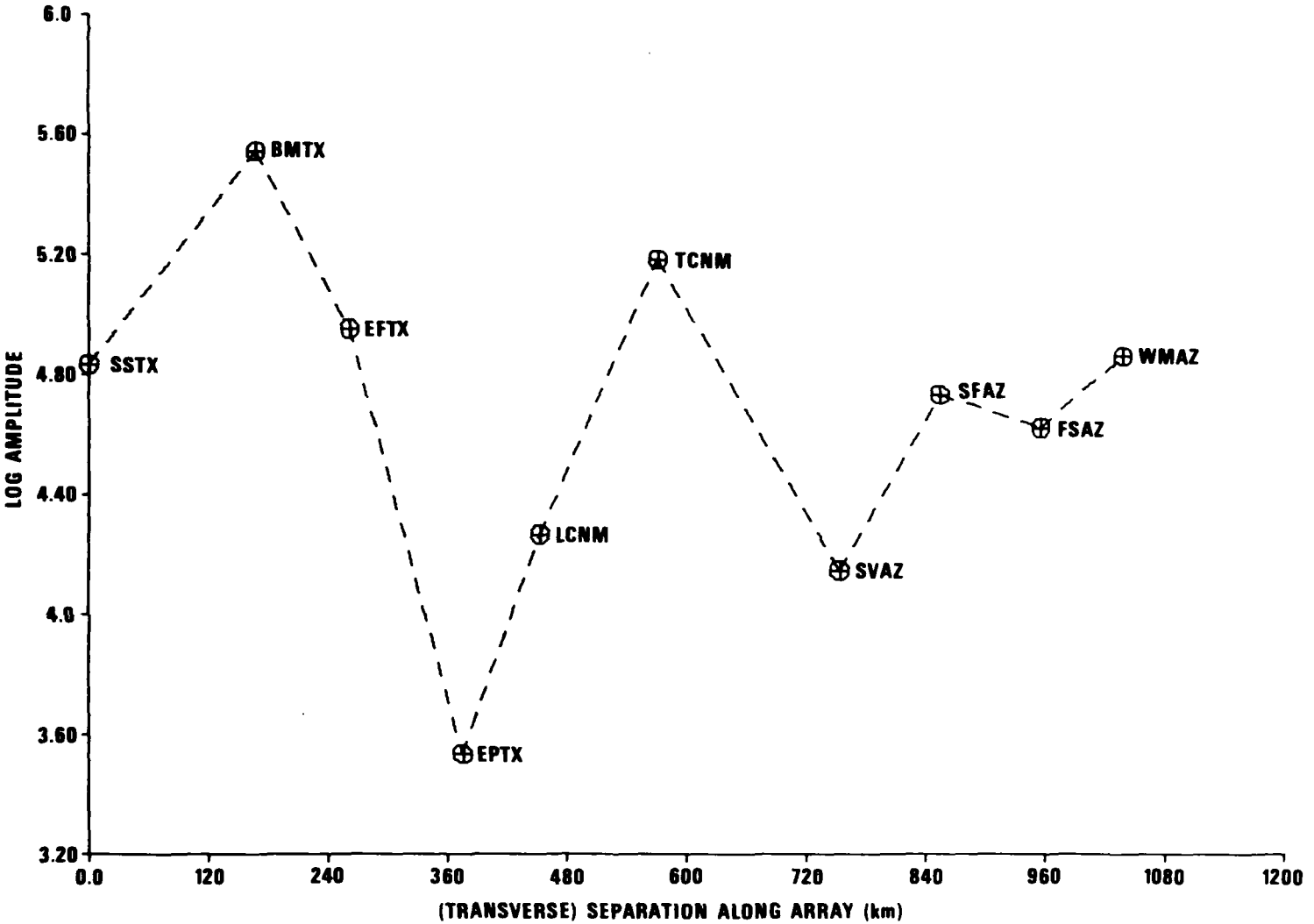

Figure 15. Logarithmic ampltudes for LR20, not corrected for attenuation or station effects, for the Kermadec earthquake.

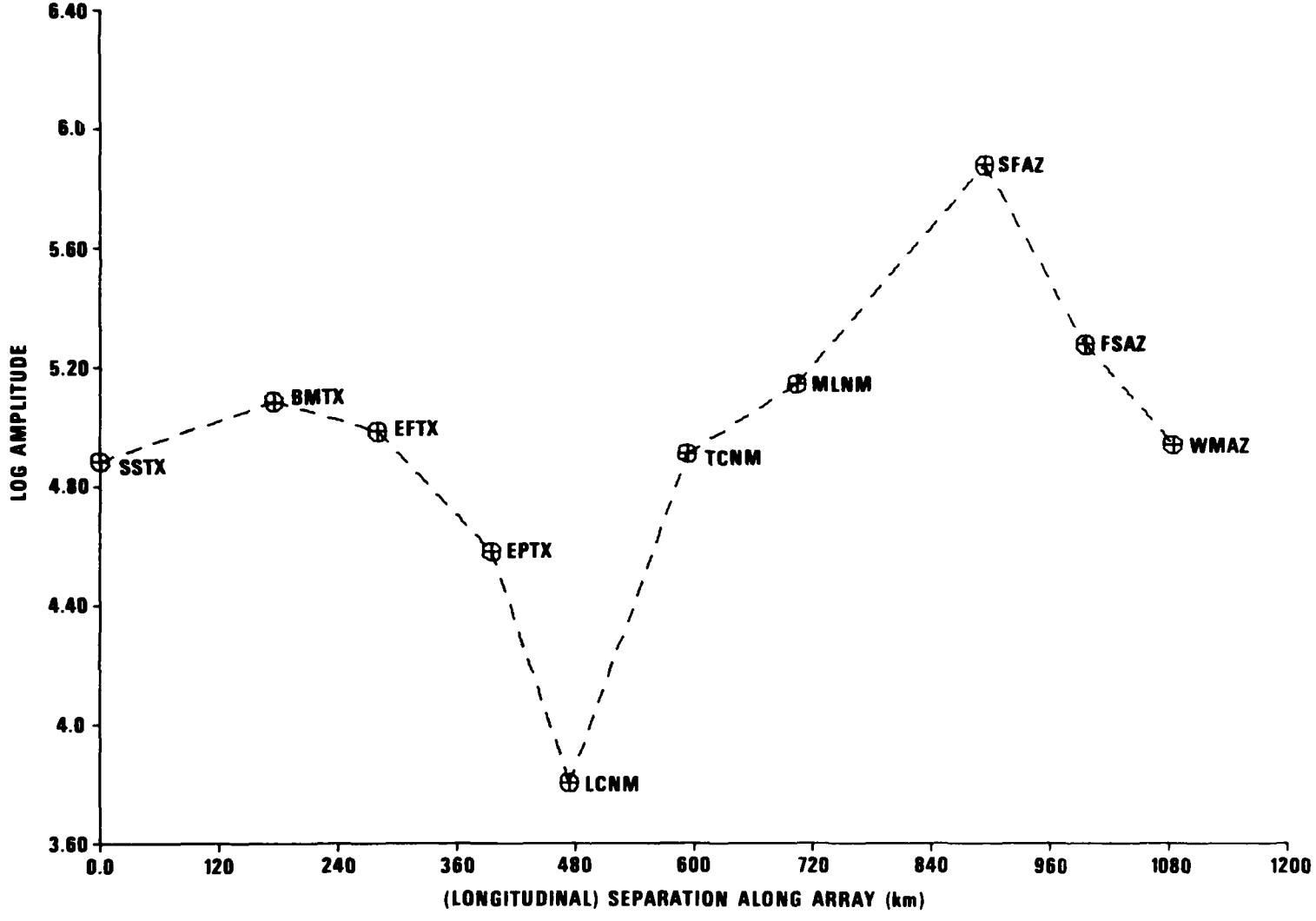

Figure 16. Logarithmic amplitudes for LR20, not corrected for attenuation or station effects, for the Nicaragua earthquake.

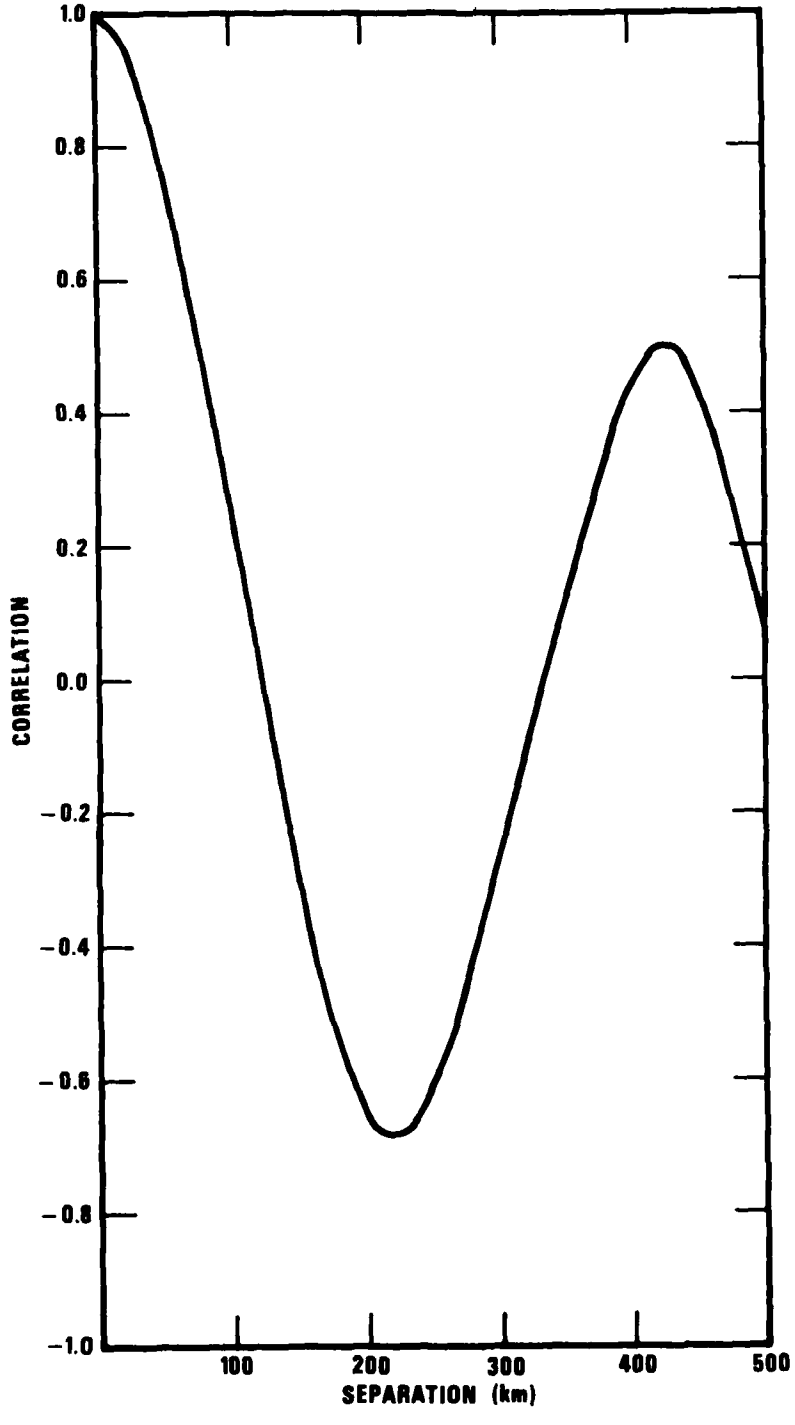

Figure 17. Spatial correlation of dashed curve in Figure 15.

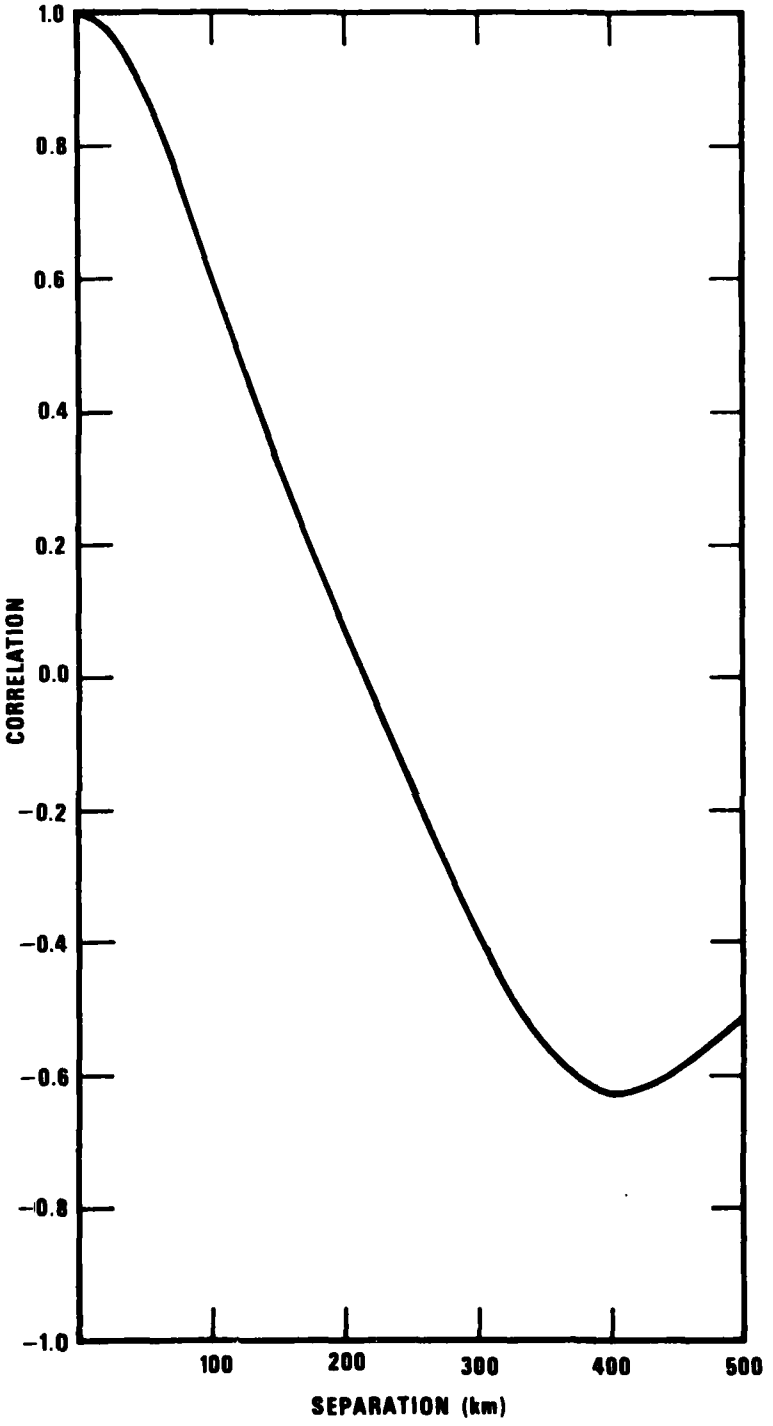

Figure 18. Spatial correlation of dashed curve in Figure 16.

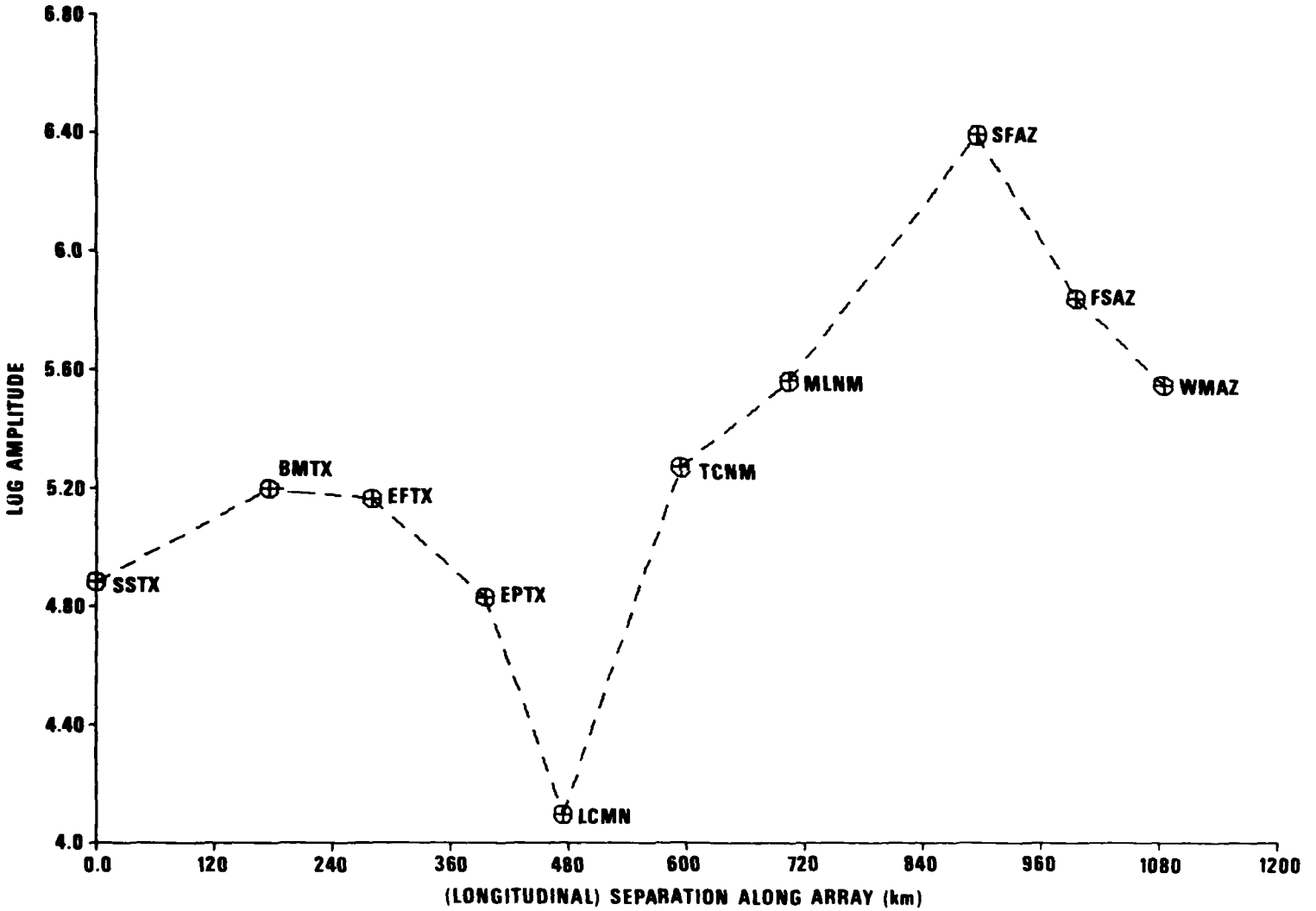

Figure 19. Logarithmic amplitudes for LR20, corrected for attentuation but not for station effects, for the Nicaragua earthquake.

stations for the Kermadec earthquake, so only its effect upon the Nicaragua earthquake data will be considered. Figure 20 shows that this correction extends the correlation in the longitudinal direction to separations of about 265 km.

Possible amplitude biases at the eleven stations in the array were calculated by measuring visual magnitudes at each of the stations for a suite of ten events (Table XIX). These events were selected for their azimuth distribution, so the effects from longitudinal or transverse orientation would not be subtracted out of the data as station effects. The residuals found for each station from these ten events (Table XXI) were removed from the logarithmic amplitudes for both the Kermadec and Nicaragua events, and R_b was calculated again (shown in Figures 21-24). This correction effectively decreased the correlation distance for the Nicaragua event and increased it for the Kermadec event. When both the attenuation and station-effect corrections are entered, as in Figures 25 and 26, the correlation extends about twice as far in the longitudinal direction as in the transverse direction.

The magnitude of the phase fluctuations made calculating R_s impossible. Since many of the spectral phases for the Kermadec earthquake could not be determined uniquely to within 360 degrees, the reliability of the phase data is highly suspect in many cases.

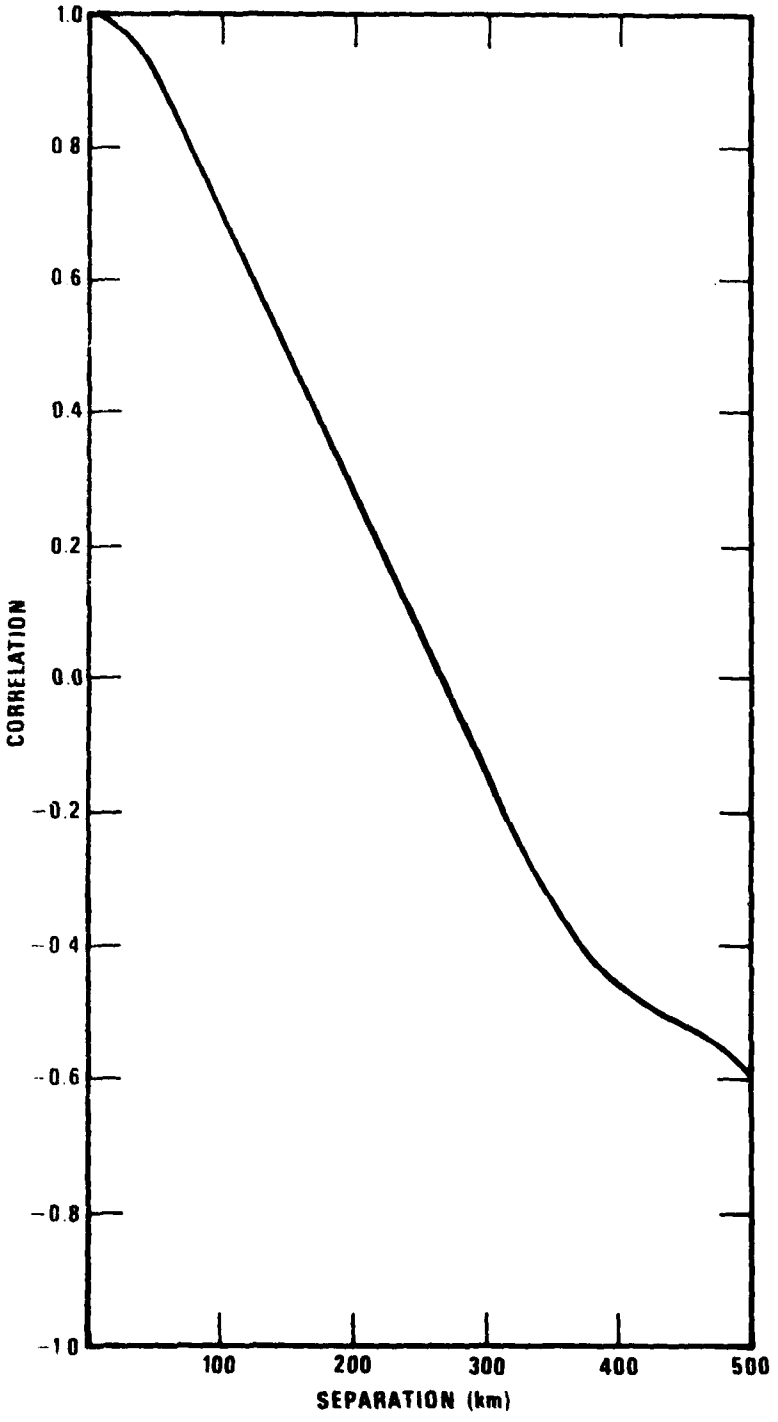

Figure 20. Spatial correlation of dashed curve in Figure 19.

TABLE XXI

Determination of station effects for Southwestern US array

Magnitude residuals $\bar{M} - M_i$

Event / Station	(Date) 1/25	1/26	1/28	1/31	2/3(A)	2/3(B)	2/4	2/8	2/10	2/11	Station effect (to be subtracted from observed mag.)
SSTX		.099	.198	.164	.175	.162	.073	.198	.276	-.075	-0.147
BMTX	-.077	-.081	-.067	-.324	-.195	-.287	-.054	.044	-.156	-.280	0.144
EFTX	-.015	.015	.140	.276	.010	.193	.107	.171	.040	.011	-0.098
EPTX	-.010	-.014	-.062	.293				.108	.006	.216	-0.082
LCNM		-.145	.020	.048	.064	.062	-.044	.552	.035	.092	-0.082
TCNM	.061	-.110	-.278		-.122	-.053	-.045			-.013	0.080
MLNM	.238	.200	.061	-.285	.014	-.072		.013	-.224	-.069	0.010
SVAZ								-.052	-.104		0.070
SFAZ	.043	-.194	-.116	.011	-.219	-.002	-.111	-.241	.030	-.106	0.087
FSAZ	-.242	.136	.120	-.343	.174	.117	.098	-.227	.101	.145	-0.011
WMAZ		.089	-.016	.156	.101	-.117	-.023	-.570	-.005	.076	0.029

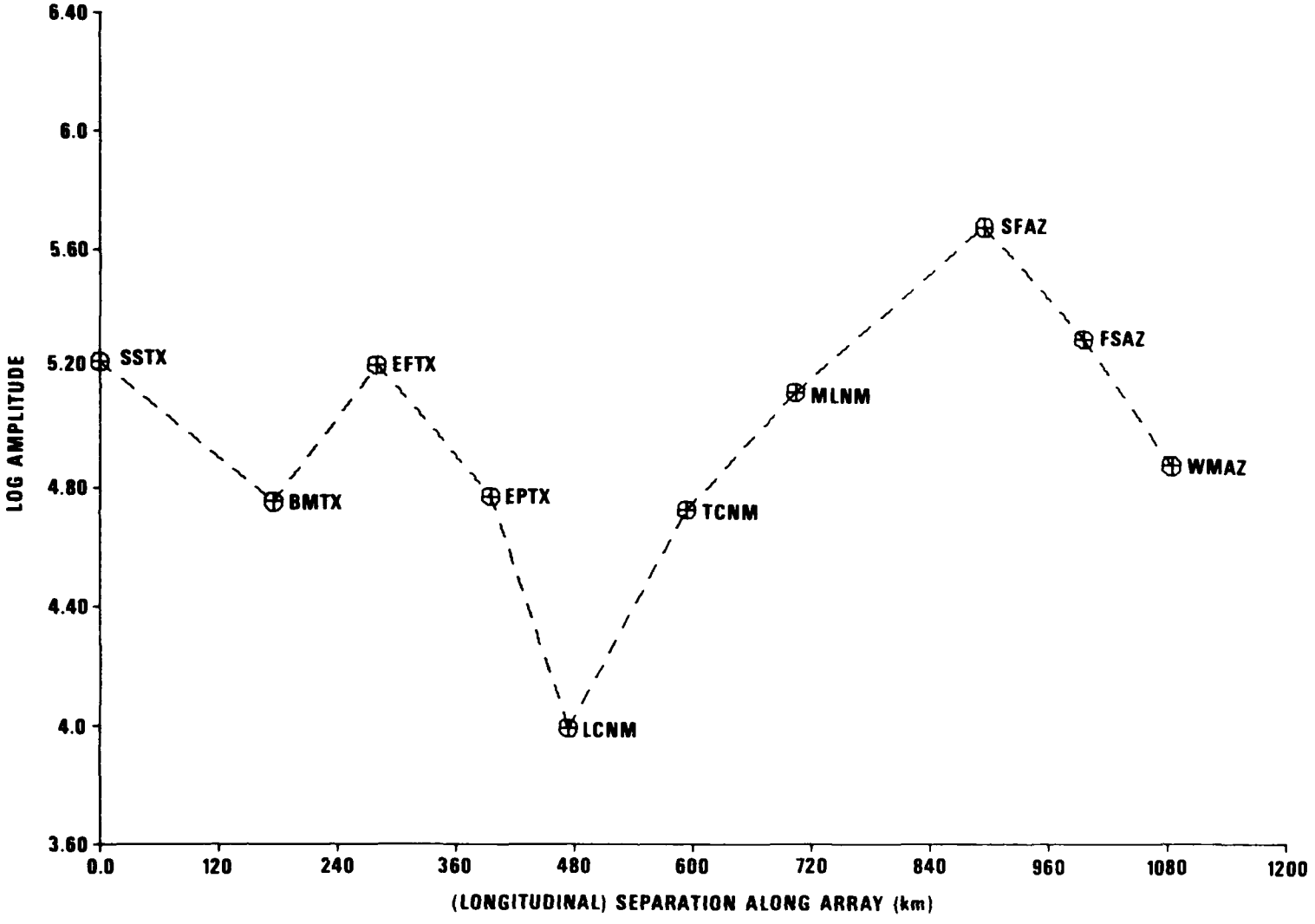

Figure 21. Logarithmic amplitudes for LR20, corrected for station effects but not for attenuation, for the Kermadec earthquake.

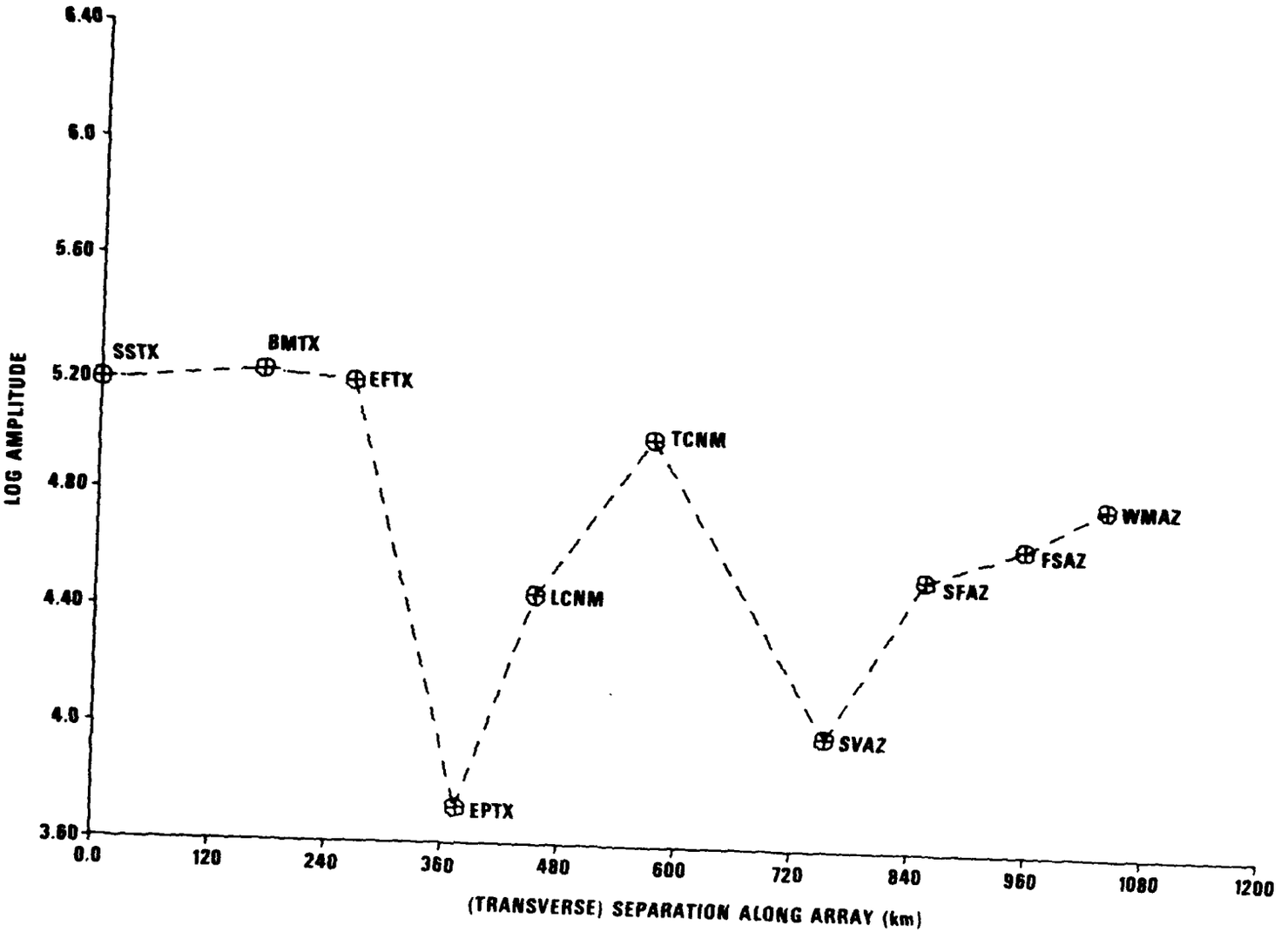

Figure 22. Logarithmic amplitudes for LR20, corrected for station effects but not for attenuation, for the Nicaragua earthquake.

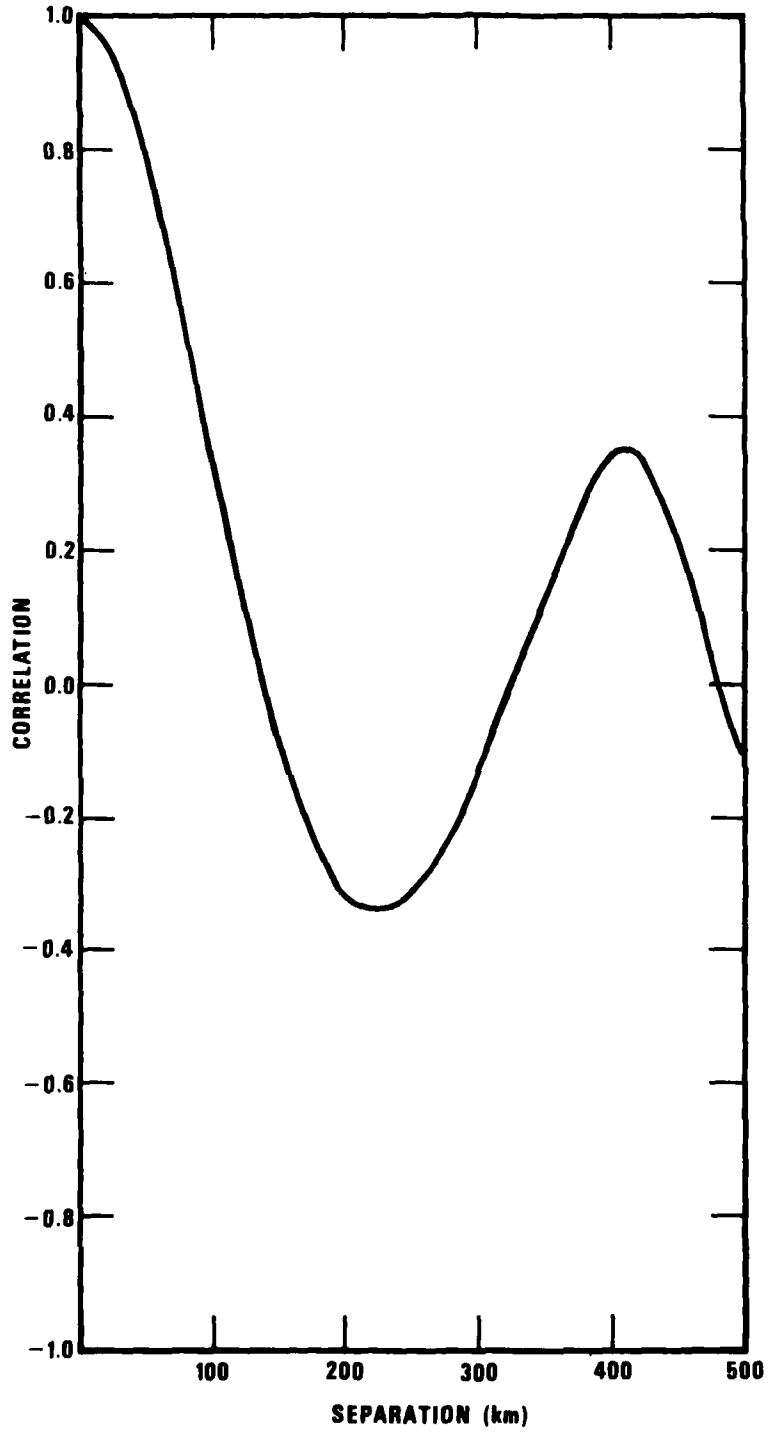

Figure 23. Spatial correlation of dashed curve in Figure 21.

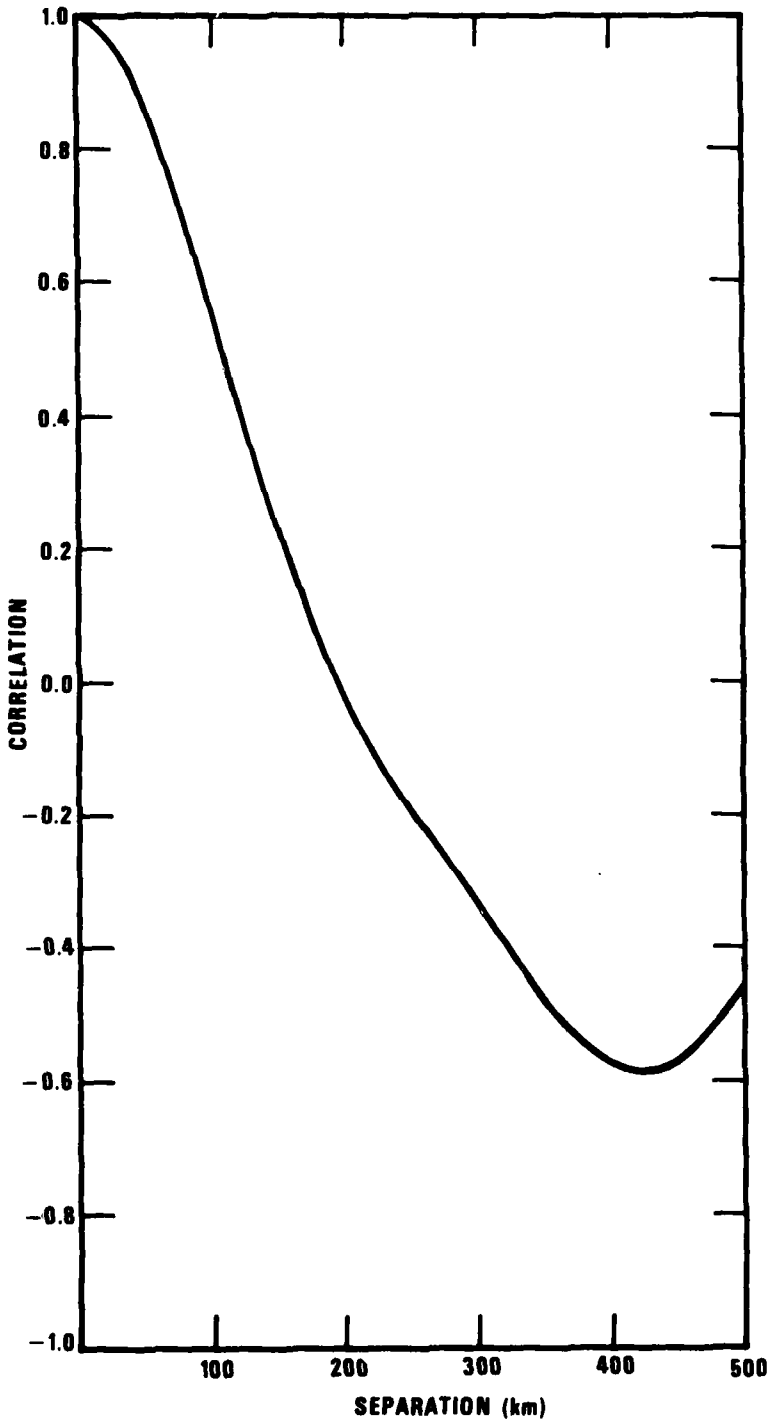

Figure 24. Spatial correlation of dashed curve in Figure 22.

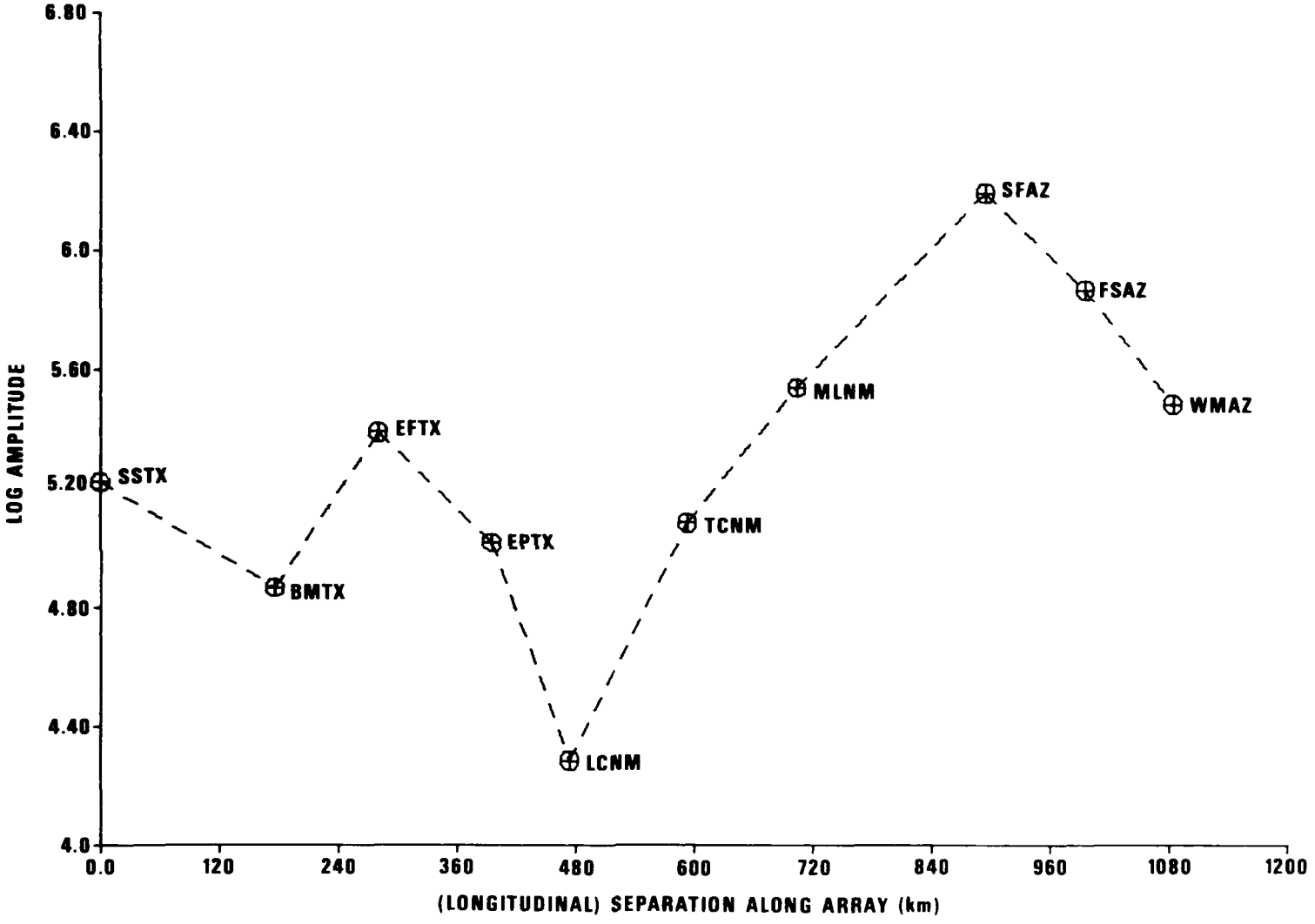

Figure 25. Logarithmic amplitudes for LR20, corrected for attenuation and for station effects, for the Nicaragua earthquake.

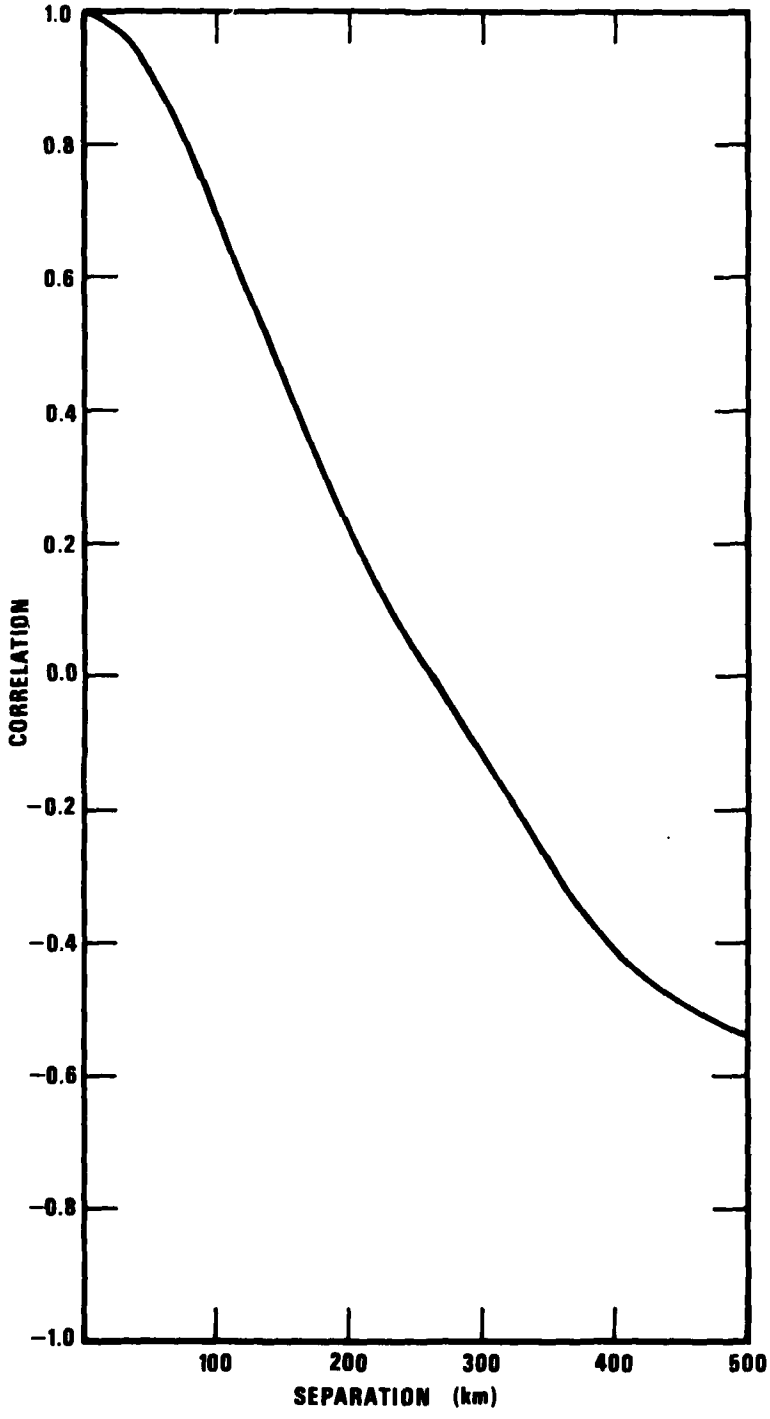

Figure 26. Spatial correlation of dashed curve in Figure 25.

IMPLICATIONS OF WAVE SCATTERING IN THE USE OF RAYLEIGH WAVES TO DETERMINE SEISMIC SOURCE PARAMETERS AND EARTH PROPERTIES

Magnitude Estimates from Long-Period Rayleigh Waves

Event Magnitude (M_s) from Rayleigh waves is commonly computed on the basis of amplitude measurements at periods near 20 sec. Previously, this report has dealt with amplitude only in the spectral domain, but we will now show that the spectral amplitude scatter is indicative of the time-domain scatter. For the events studied earlier at NORSAR (Table II), maximum seismogram amplitudes for periods near 20 sec were measured and reduced by the system response at the exact measured period. Because the propagation distance over NORSAR is small, no correction is required for differences in epicentral distance for the 22 individual sensors, and the variance of M_s over the sensors can be computed directly; the results are listed in Table XXII for the 10 events. The average standard deviation of M_s is roughly .09. For comparison, the results using average spectral amplitudes over a narrow (.0488 - .0508 Hz) and wide (.0315 - .0908) band are also listed; the narrow and wide bands comprise 2 and 11 points, respectively, in the 257-point spectra (512 seconds sampled at 1 s/sec). Narrow band (.0468 -.0547 Hz) estimates were used in previous sections of this report. Table XXII indicates that the scatter in spectral amplitude measurements is nearly the same as the seismogram measurements and also indicates that a wider bandwidth estimate will reduce the amplitude variance over NORSAR. Using the results given in Table III for average sensor bias at NORSAR, a standard deviation of .04 M_s units results from only the purely local effects of the sensors, neglecting actual wave scattering. The sensor biases are based on only 10 events and would probably be less with a larger sample. In fact, on physical grounds, NORSAR sensor effects are expected to be negligible for 20-sec waves where the wavelength is almost as long as the entire array aperture. Therefore, the "mean" σ values in Table XXII should be reduced only slightly, if at all, to give the true Rayleigh-wave scattering effects over NORSAR.

Chang and von Seggern (1977) studied m_b scatter across LASA, which has 13 subarrays and an aperture of roughly 55 km. They reported a mean σ for m_b of .15 based on a large event sample. Local effects at the subarrays, they

TABLE XXII

Surface-wave magnitude scatter over arrays of sensors

NORSAR Results

Event No.	σ(analyst M_S)	σ\{log[A(.05 Hz)]\}	σ\{log[A(.03-.05 Hz)]\}
200	.085	.039	.042
300	.092	.107	.087
400	.073	.097	.060
500	.093	.102	.054
600	.062	.134	.084
700	.173	.128	.064
800	.071	.062	.051
900	.089	.120	.070
1000	.152	.245	.106
1100	.104	.198	.134
mean σ	.089	.123	.075

Southwestern U.S. Array Results

Nicaragua EQ	.19	.31	.15
Kermadec EQ	.17	.27	.14

stated, accounted for only a small fraction of this fluctuation. Because the NORSAR array spans over 100 km, a better comparison with m_b scatter can be made if only amplitudes from a reduced NORSAR are considered. An array formed by the inner seven sensors would have an aperture of roughly 50 km, nearly equivalent to LASA. When standard deviations of spectral amplitudes over these seven sensors were computed for each of the ten events, they equalled roughly one-half the values for the full NORSAR array, in the range .04 - .05. When compared to .15 m_b scatter over LASA, a threefold decrease in magnitude scatter apparently results for M_s compared to that for m_b over an equivalent array aperture. Using the seismic reciprocity theorem, Chang and von Seggern argued that the observed level of receiver fluctuation for m_b might also apply to expected fluctuations at one distant receiver from equivalent sources spread over an area with dimensions and physical properties similar to LASA's. In this study the identical argument is made for M_s scatter, with the inference that M_s is a more stable measure of source strength as the source location is varied. Therefore, calibration of a source area will hold to larger inter-source distances for M_s than for m_b. Furthermore, results already stated in this report clearly show that this calibration will hold to significantly larger inter-source distances measured along the great-circle path to the receiver than transverse to it.

Seismograms for the events recorded in the Southwestern United States, studied earlier in this report in the spectral domain, provide additonal insight into M_s scatter. Computations identical to those for the NORSAR events in Table XXII are shown for these two events at the bottom of the same table. The result revealed that 1) the M_s scatter over the Southwestern U. S. array is roughly twice that of the NORSAR array; 2) the wide-band spectral measure of M_s is more stable than either analyst M_s or a narrow-band spectral estimate near f = .05 Hz; 3) the gross signal fluctuation, measured in either the time or frequency domain, is nearly the same for sensors aligned along the great-circle path as for sensors perpendicular to it. Also in this report we stated that for the Southwestern U. S. array the signal correlation was definitely higher over a longer space dimension for the Nicaragua earthquake than for the Kermadec earthquake. However, because the dimension of the array (~ 1100 km) is large compared to the correlation length, the overall

level of the observed amplitude fluctuations does not differ with the angle of approach.

Attenuation Estimates from Long-Period Rayleigh Waves

By expressing the observed Rayleigh-wave spectrum as:

$$A(f) = S(f) \cdot G(\Delta) \cdot e^{-\alpha(f)r}$$

where S is the source spectrum, G is the geometrical spreading factor, and r is the distance, it is possible to take the ratio of the spectra at two stations on a great-circle path as

$$\frac{A_1(f)}{A_2(f)} = \frac{G(\Delta_1)}{G(\Delta_2)} \cdot e^{-\alpha(f) \cdot (r_1 - r_2)}$$

By absorbing the known G factors into the amplitude, we find for the attenuation coefficient

$$\alpha(f) = [\log A_1(f) - \log A_2(f)]/(r_2 - r_2)$$

For 20 sec Rayleigh waves, a typical α is .0003 km^{-1} (Mitchell et al., 1976). For this value as .0002 and .0004, Figure 27 shows the term $\log A_1(f) - \log A_2(f)$ versus $r_2 - r_1$. Following the authors' observations, the measured difference of $\log A_1(f) - \log A_2(f)$ can have several tenths error due to random scattering effects. Therefore, apparently at a station separation of even 5000 km, a true α of .0003 km^{-1} could be estimated at anywhere from .0002 to .0004. This range is actually wider than necessary because it is based mer y on scattering data for one frequency while attenuation measurements are usually spread over a fairly wide bandwidth and smoothed in some manner.

Phase-Velocity Estimates from Long-Period Rayleigh Waves

Data in Tables X and XI indicate that a typical standard deviation of the measured phase over the 22 NORSAR sensors is .03 circles (12°) for Rayleigh waves at .05 Hz. For the two station method of determining phase velocity, the equation

$$C = f(r_2 - r_1)/(\Phi_2 - \Phi_1 \pm n)$$

Mitchell, B. J., L. W. B. Leite, Y. K. Yu, and R. B. Herrmann (1976). Attenuation of Love and Rayleigh waves across the Pacific at periods between 15 and 110 seconds, Bull. Seism. Soc. Am., 66, 1189-1202.

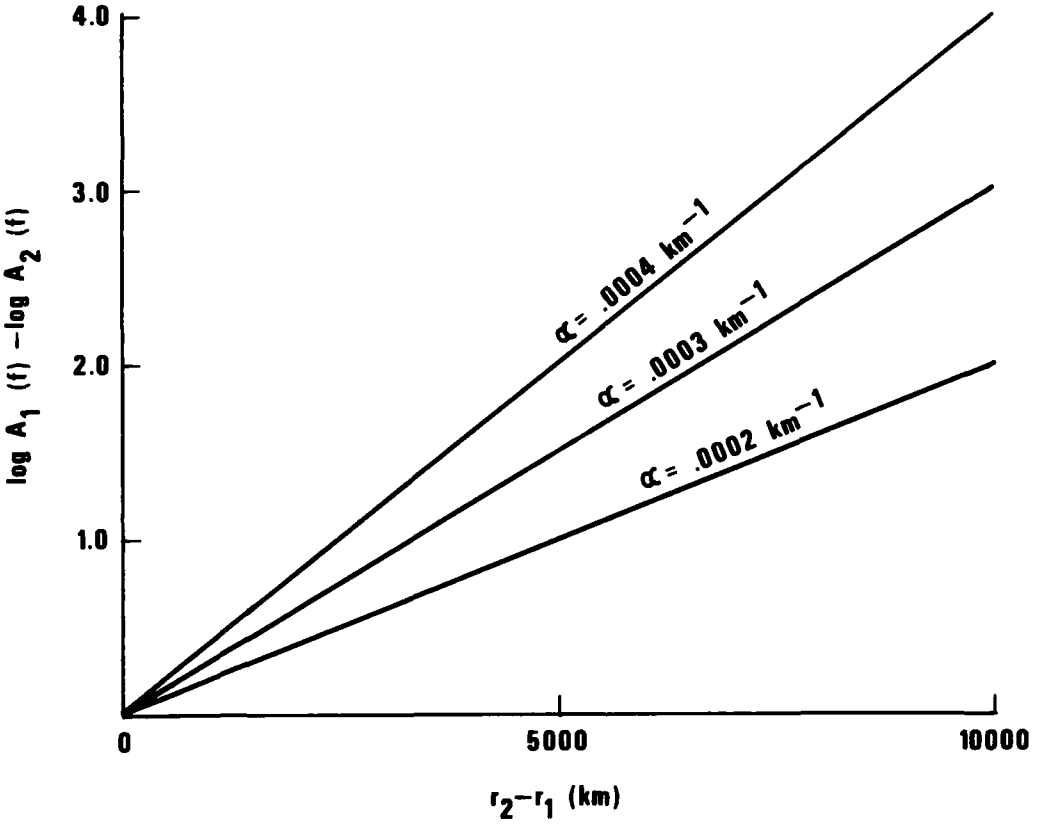

Figure 27. Predicted spectral amplitude difference at .05 Hz versus station separation for various values of α, the attenuation coefficient for surface waves.

is used where C is phase velocity in km/sec, f is frequency, ϕ is the measured phase in circles, and n is the proper integer to be adjusted to make C physically acceptable. For small errors $\Delta\phi$ in $\phi_2 - \phi_1$ due to scattering

$$C + \Delta C = f\ (r_2 - r_1)/(\phi_2 - \phi_1 + \Delta\phi_1 \pm n)$$

Using C = 4.0 and f = .05 Hz (oceanic structure), the difference ΔC is $\pm$ .04 km/sec for $\Delta\phi = \pm$ .03 circles at $r_2 - r_1 \simeq 200$ km and decreases as $r_2 - r_1$ increases, assuming that $\Delta\phi$ remains bounded for receiver separations much greater than the correlation distance. Thus, to yield a general accuracy of $\pm$ 1% to phase-velocity measurements with fair confidence, a two-station separation of only few hundred km would be sufficient if random scattering effects, like those discussed here, were the only factors in measurement error.

Source Mechanism from Surface Waves

The inversion of surface-wave spectra for obtaining the source mechanism of of earthquakes has been widely reported as a successful method. Recently, estimates of the number of spectra necessary for resolving the source mechanism have decreased; in fact, Turnbull (1976) suggested that as few as two stations would be adequate if placed favorably in relation to the source radiation pattern. However, several propagation effects seem to argue against Turnbull's view, especially laterally varying attenuation properties and large-scale refraction and multipathing. In this report, the data showed that only small-scale scattering affects the signals recorded across the Southwestern U.S. array, but that the effect was still considerable on amplitudes. As a guide to the spectral variation expected for recordings of an earthquake solely because of this effect, the LR spectra for the Kermadec and Nicaragua events are shown in Figure 28 and 29 respectively. Note the acute fluctuations for various frequencies, some of which might be interpreted as spectral "holes" related to source depth. Although the corresponding Love-wave specta were not processed here, the authors presume they display similar behavior. In view of the variations seen for these two suites of recordings, accepting that LQ and LR for as few as two stations can reliably constrain the earthquake source mechanism is difficult.

Turnbull, L.S. (1976). Determination of seismic source parameters using far-field surface wave spectra, Ph.D. Thesis, Pennsylvania State University University Park, Pennsylvania.

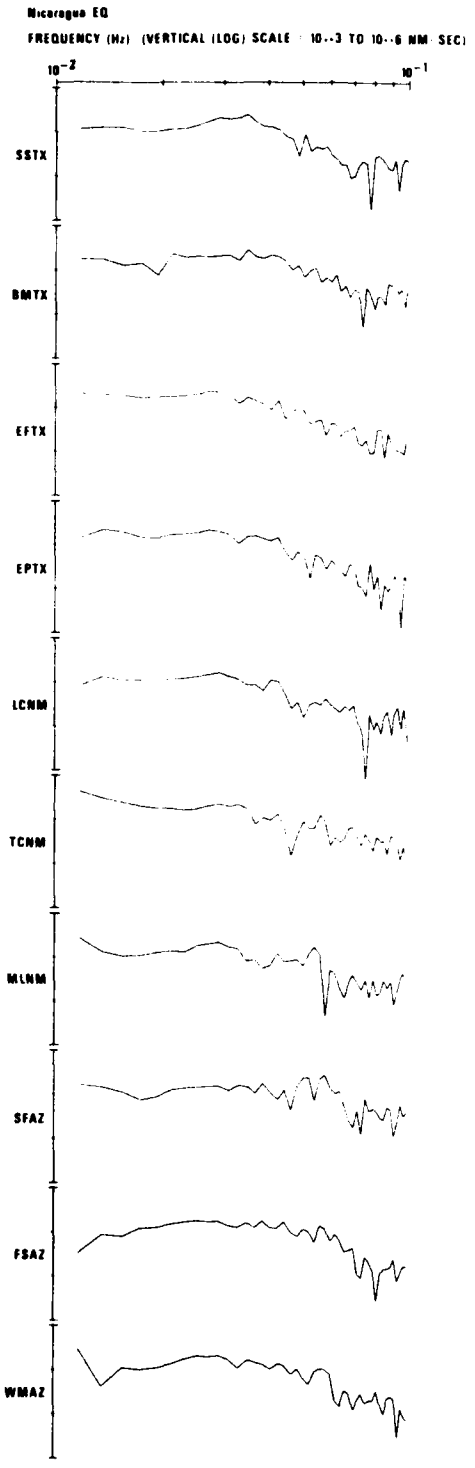

Figure 28. Spectra of the Nicaragua earthquake LR recordings at a linear array of LRSM sites in the Southwestern United States.

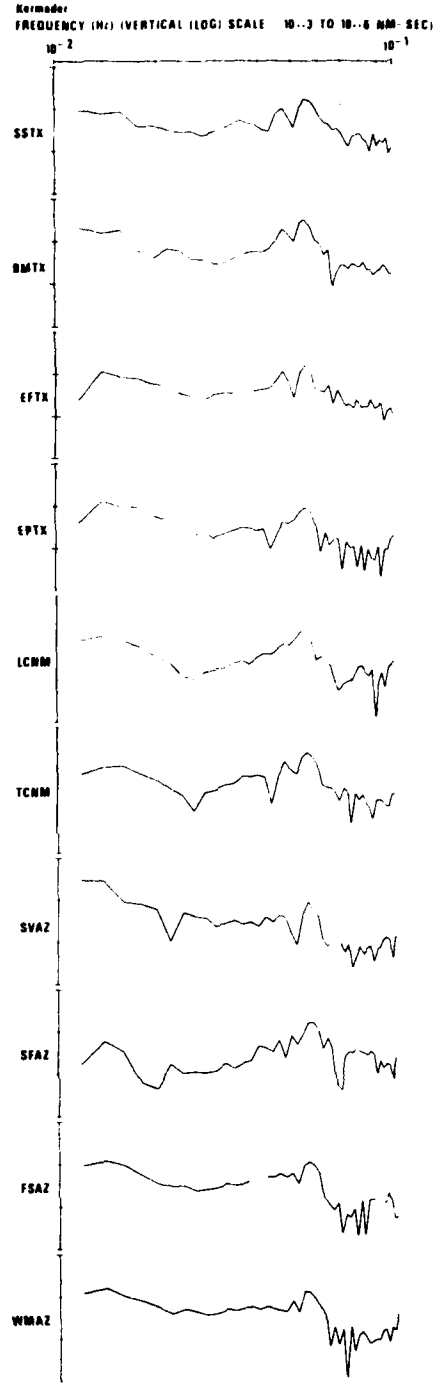

Figure 29. Spectra of the Kermadec earthquake LR recordings at a linear array of LRSM sites in the Southwestern United States.

CONCLUSIONS

Both amplitude and phase fluctuations of 20-sec Rayleigh waves were found to correlate over a longer distance in the direction of wave propagation than perpendicular to it. In addition, the report revealed that amplitude and phase fluctuations were correlated positively, in most cases. While this fact might support the hypothesis of random scattering of the Rayleigh waves according to a modified Chernov theory, the hypothesis of multipath arrivals cannot be rejected. Data available for this study was insufficient to infer the exact nature of the wavefield. In the case of the NORSAR investigation, the array aperture of 100 km was too small to define the correlation functions accurately to a large enough spatial dimension. In the case of the Southwestern United States linear array, the spacing (about 100 km) was too large to construct confidently the spatial correlation function and the entire aperture of 1000 km was so extended that large-scale multipathing, although not predicted by the ray-tracing program, might have affected the observations. From studies of recordings at the Southwestern U.S. array, indications are that the correlation length of the inhomogeneities causing the random scattering, assuming it exists, is the order of 100 km or more. The smaller-scale scattering observed at NORSAR is characterized by a correlation length of about 25 km.

The standard deviation of .05 Hz spectral amplitudes from Rayleigh-waves recorded on the NORSAR array of instruments, roughly 100 km in aperture, is approximately 0.1 log unit. For the same events used in the spectral analysis, the analyst-measured M_s values also had a standard deviation of 0.1 log unit. This figure is only somewhat less than the 0.15 standard deviation reported by Chang and von Seggern (1977) for m_b values across the 50-km aperture of LASA. However, when only the inner seven NORSAR sensors are considered (aperture about 50 km), the M_s standard deviation drops to roughly 0.05. Thus, M_s scatter is significantly less than m_b scatter over equivalent array dimensions, and by reciprocity, M_s would provide more accurate (1/3 the standard deviation) relative yield estimations for shots within a test site than would m_b.

On the basis of the observed level of amplitude fluctuations reported here, we suggest that attenuation measurements for Rayleigh waves can give highly variable results for differing sample points of the wavefield and that the attenuation coefficient can be resolved confidently to within a factor of two only

for long paths, at least of few thousand kilometers. On the other hand, the associated phase fluctuations are relatively insignificant in phase-velocity measurements; for 20-sec LR, the phase velocity can be resolved to within 1% over short (> 200-300 km) paths if instruments are well calibrated and no large-scale multipathing occurs.

Spectra of LR waves are considerably affected by small-scale scattering, and their variability would seem to preclude accurate source mechanism resolution from a small number of seismograms.

REFERENCES

Aki, K. (1973). Scattering of P waves under the Montana LASA, J. Geophys. Res., 78, 1334-1347.

Capon, J. (1970). Analysis of Rayleigh-wave multipath propagation at LASA, Bull. Seism Soc. Am., 60, 1701-1731.

Capon, J. (1974). Characterization of crust and upper mantle structure under LASA as a random medium, Bull. Seism. Soc. Am., 64, 235-266.

Chang, A. C. and D. H. von Seggern (1977). A study of amplitude variations and m_b bias at LASA subarrays, SDAC-TR-77-11, Teledyne Geotech, Alexandria, Virginia.

Chernov, L. A. (1962). Wave Propagation in a Random Medium, Dover Publications, Inc., New York, N.Y.

Herrin, E. and J. Taggart (1968). Regional variations in P travel times, Bull. Seism. Soc. Am., 58, 1325-1337.

Mack, H. (1972). Spatial coherence of surface waves, Report No. SAAC-8, Teledyne Geotech, Alexandria, Virginia.

Massé, R. P. and S. S. Alexander (1974). Compressional velocity distribution beneath Scandanavia and western Russia, Geophys. J., 39, 587-602.

Mitchell, B. J., L. W. B. Leite, Y. K. Yu, and R. B. Herrmann (1976). Attenuation of Love- and Rayleigh-waves across the Pacific at periods between 15 and 110 seconds, Bull. Seism. Soc. Am., 66, 1189-1202.

North, R. G. (1978). Station bias for ISM-reported magnitude, Geophys. J., in press.

Rivers, D. W. and D. H. von Seggern (1978). Theory of wave propagation in a two-dimensional random medium, Technical Memorandum, Teledyne Geotech, Alexandria, Virginia.

Smart, E. (1972). FKCOMB, a fast general-purpose array processor, Report No. SAAC-9, Teledyne Geotech, Alexandria, Virginia.

Sobel, P. A. and D. H. von Seggern (1978). Applications of surface-wave ray tracing, Bull. Seism. Soc. Am., in press.

Turnbull, L. S. (1976). Determination of seismic source parameters using far-field surface wave spectra, Ph.D. Thesis, Pennsylvania State University, University Park, Pennsylvania.

APPENDIX I

THEORY OF WAVE PROPAGATION IN A TWO-DIMENSIONAL RANDOM MEDIUM

APPENDIX I

THEORY OF WAVE PROPAGATION IN A TWO-DEMENSIONAL RANDOM MEDIUM

In a companion report (Rivers and von Seggern, 1979) the authors investigated fluctuations in the amplitudes and phases of 20-sec Rayleigh waves caused by random irregularities in the structure of the crust along the great-circle path of wave propagation. By analyzing these fluctuations, which were measured at NORSAR and in the southwestern United States, certain parameters can be evaluated that characterize the degree of heterogeneity in the structure of that segment of the crust through which the waves travelled. In order to perform this analysis it is necessary to have a theoretical prediction of the scattering phenomena that are expected when an elastic wave propagates through an inhomogeneous medium characterized by continuous, but random, fluctuations in the index of refraction. Chernov (1962) developed such a theory of wave propagation in three dimensions. In order to study the Rayleigh-wave problem, the authors have modified Chernov's theory to make it applicable to the two-dimensional case. This memorandum consists of the derivation of certain theoretical results summarized in Table I of Rivers and von Seggern (1979), against which the observed Rayleigh-wave amplitude and phase fluctuations are to be compared.

Although the discussion presented here of the two-dimensional random scattering problem is intended to be more or less self-contained, it necessarily requires knowledge of Chernov's (1962) text, which it follows closely.

Amplitude and Phase Fluctuations

We assume that the random medium is characterized by only small deviations of the density and acoustic velocity from their mean values, i.e.

$$\Delta\rho = \rho - \rho_0 \ll \rho_0, \quad \Delta c = c - c_0 \ll c_0. \tag{1}$$

We assume further that a plane wave having acoustic pressure p_0 and travelling in the +x direction,

$$p_0 = A_0 \exp\left[-i(\omega t - Kx)\right] \tag{2}$$

is incident upon the medium. Each element of the medium then becomes a source of secondary scattered waves p_1 which obey the equation (Chernov, p. 43, (26))*

$$\frac{1}{c_0^2}\frac{\partial^2 p_1}{\partial t^2} - \nabla^2 p_1 = -\left[2K^2\frac{\Delta c}{c_0} + \frac{iK}{\rho_0}\frac{\partial(\Delta\rho)}{\partial x}\right] A_0 \exp\left[-i(\omega t - Kx)\right]. \tag{3}$$

Taking the coordinates of the scattering element to be (ξ,η), those of the observations point to be (x, y), and their separation to be r,

$$r = \sqrt{(x-\xi)^2 + (y-\eta)^2} \tag{4}$$

we may solve the inhomogeneous equation (3) by the method of Green's functions, obtaining

$$p_1 = -\frac{iA_0}{4}\iint\left[2K^2\frac{\Delta c}{c_0} + \frac{iK}{\rho_0}\frac{\partial(\Delta\rho)}{\partial\xi}\right] e^{iK\xi} H_0^{(1)}(Kr) e^{-i\omega t}\, d\xi\, d\eta \tag{5}$$

where the integration extends over the entire region from which waves are being scattered to the observation point. The index of refraction of the medium is defined to be

$$\mu(\xi,\eta) = \frac{c_0}{c(\xi,\eta)} - 1 \approx \frac{-\Delta c(\xi,\eta)}{c_0} \tag{6}$$

so by substituting (6) into (5), dropping the time dependence $e^{-i\omega t}$, and neglecting the scattering caused by density fluctuations in comparison with that caused by velocity fluctuations, we obtain

$$p_1 = \frac{iA_0K^2}{2}\iint e^{iK\xi} H_0^{(1)}(Kr)\,\mu(\xi,\eta)\, d\xi\, d\eta \tag{7}$$

For waves of frequency 0.05 Hz and phase velocity 3.6 km/sec, the wave number K is 0.087 km^{-1}, and the asymptotic expansion of the Hankel function,

$$H_0^{(1)}(Kr) \sim \sqrt{\frac{2}{\pi Kr}}\; e^{i(Kr - \pi/4)} \tag{8}$$

* All references are to the text of Chernov (1960).

is valid to within a few percent for scatterer-to-receiver separations r of more than about 60 km. The equation obeyed by the scattered waves thus becomes

$$p_1 = A_0 \sqrt{\frac{k^3}{2\pi}} \iint \frac{e^{ik[(r+\xi)+\pi/4]}}{\sqrt{r}} \mu(\xi,\eta)\, d\xi\, d\eta \tag{9}$$

This equation is the two-dimensional analog of Chernov, p. 59, (67).

If the sum of the incident and scattered waves is expressed as

$$p = Ae^{i\varphi} = A_0 e^{i\varphi_0} + A_1 e^{i\varphi_1} \tag{10}$$

and if the amplitude $A = A_0 + \Delta A$ and phase $\phi = \phi_0 + \Delta\phi$ of the resulting wave differ only slightly from those of the incident wave, i.e.,

$$\frac{\Delta A}{A_0} \ll 1, \quad \Delta\varphi \ll 1, \tag{11}$$

it follows (cf. Chernov, pp. 58-60) that

$$\frac{\Delta A}{A_0} = \sqrt{\frac{k^3}{2\pi}} \iint \frac{1}{\sqrt{r}} \cos\left(k[r-(x-\xi)] + \frac{\pi}{4}\right) \mu(\xi,\eta)\, d\xi\, d\eta \tag{12}$$

and that

$$\Delta\varphi = \sqrt{\frac{k^3}{2\pi}} \iint \frac{1}{\sqrt{r}} \sin\left(k[r-(x-\xi)] + \frac{\pi}{4}\right) \mu(\xi,\eta)\, d\xi\, d\eta. \tag{13}$$

Equation (11) is known as the Born approximation in scattering theory. Chernov uses the method of Rytov to show that (12) and (13) hold under conditions less rigid than those imposed by (11), namely that the amplitude fluctuation $\Delta A/A_0$ and phase fluctuation $\Delta\phi$ be small over the distance of a single wavelength, rather than over the entire path length of the wave through the medium. This is an important loosening of restrictions, since the observed fluctuations are not always small. In the event that the amplitude fluctuations are not to be regarded as small perturbations, Rytov's method dictates that the left side of equation (12) be replaced by the logarithmic amplitude fluctuation $\ln \Delta A/A_0$. We must note, however, that Rytov's method has been criticized by Aki (1973), so we should be cautious about the applicability of the theory to those cases for which (11) is not satisfied.

Introducing the dimensionless variables

$$x' = kx, \quad y' = ky, \quad \xi' = k\xi, \quad \eta' = k\eta, \quad r' = kr, \tag{14}$$

and denoting the phase fluctuation by S and the logarithmic amplitude fluctua-

tion by B, equations (13) and (12) become

$$S(x',y') = \frac{1}{\sqrt{2\pi}} \iint \frac{1}{\sqrt{r'}} \sin\left(r' - (x' - \xi') + \frac{\pi}{4}\right) \mu(\xi',\eta')\, d\xi'\, d\eta' \tag{15}$$

$$B(x',y') = \frac{1}{\sqrt{2\pi}} \iint \frac{1}{\sqrt{r'}} \cos\left(r' - (x' - \xi') + \frac{\pi}{4}\right) \mu(\xi',\eta')\, d\xi'\, d\eta'. \tag{16}$$

We will treat only the case in which the medium is composed of large-scale inhomogeneities, i.e.,

$$Ka \gg 1 \tag{17}$$

where a is the characteristic dimension of the scatterers. For this case we are able to neglect back-scattering and assume that all secondary waves p_1 are emitted into a cone (actually a two-dimensional sector) which has an aperture angle of the order of 1/Ka and which is centered about the direction of the incident wave p_0 (i.e., the +x-axis)(Chernov, pp. 56-57). It follows that the receiver at (x',y') will detect ratiation scattered only from those inhomogeneities located inside a similar cone with apex at the receiver and oriented in the -x-direction. Within this cone we may approximate (4) by

$$r' \approx (x' - \xi') + \frac{1}{2} \frac{(y' - \eta')^2}{x' - \xi'} \tag{18}$$

and substitute (18) into the arguments of the trigonometric functions in (15) and (16). Since $1/\sqrt{r'}$ varies much more slowly than do the trigonometric functions, we may make the rougher approximation

$$\frac{1}{\sqrt{r'}} \approx \frac{1}{\sqrt{x' - \xi'}} \tag{19}$$

in these same equations. Since we need consider only scatterers lying between the planes $\xi' = 0$ and $\xi' = x'$, (15) and (16) become

$$S(x',y') = \frac{1}{\sqrt{2\pi}} \int_{-\infty}^{\infty} \int_{0}^{x'} \frac{1}{\sqrt{x' - \xi'}} \sin\left(\frac{(y' - \eta')^2}{2(x' - \xi')} + \frac{\pi}{4}\right) \mu(\xi',\eta')\, d\xi'\, d\eta' \tag{20}$$

$$B(x',y') = \frac{1}{\sqrt{2\pi}} \int_{-\infty}^{\infty} \int_{0}^{x'} \frac{1}{\sqrt{x' - \xi'}} \cos\left(\frac{(y' - \eta')^2}{2(x' - \xi')} + \frac{\pi}{4}\right) \mu(\xi',\eta')\, d\xi'\, d\eta'. \tag{21}$$

We emphasize that our neglect of waves not scattered forward into a small cone (the Fresnel approximation of diffraction theory) is valid only if (17) applies. If, as previously supposed, $K \approx 0.09$ km^{-1}, our theory will not be valid for media composed of scatterers for which the characteristic dimension is much less than 100 km. Since we wish to consider the effect of inhomogeneities smaller than this, it will be necessary to make approximations, wherever possible, which are not so strongly dependent upon the condition imposed by (17).

We assume that the receiver is located at (L,0) where L is the distance through the medium travelled by incident wave. We now write (20) and (21) as

$$C(L',0) = \int_{-\infty}^{\infty}\int_{0}^{L'} A_1(L'-\xi',\eta')\,\mu(\xi',\eta')\,d\xi'd\eta' \tag{22}$$

$$B(L',0) = \int_{-\infty}^{\infty}\int_{0}^{L'} A_2(L'-\xi',\eta')\,\mu(\xi',\eta')\,d\xi'd\eta' \tag{23}$$

where we have adopted the abbreviations

$$A_1(\alpha,\beta) = \frac{1}{\sqrt{2\pi\alpha}}\sin\left(\frac{\beta^2}{2\alpha}+\frac{\pi}{4}\right) \tag{24}$$

$$A_2(\alpha,\beta) = \frac{1}{\sqrt{2\pi\alpha}}\cos\left(\frac{\beta^2}{2\alpha}+\frac{\pi}{4}\right) \tag{25}$$

and where $L' = K\,L$.

For the moment, let us make explicit the fact that we have oriented the +x-axis of our coordinate system along the source-to-receiver line by expressing coordinates in this system as (x,y,θ), where θ is the geometrical azimuth of the source as measured in a geographical (i.e., fixed) coordinate system centered at the receiver. Considering coordinate systems oriented toward two different sources, we see that the points (x_1,y_1,θ_1) and (x_1, y_1,θ_2) are physically distinct, but in the two different coordinate systems they bear an identical geometrical relationship to the source and the receiver (see Figure 1). (We assume all sources to be at the same distance, L, from the receiver.) We now introduce the spatial correlation function of the index of refraction

$$N_{12} = \overline{\mu(x_1,y_1,\theta)\,\mu(x_2,y_2,\theta)} \tag{26}$$

where the overbar denotes the average taken over all receiver-to-source azimuths θ, i.e.,

$$N_{12} = \frac{1}{2\pi}\int_{0}^{2\pi} \mu(x_1,y_1,\theta)\,\mu(x_2,y_2,\theta)\,d\theta. \tag{27}$$

Due to the random arrangement of scatterers, the correlation function N_{12} depends only on the separation between the points (x_1,y_1,θ) and (x_2,y_2,θ) and not on the points themselves, so we may write

$$N_{12} = \overline{\mu^2}\,N\left(\sqrt{(x_2-x_1)^2+(y_2-y_1)^2}\right) \tag{28}$$

where $\overline{\mu^2}$ is the mean square fluctuation of the refractive index (i.e., N_{11}) and where N is the correlation coefficient. Now the geometrical functions A_1 and A_2 in (22) and (23) depend only on the coordinates of the points $(L,0)$ and (ξ,η) and not on any physical property corresponding to the actual points in space themselves (such as μ), hence they are the same whether evaluated at the point (ξ,η,θ_1) or at the point (ξ,η,θ_2). It then follows that by squaring (22) and (23) and by averaging over all receiver-to-source azimuths θ, we find the mean square phase and amplitude fluctuations to be

$$\overline{S^2} = \overline{\mu^2} \int_0^{L'}\int_0^{L'}\int_{-\infty}^{\infty}\int_{-\infty}^{\infty} A_1(L'-\xi_1',\eta_1')\,A_1(L'-\xi_2',\eta_2')\,N(r')\,d\eta_1'\,d\eta_2'\,d\xi_1'\,d\xi_2' \quad (29)$$

$$\overline{B^2} = \overline{\mu^2} \int_0^{L'}\int_0^{L'}\int_{-\infty}^{\infty}\int_{-\infty}^{\infty} A_1(L'-\xi_1',\eta_1')\,A_2(L'-\xi_2',\eta_2')\,N(r')\,d\eta_1'\,d\eta_2'\,d\xi_1'\,d\xi_2' \quad (30)$$

where

$$r' = \sqrt{(\xi_1'-\xi_2')^2+(\eta_1'-\eta_2')^2}. \quad (31)$$

We rewrite (29) and (30) in terms of new coordinates η and y, defined by

$$\eta = \eta_1' - \eta_2' \quad (32)$$

$$y = \tfrac{1}{2}(\eta_1'+\eta_2'). \quad (33)$$

Our expressions then become

$$\overline{S^2} = \overline{\mu^2} \int_0^{L'}\int_0^{L'}\int_{-\infty}^{\infty}\int_{-\infty}^{\infty} A_1(L'-\xi_1',y+\tfrac{\eta}{2})\,A_1(L'-\xi_2',y-\tfrac{\eta}{2})\,N(r')\,d\eta\,dy\,d\xi_1'\,d\xi_2' \quad (34)$$

$$\overline{B^2} = \overline{\mu^2} \int_0^{L'}\int_0^{L'}\int_{-\infty}^{\infty}\int_{-\infty}^{\infty} A_2(L'-\xi_1',y+\tfrac{\eta}{2})\,A_2(L'-\xi_2',y-\tfrac{\eta}{2})\,N(r')\,d\eta\,dy\,d\xi_1'\,d\xi_2'. \quad (35)$$

It is shown in Appendix II that performing the integration with respect to y yields

$$\overline{S^2} = \overline{\mu^2} \int_0^{L'}\int_0^{L'}\int_{-\infty}^{\infty} \tfrac{1}{2}\left[A_1(2L'-\xi_1'-\xi_2',\eta) + A_1(|\xi_1'-\xi_2'|,\eta)\right] N(r')\,d\eta\,d\xi_1'\,d\xi_2' \quad (36)$$

$$\overline{B^2} = \overline{\mu^2} \int_0^{L'}\int_0^{L'}\int_{-\infty}^{\infty} \tfrac{1}{2}\left[-A_1(2L'-\xi_1'-\xi_2',\eta) + A_1(|\xi_1'-\xi_2'|,\eta)\right] N(r')\,d\eta\,d\xi_1'\,d\xi_2'. \quad (37)$$

which we write as

$$\overline{S^2} = \tfrac{1}{2}\,\overline{\mu^2}\,(I_1 + I_2) \tag{38}$$

$$\overline{B^2} = \tfrac{1}{2}\,\overline{\mu^2}\,(I_1 - I_2) \tag{39}$$

where we have defined

$$I_1 = \int_0^{L'}\int_0^{L'}\int_{-\infty}^{\infty} A_1(|\xi_1' - \xi_2'|, \eta)\, N(r')\, d\eta\, d\xi_1'\, d\xi_2' \tag{40}$$

$$I_2 = \int_0^{L'}\int_0^{L'}\int_{-\infty}^{\infty} A_1(2L' - \xi_1' - \xi_2', \eta)\, N(r')\, d\eta\, d\xi_1'\, d\xi_2'. \tag{41}$$

Introducing new variables x and ξ, defined by

$$x = \tfrac{1}{2}(\xi_1' + \xi_2') \tag{43}$$

$$\xi = \xi_1' - \xi_2', \tag{44}$$

and allowing the integration over ξ to extend from $-\infty$ to $+\infty$ (which we may do if $L >> a$, since $N(r) = 0$ for $r >> a$), we have

$$I_1 = \int_0^{L'}\int_{-\infty}^{\infty}\int_{-\infty}^{\infty} A_1(|\xi|, \eta)\, N(r')\, d\eta\, d\xi\, dx \tag{45}$$

$$I_2 = \int_0^{L'}\int_{-\infty}^{\infty}\int_{-\infty}^{\infty} A_1(2L' - 2x, \eta)\, N(r')\, d\eta\, d\xi\, dx \tag{46}$$

where we now write

$$r' = \sqrt{\xi^2 + \eta^2} \tag{47}$$

Since the integrand of (45) is independent of x, we find

$$I_1 = L'\int_{-\infty}^{\infty}\int_{-\infty}^{\infty} A_1(|\xi|, \eta)\, N(r')\, d\eta\, d\xi. \tag{48}$$

Recalling our definition of A_1, (24), and noting that r' is an even function of both ξ and η, we write this as

$$I_1 = \frac{4L'}{\sqrt{2\pi}} \int_0^\infty \int_0^\infty \frac{1}{\sqrt{\xi}} \sin\left(\frac{\eta^2}{2\xi} + \frac{\pi}{4}\right) N(r')\, d\eta\, d\xi$$

$$= \frac{2L'}{\sqrt{2\pi}} \int_0^\infty \int_0^\infty \frac{1}{\sqrt{\xi}} \left[\sin\left(\frac{\eta^2}{2\xi}\right) + \cos\left(\frac{\eta^2}{2\xi}\right)\right] N(r')\, d\eta\, d\xi. \tag{49}$$

We now assume (Chernov, pp. 7-11) that the correlation coefficient of the refractive index has the form of a Gaussian density, i.e.,

$$N(r) = e^{-r^2/a^2} = e^{-r'^2/a'^2} \tag{50}$$

where, as before, a is the characteristic dimension of the scatterers and where $a' = Ka$. It follows from (47), (49), and (50) that by setting $\frac{\eta^2}{2\xi} = q$ we obtain

$$I_1 = \sqrt{\frac{2}{\pi}}\, L' \int_0^\infty \int_0^\infty \frac{1}{\sqrt{q}} (\sin q + \cos q)\, e^{-(\xi^2 + 2\xi q)/a'^2}\, dq\, d\xi$$

$$= L' \int_0^\infty e^{-\frac{\xi^2}{a'^2}} \frac{1}{\sqrt{\zeta^2+1}} \left[\sqrt{(\zeta^2+1)^{\frac{1}{2}} + \zeta} + \sqrt{(\zeta^2+1)^{\frac{1}{2}} - \zeta}\right] d\xi \tag{51}$$

where $\zeta = \frac{2\xi}{a'^2}$. We may evaluate the integral in (51) approximately by noting although the range of integration extends from $\xi = 0$ to $\xi = +\infty$, the $\exp(-\xi^2/a'^2)$ term causes the integrand to vanish for $\xi >> a'$, so the effective range of ξ is actually of the order of a'. Then throughout this effective range of ξ we have $\zeta = \frac{2\xi}{a'^2} \leq \frac{2}{a'} << 1$, where we have used the restriction (17) that $a' = Ka >> 1$. We thus set $\zeta = 0$ in (51), obtaining

$$I_1 \approx 2L' \int_0^\infty e^{-\frac{\xi^2}{a'^2}}\, d\xi$$

$$= \sqrt{\pi}\, L' a'$$

$$= \sqrt{\pi}\, K^2 L a \tag{52}$$

which is identical to Chernov's I_1 for the analogous three-dimensional case (Chernov, p. 73 and p. 83).

We may obtain a more cumbersome, but exact, representation of I_1 by writing (51) as

$$I_1 = L' \int_0^\infty e^{-\frac{a'^2}{4}\zeta^2} \frac{1}{\sqrt{\zeta^2+1}} \sqrt{\alpha^2 + 2\alpha\beta + \beta^2}\, \frac{a'^2}{2}\, d\zeta \tag{53}$$

where $\alpha = \sqrt{(\zeta^2 + 1)^{1/2} + \zeta}$ and $\beta = \sqrt{(\zeta^2 + 1)^{1/2} - \zeta}$. This reduces to

$$I_1 = \frac{L'a'}{\sqrt{2}} \int_0^\infty e^{-\frac{a'^2}{4}\zeta^2} \frac{1}{\sqrt{\zeta^2+1}} \left[\sqrt{\zeta^2+1} + 1\right]^{\frac{1}{2}} d\zeta$$

$$= \frac{L'a'}{\sqrt{2}} \int_0^\infty e^{-\frac{a'^2}{4}z^2 - \frac{a'^2}{2}z} \frac{1}{\sqrt{z}} dz \qquad (54)$$

where $z = \sqrt{\zeta^2 + 1}$. Equation (54) has the form of a tabulated Laplace transform, and it reduces to

$$I_1 = \frac{L'a'^2}{2} e^{\frac{a'^2}{8}} K_{1/4}\left(\frac{a'^2}{4}\right)$$

$$= \frac{K^2 L a^2}{2} e^{\frac{K^2 a^2}{8}} K_{1/4}\left(\frac{K^2 a^2}{8}\right). \qquad (55)$$

We note that the asymptotic expansion of the modified Bessel function $K_\nu(x)$,

$$K_\nu(x) \sim \sqrt{\frac{2\pi}{x}}\, e^{-x}\left(1 + \frac{4\nu^2 - 1}{8x} + \ldots\right) \qquad (56)$$

implies that (55) reduces to (52) if $Ka \gg 1$. We may thus use (52) when (17) is valid, but we should use (55) when considering scatterers of size $a \lesssim 100$ km.

Substituting from equations (47) and (50) into (46) and performing the integration over ξ, we find

$$I_2 = \sqrt{\pi}\, a' \int_0^{L'} \int_{-\infty}^{\infty} A_1(2L' - 2x, \eta)\, e^{-\frac{\eta^2}{a'^2}} d\eta\, dx \qquad (57)$$

Reversing the order of integration and noting that the integrand is an even function of η, we have

$$I_2 = 2a' \int_0^\infty \int_0^{L' - \frac{\eta^2}{4x}} \sin\left(\frac{\eta^2}{4L' - 4x} + \frac{\pi}{4}\right) e^{-\frac{\eta^2}{a'^2}} dx\, d\eta \qquad (58)$$

Substituting $t = \sqrt{4L' - 4x}/\eta$, this becomes

$$I_2 = a' \int_0^\infty \left[\int_{\eta/2\sqrt{L'}}^\infty \frac{1}{t^2} \sin\left(t^2 + \frac{\pi}{4}\right) dt\right] \eta\, e^{-\frac{\eta^2}{a'^2}} d\eta$$

$$= 4a'L' \int_0^\infty \left[\int_\zeta^\infty \frac{1}{t^2} \sin\left(t^2 + \frac{\pi}{4}\right) dt\right] \zeta\, e^{-\frac{4L'\zeta^2}{a'^2}} d\zeta$$

$$= 4a'L' \int_0^\infty \left[\int_0^t \zeta\, e^{-\frac{4L'\zeta^2}{a'^2}} d\zeta\right] \frac{1}{t^2} \sin\left(t^2 + \frac{\pi}{4}\right) dt$$

$$= -\frac{a'^2}{2} \int_0^\infty \left(e^{-\frac{4L't^2}{a'^2}} - 1\right) \frac{1}{t^2} \sin\left(t^2 + \frac{\pi}{4}\right) dt$$

$$= -\frac{a'^2}{2} \operatorname{Im} \int_0^\infty \left(e^{-bt^2} - 1\right) \frac{1}{t^2} e^{i\left(t^2 + \frac{\pi}{4}\right)} dt \qquad (59)$$

where we have adopted Chernov's (p. 74) definition of the so-called "wave parameter" D,

$$D = \frac{4L'}{a'^2} = \frac{4L}{Ka^2}. \tag{60}$$

Physically, the wave parameter represents approximately the ratio of the size of the first Fresnel zone $\pi\lambda L$ to the scale of the inhomogeneities.

Making the change of variable $p = e^{-i\pi/4}\, t$ in equation (59), we find

$$\begin{aligned} I_2 &= -\frac{a'^3}{2} \int_0^\infty \left(e^{-iDp^2} - 1\right) \frac{1}{ip}\, e^{-p^2 + i\pi/4}\, e^{i\pi/4}\, dp \\ &= \frac{a'^3}{2} \int_0^\infty \sin Dp^2\, \frac{e^{-p^2}}{p}\, dp \\ &= \frac{a'^2}{4} \int_0^\infty \sin Dq\, \frac{e^{-q}}{q^{3/2}}\, dq. \end{aligned} \tag{61}$$

This last integral has the form of a Laplace transform, and it reduces to

$$\begin{aligned} I_2 &= \frac{\sqrt{2\pi}\, a'^3}{4} \left[\sqrt{D^2+1} - 1\right]^{\frac{1}{2}} \\ &= \frac{\sqrt{2\pi}\, L'a'}{D} \left[\sqrt{D^2+1} - 1\right]^{\frac{1}{2}} \\ &= \frac{\sqrt{2\pi}\, K^2 La}{D} \left[\sqrt{D^2+1} - 1\right]^{\frac{1}{2}}. \end{aligned} \tag{62}$$

We finally obtain the desired expressions for the phase and amplitude fluctuations by substituting the equation for I_1, either (52) or (55), and those for I_2, (60) and (62), into equations (38) and (39). We see that the form of these expressions depends in an essential way on the value of the wave parameter D:

$$\begin{aligned} &\text{for } D \gg 1: \quad I_2 = 0 \\ &\qquad\qquad \overline{\varsigma^2} = \overline{\beta^2} = \frac{\sqrt{\pi}}{2}\, \overline{\mu^2}\, K^2 L a \\ &\text{for } D \ll 1: \quad I_2 = \sqrt{\pi}\, K^2 La \\ &\qquad\qquad \overline{\varsigma^2} = \sqrt{\pi}\, \overline{\mu^2}\, K^2 L a, \quad \overline{\beta^2} = 0. \end{aligned} \tag{63}$$

These limiting values are the same as those for the three-dimensional case treated by Chernov (p. 83, (159) and (160)). We note that use of the exact value of I_1, given by (55), would have yielded a negative value for B^2 in the case $D \ll 1$. We also note, however, that the limit $K \to \infty$ (which would imply $D \to 0$) must not be approached too closely, since our scattering formulas are invalid in the very high frequency case corresponding to geometrical acoustics (Chernov, p. 56).

Correlation of the Amplitudes and Phase Fluctuations at the Receiver

Having determined the magnitude of both the amplitude and phase fluctuations, we now examine the correlation between them. We determine the average (over receiver-to-event azimuths) of the product of the two fluctuations by the same method as was used to determine the average of their squares, (34) and (35), thereby obtaining

$$\overline{BS} = \overline{\mu^2} \int_0^{L'} \int_0^{L'} \int_{-\infty}^{\infty} \cdots \int_{-\infty}^{\infty} A_1(L'-\xi_1', y+\tfrac{\eta}{2}) A_2(L'-\xi_2', y-\tfrac{\eta}{2}) N(r')\, d\eta\, dy\, d\xi_1'\, d\xi_2' \quad (64)$$

It is shown in the Appendix II that performing the integration with respect to y yields

$$\overline{BS} = \tfrac{1}{2}\overline{\mu^2} \int_0^{L'} \int_0^{L'} \int_{-\infty}^{\infty} \left[A_2(2L'-(\xi_1'+\xi_2'), \eta) + \operatorname{sgn}(\xi_1'-\xi_2') A_2(|\xi_1'-\xi_2'|, \eta) \right] N(r')\, d\eta\, d\xi_1'\, d\xi_2' \quad (65)$$

Changing variables as indicated in (43) and (44) and, as before, allowing the integration with respect to ξ to extend from $\xi = -\infty$ to $\xi = +\infty$, we find

$$\overline{BS} = \tfrac{1}{2}\overline{\mu^2} \int_0^{L'} \int_{-\infty}^{\infty} \int_{-\infty}^{\infty} \left[A_2(2L'-2x, \eta) + \operatorname{sgn}(\xi) A_2(|\xi|, \eta) \right] N(r')\, d\eta\, d\xi\, dx$$

$$= \tfrac{1}{2}\overline{\mu^2} \int_0^{L'} \int_{-\infty}^{\infty} \int_{-\infty}^{\infty} A_2(2L'-2x, \eta) N(r')\, d\eta\, d\xi\, dx. \quad (66)$$

We now substitute (47) and (50) into (66) and perform the integration over ξ, obtaining

$$\overline{BS} = \frac{\overline{\mu^2}}{2} \sqrt{\pi}\, a' \int_0^{L'} \int_{-\infty}^{\infty} \frac{1}{\sqrt{\pi(4L'-4x)}} \cos\left(\frac{\eta^2}{4L'-4x} + \frac{\pi}{4}\right) e^{-\frac{\eta^2}{a'^2}}\, d\eta\, dx$$

$$= \frac{\overline{\mu^2}}{2} a' \int_0^{\infty} \int_0^{L'} \frac{1}{\sqrt{4L'-4x}} \cos\left(\frac{\eta^2}{4L'-4x} + \frac{\pi}{4}\right) e^{-\frac{\eta^2}{a'^2}}\, dx\, d\eta. \quad (67)$$

By inspection of equations (58)-(61), we see that

$$\overline{BS} = -\overline{\mu^2}\, \frac{a'^3}{4} P_e \int_0^{\infty} \left(e^{-iDp^2} - 1\right) \frac{1}{ip} e^{-p^2 + i\pi/4} e^{i\pi/4}\, dp$$

$$= -\overline{\mu^2}\, \frac{a'^3}{4} \int_0^{\infty} \left(\cos Dp^2 - 1\right) \frac{e^{-p^2}}{p^2}\, dp$$

$$= \overline{\mu^2}\, \frac{a'^3}{8} \int_0^{\infty} \left(\cos Dq - 1\right) \frac{e^{-q}}{q^{3/2}}\, dq. \quad (68)$$

Equation (68) is tabulated Laplace transform, so finally we have

$$\overline{BS} = -\frac{\sqrt{\pi}\,\overline{\mu^2}\,a'^3}{4}\left[1-\frac{1}{\sqrt{2}}\left(\sqrt{D^2+1}+1\right)^{\frac{1}{2}}\right]$$

$$= -\frac{\sqrt{\pi}\,\overline{\mu^2}\,K^3a^3}{4}\left[1-\frac{1}{\sqrt{2}}\left(\sqrt{D^2+1}+1\right)^{\frac{1}{2}}\right]. \tag{69}$$

The correlation coefficient for amplitude fluctuations and phase fluctuations is given by

$$\rho = \frac{\overline{BS}}{\sqrt{\overline{B^2}}\sqrt{\overline{S^2}}}. \tag{70}$$

If we approximate I_1 in (38) and (39) by (52), we have

$$\overline{S^2} = \frac{\sqrt{\pi}}{2}\,\overline{\mu^2}\,K^2aL\left[1+\frac{\sqrt{2}}{D}\left(\sqrt{D^2+1}-1\right)^{\frac{1}{2}}\right] \tag{71}$$

$$\overline{B^2} = \frac{\sqrt{\pi}}{2}\,\overline{\mu^2}\,K^2aL\left[1-\frac{\sqrt{2}}{D}\left(\sqrt{D^2+1}-1\right)^{\frac{1}{2}}\right], \tag{72}$$

and (70) reduces to

$$\rho = \frac{-2+\left[2\sqrt{D^2+1}+2\right]^{\frac{1}{2}}}{\left[D^2+2-2\sqrt{D^2+1}\right]^{\frac{1}{2}}}. \tag{73}$$

We see that for large values of the wave parameter ($D \gg 1$) we have $\rho = 0$, and for small values of the wave parameter ($D \ll 1$) we have $\rho = 1/2$. For the three-dimensional case Chernov (p. 89) finds corresponding values of 0 and $\sqrt{3/2}\,/2$, respectively.

Longitudinal Autocorrelation of Amplitude and Phase Fluctuations

We now examine the correlation of both amplitude and phase fluctuations which are measured at two separate receivers. By "longitudinal" autocorrelation we mean the special case in which the separation of the two receivers is parallel to the direction of propagation of the incident wave (i.e., normal to the wavefront). We thus take the coordinates of the receivers to be $(L_1,0)$ and $(L_2,0)$. Taking the product of the fluctuations at the two receivers and averaging over azimuths (changing the actual location in space of the geometrical point $(L_2,0,\theta)$ so that the separation is longitudinal for each azimuth), we find

$$\overline{S_1S_2} = \overline{\mu^2}\int_0^{L_1'}\int_0^{L_1'}\int_{-\infty}^{\infty}\int_{-\infty}^{\infty} A_1(L_1'-\xi_1',\eta_1')A_1(L_2'-\xi_2',\eta_2')N(r')\,d\eta_1'\,d\eta_2'\,d\xi_1'\,d\xi_2' \tag{74}$$

$$\overline{B_1B_2} = \overline{\mu^2}\int_0^{L_1'}\int_0^{L_1'}\int_{-\infty}^{\infty}\int_{-\infty}^{\infty} A_2(L_1'-\xi_1',\eta_1')A_2(L_2'-\xi_2',\eta_2')N(r')\,d\eta_1'\,d\eta_2'\,d\xi_1'\,d\xi_2' \tag{75}$$

where $L_1' = KL_1$ and $L_2' = KL_2$.

We assume that the effect of waves scattered in the region between the two receivers is negligible, since such waves are incident upon only the second receiver. We thus set the upper limit on the integrals over ξ_2' to be L_1'. Inspection of equations (29)-(41) enables us to write

$$\overline{S_1 S_2} = \tfrac{1}{2}\overline{\mu}^2 (I_1 + I_2) \tag{76}$$

$$\overline{B_1 B_2} = \tfrac{1}{2}\overline{\mu}^2 (I_1 - I_2) \tag{77}$$

where we have now defined

$$I_1 = \int_0^{L_1'}\int_0^{L_1'}\int_{-\infty}^{\infty} A_1(|L_2' - L_1' - (\xi_2' - \xi_1')|, \eta)\, N(r')\, d\eta\, d\xi_1'\, d\xi_2' \tag{78}$$

$$I_2 = \int_0^{L_1'}\int_0^{L_1'}\int_{-\infty}^{\infty} A_1(L_2' + L_1' - (\xi_2' + \xi_1'), \eta)\, N(r')\, d\eta\, d\xi_1'\, d\xi_2'. \tag{79}$$

Making the substitutions (43) and (44) and setting the limits on the ξ integral equal to $-\infty$ and $+\infty$, we find

$$I_1 = \int_0^{L_1'}\int_{-\infty}^{\infty}\int_{-\infty}^{\infty} \frac{1}{\sqrt{2\pi|L_2' - L_1' - \xi|}} \sin\left(\frac{\eta^2}{2|L_2' - L_1' - \xi|} + \frac{\pi}{4}\right) N(r')\, d\eta\, d\xi\, dx$$

$$= \sqrt{\frac{2}{\pi}} L_1' \int_{-\infty}^{\infty}\int_0^{\infty} \frac{1}{\sqrt{|\Delta L' - \xi|}} \sin\left(\frac{\eta^2}{2|\Delta L' - \xi|} + \frac{\pi}{4}\right) N(r')\, d\eta\, d\xi \tag{80}$$

where $\Delta L = L_2 - L_1$. Proceeding as in equations (49)-(53), we have

$$I_1 = \frac{L_1'}{\sqrt{2}} \int_{-\infty}^{\infty} e^{-\frac{\xi^2}{a'^2}} \frac{1}{\sqrt{\zeta^2+1}} \left[\sqrt{\zeta^2+1} + 1\right]^{\frac{1}{2}} d\xi \tag{81}$$

where now $\zeta = \dfrac{2|\Delta L' - \xi|}{a'^2}$. We divide (81) into two integrals

$$I_1 = \frac{L_1'}{\sqrt{2}} \left\{ \int_{-\infty}^{\Delta L'} e^{-\frac{\xi^2}{a'^2}} \frac{1}{\sqrt{\zeta_1^2+1}} \left[\sqrt{\zeta_1^2+1} + 1\right]^{\frac{1}{2}} d\xi + \int_{\Delta L'}^{\infty} e^{-\frac{\xi^2}{a'^2}} \frac{1}{\sqrt{\zeta_2^2+1}} \left[\sqrt{\zeta_2^2+1} + 1\right]^{\frac{1}{2}} d\xi \right\} \tag{82}$$

where $\zeta_1 = \dfrac{2(\Delta L' - \xi)}{a'^2}$ and $\zeta_2 = \dfrac{2(\xi - \Delta L')}{a'^2}$. We now write

$$I_1 = \frac{L_1'}{\sqrt{2}} \left\{ \int_{\infty}^{0} e^{-\frac{1}{a'^2}\left(\frac{a'^2\zeta_1}{2} - \Delta L'\right)^2} \frac{1}{\sqrt{\zeta_1^2+1}} \left[\sqrt{\zeta_1^2+1} + 1\right]^{\frac{1}{2}} \left(-\frac{a'^2}{2} d\zeta_1\right) + \right.$$

$$\left. \int_0^{\infty} e^{-\frac{1}{a'^2}\left(\frac{a'^2\zeta_2}{2} + \Delta L'\right)^2} \frac{1}{\sqrt{\zeta_2^2+1}} \left[\sqrt{\zeta_2^2+1} + 1\right]^{\frac{1}{2}} \left(\frac{a'^2}{2} d\zeta_2\right) \right\}$$

$$= \frac{L_1' a'^2}{2\sqrt{2}} \int_0^{\infty} \left[e^{-\frac{1}{a'^2}\left(\frac{a'^2\zeta}{2} - \Delta L'\right)^2} + e^{-\frac{1}{a'^2}\left(\frac{a'^2\zeta}{2} + \Delta L'\right)^2} \right] \frac{1}{\sqrt{\zeta^2+1}} \left[\sqrt{\zeta^2+1} + 1\right]^{\frac{1}{2}} d\zeta$$

$$= \frac{L_1' a'^2}{\sqrt{2}} e^{-\frac{\Delta L'^2}{a'^2}} \int_0^{\infty} e^{-\frac{a'^2\zeta^2}{4}} \cosh(\Delta L'\zeta) \frac{1}{\sqrt{\zeta^2+1}} \left[\sqrt{\zeta^2+1} + 1\right]^{\frac{1}{2}} d\zeta. \tag{83}$$

Inspection of (83) reveals that when the separation between receivers, ΔL, is small compared to the size of the scatterers, a, we may neglect the dependence of I_1 upon ΔL, whereupon I_1 takes on the value found in the single-receiver case,

$$I_1 \approx \sqrt{\pi}\, K^2 L a, \qquad a \gg \Delta L. \tag{84}$$

We may treat the general case by evaluating the integral in (83) numerically.

We substitute (43), (44), (47), and (50) into equation (79) and once again set the limits on the ξ integral equal to $-\infty$ and $+\infty$, thereby obtaining

$$I_2 = \int_0^{L'} \int_{-\infty}^{\infty} \int_{-\infty}^{\infty} \frac{1}{\sqrt{2\pi(L_1'+L_2'-2x)}} \sin\left(\frac{\eta^2}{2(L_1'+L_2'-2x)} + \frac{\pi}{4}\right) e^{-\frac{\xi^2+\eta^2}{a'^2}}\, d\eta\, d\xi\, dx$$

$$= 2a' \int_0^{\infty} \int_0^{L'} \frac{1}{\sqrt{2(L_1'+L_2')-4x}} \sin\left(\frac{\eta^2}{2(L_1'+L_2')-4x} + \frac{\pi}{4}\right) e^{-\frac{\eta^2}{a'^2}}\, dx\, d\eta. \tag{85}$$

By comparison with equations (58)-(62) we see that

$$I_2 = a' \int_0^{\infty} \left[\int_{\eta/\sqrt{2(L_1'+L_2')}}^{\eta/\sqrt{2(L_1'-L_2')}} \frac{1}{t^2} \sin\left(t^2 + \frac{\pi}{4}\right) dt \right] \eta\, e^{-\frac{\eta^2}{a'^2}}\, d\eta$$

$$= \frac{\sqrt{2\pi}\, a'^3}{4} \left\{ \left[\sqrt{D_1^2+1} - 1\right]^{\frac{1}{2}} - \left[\sqrt{D_2^2+1} - 1\right]^{\frac{1}{2}} \right\} \tag{86}$$

where now

$$D_1 = \frac{2}{a'^2}\left(L_1' + L_2'\right) \tag{87}$$

$$D_2 = \frac{4}{a'^2}\Delta L'. \tag{88}$$

For the case in which the receiver separation, ΔL, is small compared with the source-to-receiver distance, $L \approx L_1 \approx L_2$, the expression for I_2 reduces to the constant value found for the single-receiver case,

$$I_2 \approx \frac{\sqrt{2\pi}\, K^2 L a}{D} \left[\sqrt{D^2+1} - 1\right]^{\frac{1}{2}}. \tag{89}$$

The correlation coefficient for phase fluctuations as a function of receiver separation in the longitudinal direction is given by

$$R_{s,\,\text{long}} = \frac{(\overline{S_1 S_2})_{\text{long}}}{\overline{S^2}}$$

$$= \frac{I_1(\Delta L) + I_2(\Delta L)}{I_1(0) + I_2(0)} \tag{90}$$

and that for amplitude fluctuations is

$$R_{b,\,long} = \frac{(\overline{B_1 B_2})_{long}}{\overline{B^2}}$$

$$= \frac{I_1(\Delta L) - I_2(\Delta L)}{I_1(0) - I_2(0)} \tag{91}$$

Transverse Autocorrelation of Amplitude and Phase Fluctuations

We now examine the case in which two receivers are separated in the direction "transverse" to the direction of the incident wave (i.e., parallel to the wavefront). We take the coordinates of these receivers to be (L,0) and (L,ℓ). By the same procedure as was used to derive equations (29)-(30) and (74)-(75), we see that for this case

$$\overline{S_1 S_2} = \overline{\mu^2} \int_0^{L'} \int_0^{L'} \int_{-\infty}^{\infty} \int_{-\infty}^{\infty} A_1(L' - \xi_1', \eta_1') A_2(L' - \xi_2', \eta_2' - \ell') N(r')\, d\eta_1'\, d\eta_2'\, d\xi_1'\, d\xi_2' \tag{92}$$

$$\overline{B_1 B_2} = \overline{\mu^2} \int_0^{L'} \int_0^{L'} \int_{-\infty}^{\infty} \int_{-\infty}^{\infty} A_1(L' - \xi_1', \eta_1') A_2(L' - \xi_2', \eta_2' - \ell') N(r')\, d\eta_1'\, d\eta_2'\, d\xi_1'\, d\xi_2' \tag{93}$$

where $\ell' = K\ell$.

Following the same procedure as in equation (29)-(41) we obtain

$$\overline{S_1 S_2} = \tfrac{1}{2}\,\overline{\mu^2}\,(I_1 + I_2) \tag{94}$$

$$\overline{B_1 B_2} = \tfrac{1}{2}\,\overline{\mu^2}\,(I_1 - I_2) \tag{95}$$

where now

$$I_1 = \int_0^{L'} \int_0^{L'} \int_{-\infty}^{\infty} A_1(|\xi_1' - \xi_2'|, \eta + \ell')\, N(r')\, d\eta\, d\xi_1'\, d\xi_2' \tag{96}$$

$$I_2 = \int_0^{L'} \int_0^{L'} \int_{-\infty}^{\infty} A_1(2L' - \xi_1' - \xi_2', \eta + \ell')\, N(r')\, d\eta\, d\xi_1'\, d\xi_2'. \tag{97}$$

In order to evaluate I_1, we make the substitutions (43) and (44) and allow the integration over ξ to extend from $-\infty$ to $+\infty$, whence

$$I_1 = \int_0^{L'} \int_{-\infty}^{\infty} \int_{-\infty}^{\infty} A_1(|\xi|, \eta + \ell')\, N(r')\, d\eta\, d\xi\, dx$$

$$= 2L' \int_0^{\infty} \int_{-\infty}^{\infty} A_1(\xi, \eta + \ell')\, N(r')\, d\eta\, d\xi$$

$$= \sqrt{\tfrac{2}{\pi}}\, L' \int_0^{\infty} \frac{1}{\sqrt{\xi}}\, e^{-\frac{\xi^2}{a'^2}} \left[\int_{-\infty}^{\infty} e^{-\frac{\eta^2}{a'^2}} \sin\left(\frac{(\eta + \ell')^2}{2\xi} + \frac{\pi}{4} \right) d\eta \right] d\xi. \tag{98}$$

The second integral in (98) may be written as

$$\int_{-\infty}^{\infty} e^{-\frac{\eta^2}{a'^2}} \sin\left(\frac{(\eta+\ell')^2}{2\xi} + \frac{\pi}{4}\right) d\eta = \mathrm{Im} \int_{-\infty}^{\infty} \exp\left[\eta^2\left(-\frac{1}{a'^2} + \frac{i}{2\xi}\right) + \frac{i\ell'\eta}{\xi} + i\left(\frac{\ell'^2}{2\xi} + \frac{\pi}{4}\right)\right] d\eta$$

$$= \mathrm{Im}\left\{\exp\left[i\left(\frac{\ell'^2}{2\xi} + \frac{\pi}{4}\right)\right] \int_{-\infty}^{\infty} e^{-p\eta^2 + q\eta}\, d\eta\right\} \qquad (99)$$

where $p = \frac{1}{a'^2} - \frac{i}{2\xi}$ and $q = \frac{i\ell'}{\xi}$. Since the real part of p is positive, we may write

$$\int_{-\infty}^{\infty} e^{-(p\eta^2 - q\eta)}\, d\eta = e^{\frac{q^2}{4p}} \int_{-\infty}^{\infty} e^{-\left(\sqrt{p}\,\eta - \frac{q}{2\sqrt{p}}\right)^2} d\eta$$

$$= e^{\frac{q^2}{4p}} \int_{-\infty}^{\infty} e^{-\zeta^2} \frac{1}{\sqrt{p}}\, d\zeta$$

$$= \sqrt{\frac{\pi}{p}}\, e^{\frac{q^2}{4p}}$$

$$= \sqrt{\frac{\pi}{\frac{1}{a'^2} - \frac{i}{2\xi}}} \exp\left[\frac{-\ell'^2}{\frac{4\xi^2}{a'^2} - 2i\xi}\right] \qquad (100)$$

Substituting (100) into (99), we obtain

$$\int_{-\infty}^{\infty} e^{-\frac{\eta^2}{a'^2}} \sin\left(\frac{(\eta+\ell')^2}{2\xi} + \frac{\pi}{4}\right) d\eta = \sqrt{\pi}\, \mathrm{Im}\left\{\frac{1}{\sqrt{1/a'^2 - i/2\xi}} \exp\left[i\left(\frac{\ell'^2}{2\xi} + \frac{\pi}{4}\right) - \frac{\ell'^2/2\xi}{2\xi/a'^2 - i}\right]\right\}$$

$$= \sqrt{\pi}\, \mathrm{Im}\left\{\frac{1}{\sqrt{1/a'^2 - i/2\xi}}\, e^{i\frac{\pi}{4}} \exp\left[\frac{i\ell'^2/a'^2}{2\xi/a'^2 - i}\right]\right\} \qquad (101)$$

and our expression for I_1 becomes

$$I_1 = 2L'\, \mathrm{Im}\left\{e^{i\frac{\pi}{4}} \int_0^{\infty} \frac{1}{\sqrt{2\xi/a'^2 - i}} \exp\left[\frac{i\ell'^2/a'^2}{2\xi/a'^2 - i}\right] e^{-\frac{\xi^2}{a'^2}}\, d\xi\right\}. \qquad (102)$$

It is not apparent from the form of equation (102) that the expression for I_1 reduces to the value found for the single-receiver case, equation (54), in the limit as the separation between the receivers, ℓ, approaches zero. In order to make the relation between (102) and (54) more apparent, we substitute $\zeta = \frac{2\xi}{a'^2}$ and remove the complex numbers from the denominators in (102), obtaining

$$I_1 = L'a'^2\, \mathrm{Im}\left\{e^{i\frac{\pi}{4}} \int_0^{\infty} \frac{\sqrt{\zeta+i}}{\sqrt{\zeta^2+1}} \exp\left[\frac{i\zeta\ell'^2/a'^2 - \ell'^2/a'^2}{\zeta^2+1}\right] e^{-\frac{a'^2\zeta^2}{4}}\, d\zeta\right\}. \qquad (103)$$

We may set

$$\zeta + i = r(\cos\theta + i\sin\theta) \qquad (104)$$

where $r = \sqrt{\zeta^2 + 1}$, $\cos\theta = \frac{\zeta}{r}$, and $\sin\theta = \frac{1}{r}$. De Moivre's theorem then implies that

$$\sqrt{\zeta + i} = \sqrt{r}\left(\cos\frac{\theta}{2} + i\sin\frac{\theta}{2}\right)$$

$$= \sqrt{r}\left(\sqrt{\frac{1+\cos\theta}{2}} + i\sqrt{\frac{1-\cos\theta}{2}}\right)$$

$$= \left[\tfrac{1}{2}\left(\sqrt{\zeta^2+1} + \zeta\right)\right]^{\frac{1}{2}} + i\left[\tfrac{1}{2}\left(\sqrt{\zeta^2+1} - \zeta\right)\right]^{\frac{1}{2}}. \tag{105}$$

and hence

$$\sqrt{\zeta + i}\, e^{i\frac{\pi}{4}} = \tfrac{1}{2}\left(\sqrt{\zeta^2+1} + \zeta\right)^{\frac{1}{2}} - \tfrac{1}{2}\left(\sqrt{\zeta^2+1} - \zeta\right)^{\frac{1}{2}} + \tfrac{i}{2}\left(\sqrt{\zeta^2+1} + \zeta\right)^{\frac{1}{2}} + \tfrac{i}{2}\left(\sqrt{\zeta^2+1} - \zeta\right)^{\frac{1}{2}}$$

$$= \tfrac{1}{2}\sqrt{\alpha^2 - 2\alpha\beta + \beta^2} + \tfrac{i}{2}\sqrt{\alpha^2 + 2\alpha\beta + \beta^2} \tag{106}$$

where $\alpha = \left(\sqrt{\zeta^2 + 1} + \zeta\right)^{\frac{1}{2}}$ and $\beta = \left(\sqrt{\zeta^2 + 1} - \zeta\right)^{\frac{1}{2}}$. This last expression reduces to

$$\sqrt{\zeta + i}\, e^{i\frac{\pi}{4}} = \tfrac{1}{2}\left(2\sqrt{\zeta^2+1} - 2\right)^{\frac{1}{2}} + \tfrac{i}{2}\left(2\sqrt{\zeta^2+1} + 2\right)^{\frac{1}{2}}, \tag{107}$$

so equation (103) becomes

$$I_1 = \frac{L'a'^2}{\sqrt{2}} \int_0^\infty \frac{1}{\sqrt{\zeta^2+1}}\, e^{-\frac{k'^2/a'^2}{\zeta^2+1}}\, e^{-\frac{a'^2\zeta^2}{4}} \left\{\left(\sqrt{\zeta^2+1} - 1\right)^{\frac{1}{2}} \sin\left(\frac{\zeta k'^2/a'^2}{\zeta^2+1}\right)\right.$$

$$\left. + \left(\sqrt{\zeta^2+1} + 1\right)^{\frac{1}{2}} \cos\left(\frac{\zeta k'^2/a'}{\zeta^2+1}\right)\right\} d\zeta \tag{108}$$

which reduces to (54) when $k' = 0$.

If the restriction imposed by (17) is valid, the term $e^{-\frac{a'^2\zeta^2}{4}}$ will cause the integrand to vanish for $\zeta \gtrsim 1$, so throughout the effective range of integration we may neglect ζ^2 im comparison with unity. For this case equation (108) reduces to

$$I_1 = L'a'^2 e^{-\frac{k'^2}{a'^2}} \int_0^\infty e^{-\frac{a'^2\zeta^2}{4}} \cos\left(\frac{\zeta k'^2}{a'^2}\right) d\zeta$$

$$= \sqrt{\pi}\, L'a' e^{-\frac{k'^2}{a'^2}}\, e^{-\frac{k'^4}{a'^6}}$$

$$= \sqrt{\pi}\, La K^2 e^{-\frac{k^2}{a^2}}\, e^{-\frac{k^4}{K^2a^6}} \tag{109}$$

which is the same value as that which Chernov derived for the three-dimensional case (p. 102, (213)). For small-scale inhomogeneities (i.e., those for which

equation (17) is not valid) we shall have to evaluate (108) numerically.

We may evaluate I_2 by substituting (43) and (44) into (97) and setting the limits on the integral over ξ equal to $-\infty$ and $+\infty$, thereby obtaining

$$I_2 = \int_0^{L'} \int_{-\infty}^{\infty} \int_{-\infty}^{\infty} A_1(2L'-2x, \eta+\ell') N(r')\, d\eta\, d\xi\, dx. \tag{110}$$

Inspection of equations (98)-(102) enables us to write

$$\begin{aligned} I_2 &= \mathrm{Im}\left\{ e^{i\frac{\pi}{4}} \int_0^{L'} \int_{-\infty}^{\infty} \frac{1}{\sqrt{4(L'-x)/a'^2 - i}} \exp\left[\frac{i\ell'^2/a'^2}{4(L'-x)/a'^2 - i} \right] e^{-\frac{\xi^2}{a'^2}}\, d\xi\, dx \right\} \\ &= \sqrt{\pi}\, a' \,\mathrm{Im}\left\{ e^{i\frac{\pi}{4}} \int_0^{L'} \frac{1}{\sqrt{4(L'-x)/a'^2 - i}} \exp\left[\frac{i\ell'^2/a'^2}{4(L'-x)/a'^2 - i} \right] dx \right\} \\ &= \frac{\sqrt{\pi}\, a'^3}{4} \,\mathrm{Im}\left\{ e^{i\frac{\pi}{4}} \int_0^{D} \frac{1}{\sqrt{\zeta - i}} \exp\left[\frac{i\ell'^2/a'^2}{\zeta - i} \right] d\zeta \right\} \end{aligned} \tag{111}$$

where we have used the definition of the wave parameter D, equation (60). If we substitute $t = -\dfrac{i\ell'^2/a'^2}{\zeta - i}$ into equation (111), we find

$$\begin{aligned} I_2 &= -\frac{\sqrt{\pi}\,\ell' a'^2}{4} \,\mathrm{Im}\left\{ \int_{\ell'^2/a'^2}^{-\frac{i\ell'^2/a'^2}{D-i}} e^{-t}\, t^{-\frac{3}{2}}\, dt \right\} \\ &= -\frac{\sqrt{\pi}\, k^2 \ell a'}{4} \,\mathrm{Im}\left\{ \Gamma\left(-\tfrac{1}{2}, \frac{\ell^2}{a^2}\right) - \Gamma\left(-\tfrac{1}{2}, \frac{-i\ell^2/a^2}{D-i}\right) \right\} \end{aligned} \tag{112}$$

where $\Gamma(\alpha, z)$ is the incomplete gamma function, defined by

$$\Gamma(\alpha, z) = \int_z^{\infty} e^{-t}\, t^{\alpha-1}\, dt. \tag{113}$$

We now show that equation (112) reduces to the value which was found for the single-receiver case, equation (62), as the separation between receivers, ℓ, approaches zero. Expanding the incomplete gamma function in a power series, we find

$$\begin{aligned} \lim_{z\to 0} \Gamma\left(-\tfrac{1}{2}, z\right) &= \lim_{z\to 0} \left\{ \Gamma\left(-\tfrac{1}{2}\right) - \sum_{n=0}^{\infty} \frac{(-1)^n z^{-\frac{1}{2}+n}}{n!\left(-\frac{1}{2}+n\right)} \right\} \\ &= 2 z^{-\frac{1}{2}}, \end{aligned} \tag{114}$$

hence

$$\lim_{\ell \to 0} I_2 = \frac{\sqrt{\pi} K^3 \ell a^2}{4} \operatorname{Im}\left\{2\left(\frac{-i\ell^2/a^2}{D-i}\right)^{-\frac{1}{2}} - 2\left(\frac{\ell^2}{a^2}\right)^{-\frac{1}{2}}\right\}$$

$$= \frac{\sqrt{\pi} K^3 a^2}{2} \operatorname{Im}\left\{(1+iD)^{\frac{1}{2}}\right\}$$

$$= \frac{\sqrt{\pi} K^3 a^2}{2\sqrt{2}} \left[(D^2+1)^{\frac{1}{2}} - 1\right]^{\frac{1}{2}}$$

$$= \sqrt{2\pi}\, K^2 a \left(\frac{1}{D}\right)\left[(D^2+1)^{\frac{1}{2}} - 1\right]^{\frac{1}{2}} \tag{115}$$

which agrees with (62). Having demonstrated the behavior of I_2 for small ℓ, we may now delete the first term inside the braces in equation (112), since it has no imaginary part and contributes nothing.

Since the incomplete gamma function is not tabulated for complex arguments, it will be necessary to evaluate I_2 by means of the power series expansion which is shown in (114). Because this series is only slowly convergent when the wave parameter D is small, we will find it helpful to treat this particular case by expanding (112) in a Taylor series:

$$I_2 = \frac{\sqrt{\pi} K^2 L \ell}{D} \operatorname{Im}\left\{\Gamma'\left(-\tfrac{1}{2}, \tfrac{\ell^2}{a^2}\right)\Delta\epsilon + \tfrac{1}{2}\Gamma''\left(-\tfrac{1}{2}, \tfrac{\ell^2}{a^2}\right)\Delta\epsilon^2 + \tfrac{1}{6}\Gamma'''\left(-\tfrac{1}{2}, \tfrac{\ell^2}{a^2}\right)\Delta\epsilon^3 + \ldots\right\} \tag{116}$$

where

$$\Delta\epsilon = \frac{-i\ell^2/a^2}{D-i} - \frac{\ell^2}{a^2}$$

$$= -iD\frac{\ell^2}{a^2} - D^2\frac{\ell^2}{a^2} + iD^3\frac{\ell^2}{a^2} + \ldots \tag{117}$$

We see from the definition (113) that

$$\Gamma'(\alpha, z) = -e^{-z} z^{\alpha-1} \tag{118}$$

$$\Gamma''(\alpha, z) = e^{-z} z^{\alpha-1} + (1-\alpha) e^{-z} z^{\alpha-2} \tag{119}$$

Retaining terms of up to third order in the small quantity D, we find

$$I_2 \approx \frac{\sqrt{\pi} K^2 L \ell}{D} e^{-\frac{\ell^2}{a^2}} \left[D\frac{a}{\ell} + D^3\left(-\frac{\ell^3}{6a^3} + \frac{\ell}{2a} - \frac{a}{8\ell}\right)\right] \qquad D \ll 1 \tag{120}$$

As was done for the case of longitudinal receiver separation in equations (90) and (91), we write the expressions for the correlation coefficients for phase fluctuations and for amplitude fluctuations:

$$R_{s,trans} = \frac{I_1(l) + I_2(l)}{I_1(0) + I_2(0)} \tag{121}$$

$$R_{b,trans} = \frac{I_1(l) - I_2(l)}{I_1(0) - I_2(0)} \tag{122}$$

We note that we may obtain convenient expressions for the correlation coefficients in the particular case D << 1 by expanding (62) in a power series:

$$I_1(0) = \frac{\sqrt{2\pi}\, K^2 L a}{D}\left[1 + \frac{D^2}{2} - \frac{D^4}{8} + \frac{D^6}{16} + \ldots - 1\right]^{\frac{1}{2}} \qquad D \ll 1$$

$$= \sqrt{\pi}\, K^2 L a \left[1 + \frac{1}{2}\left(-\frac{D^2}{4} + \frac{D^4}{8} + \ldots\right) - \frac{1}{8}\left(-\frac{D^2}{16} + \ldots\right) + \ldots\right]$$

$$= \sqrt{\pi}\, K^2 L a \left[1 - \frac{D^2}{8} + \frac{7D^4}{128} + \ldots\right]. \tag{123}$$

Substituting (109), (120), (52), and (123) into (122), we find

$$R_b = \frac{e^{-\frac{l^2}{a^2}} e^{-\frac{l^4}{K^2a^4}} - \frac{l}{aD} e^{-\frac{l^2}{a^2}}\left[D\frac{a}{l} + D^3\left(-\frac{l^3}{6a^3} + \frac{l}{2a} - \frac{a}{8l}\right)\right]}{1 - \left(1 - \frac{D^2}{8} + \frac{7D^4}{128}\right)}$$

$$\approx \left(\frac{4l^4}{3a^4} - \frac{4l^2}{a^2} + 1\right) e^{-\frac{l^2}{a^2}} \qquad D \ll 1,\ Ka \gg 1,\ l \lesssim a. \tag{124}$$

For the corresponding three-dimension case Chernov finds the value (p. 102, (227)) $R_b = (l^4/2a^4 - 2l^2/a^2 + 1)\exp(-l^2/a^2)$. Similarly, equation (121) in this particular case reduces to

$$R_s \approx e^{-\frac{l^2}{a^2}} \tag{125}$$

which is the same value found by Chernov (p. 107, (227a)).

Summary of Theoretical Results

The expression for $\overline{B^2}$, $\overline{S^2}$, ρ, $R_{b,long}(\Delta L)$, $R_{b,trans}(l)$, and $R_{s,trans}(l)$ are summarized and compared with Chernov's values for the three-dimensional case in Table I of Rivers and von Seggern (1979). It may be seen that the ratio of the amplitude and phase fluctuations, B^2/S^2, and the correlation between them, ρ, can be expressed parametrically as

$$\frac{\overline{B^2}}{\overline{S^2}} = f_1(K,L,a) \tag{126}$$

$$\rho = g_1(K,L,a). \tag{127}$$

If we make the approximation Ka >> 1, these equations take on the even simpler form

$$\frac{\overline{B^2}}{\overline{S^2}} = f_2(D) \tag{128}$$

$$\rho = g_2(D). \tag{129}$$

Figures 2, 3, and 4 show $\overline{B^2}$, $\overline{S^2}$, and ρ as functions of D. We may eliminate D from (128) and (129) and plot $\overline{B^2}/\overline{S^2}$ versus ρ, in Figure 5. The values of D corresponding to selected points along this curve are shown on it. Analogous plots may be obtained from the more exact relations (126) and (127) by taking K and L to be given and eliminating a. This is done, for three different source-to-receiver distances L, in Figures 6, 7, and 8. Comparison of these three plots shows that the values of $\overline{B^2}/\overline{S^2}$ and ρ are insensitive to the value of L, so long as L >> a. It was this insensitivity to the length of the path through the scattering medium (after the incident wave has been scattered several times) which enabled us to assume that all paths were of the same length L when computing the averages (29) and (30).

By once again assuming K and L to be given constants, we may calculate the longitudinal amplitude and phase correlation coefficient, $R_b(\Delta L)$ and $R_s(\Delta L)$, as functions of a. This is done in Tables I and II for separation between receivers of up to 100 km, approximately the distance across NORSAR. It is seen that both $R_b(\Delta L)$ and $R_s(\Delta L)$ fall off slowly with increasing separation between receivers. (The apparent increase in R_b with increasing ΔL for large values of a is an artifact of the computation process; in fact, $R_b(\Delta L) \approx 1.0$ for $\Delta L \ll a$.) The tabulated values were computed for source-to-receiver distance L = 3000 km; they were found to be scarcely different for the case L = 9000 km.

The transverse amplitude and phase correlation coefficients, $R_b(\ell)$ and $R_s(\ell)$, were similarly calculated for fixed K and L and for various values of a. As shown in Tables III and IV, $R_s(\ell)$ fall off in an approximately Gaussian curve with increasing separation between receivers, but $R_b(\ell)$ decreases to negative values for $\ell \approx a$. Inspection of Table V shows that the values of $R_b(\ell)$ are relatively insensitive to the assumed value of L; $R_s(\ell)$ is even less sensitive to L. The behavior of $R_b(\ell)$ and of $R_s(\ell)$ are shown graphically, for both large and moderate values of the wave parameter, in Figures 9-12. These graphs demonstrate the same general behavior with increasing ℓ as do those given by Chernov for the three-dimensional case. (Chernov, Figs. 5 and 6) Figure 13 shows $R_b(\ell)$ for five values of D and extends the separation ℓ to distances beyond the 100 km considered in Table III.

REFERENCES

Aki, K. (1973). Scattering of P waves under the Montana LASA, J. Geophys. Res., 78, 1334-1347.

Chernov, L. A. (1962). Wave Propagation in a Random Medium, Dover Publications, Inc., New York, N.Y.

Rivers, D. W. and D. H. von Seggern (1979). Random scattering effect on Rayleigh-wave amplitudes and phases, SDAC-TR-78-3, Teledyne Geotech, Alexandria, Virginia.

Table I

Theoretical Amplitude Correlation Coefficient

R_b (ΔL) for Longitudinal Separation of Receivers

Source-to-Receiver Distance L = 3000 km

Period T = 19.7 sec

Phase Velocity C = 3.641 $\frac{km}{sec}$

Wave Number K = 0.0876 km^{-1}

Separation ΔL(km)	Characteristic Dimension of Scatterers a (km)											
	300	250	200	150	125	100	75	50	40	30	20	10
0	1.00	1.00	1.00	1.00	1.00	1.00	1.00	1.00	1.00	1.00	1.00	.98
5	1.00	1.00	1.00	1.00	1.00	1.00	1.00	1.00	1.00	1.00	.99	.90
10	1.01	1.01	1.01	1.00	1.00	1.00	1.00	1.00	1.00	.99	.96	.75
15	1.02	1.01	1.01	1.01	1.01	1.00	1.00	1.00	.99	.97	.91	.59
20	1.02	1.01	1.01	1.01	1.01	1.01	1.01	1.00	.98	.95	.84	.48
25	1.03	1.02	1.01	1.01	1.01	1.01	1.01	.99	.97	.92	.77	.41
30	1.03	1.02	1.01	1.01	1.01	1.01	1.01	.98	.96	.89	.71	.36
35	1.04	1.02	1.02	1.01	1.01	1.01	1.00	.98	.94	.86	.65	.32
40	1.04	1.03	1.02	1.01	1.01	1.01	1.00	.97	.92	.83	.60	.29
45	1.05	1.03	1.02	1.02	1.01	1.01	1.00	.96	.91	.79	.55	.27
50	1.05	1.04	1.02	1.02	1.02	1.01	1.00	.95	.89	.76	.51	.25
55	1.06	1.04	1.03	1.02	1.02	1.01	.99	.93	.87	.72	.48	.24
60	1.06	1.04	1.03	1.02	1.02	1.01	.99	.92	.84	.69	.45	.22
65	1.07	1.05	1.03	1.02	1.02	1.01	.99	.91	.82	.66	.42	.21
70	1.07	1.05	1.03	1.03	1.02	1.01	.98	.90	.80	.63	.40	.20
75	1.08	1.05	1.04	1.03	1.02	1.01	.98	.88	.78	.60	.38	.19
80	1.09	1.06	1.04	1.03	1.02	1.01	.98	.87	.76	.58	.37	.19
85	1.09	1.06	1.04	1.03	1.02	1.01	.97	.85	.74	.56	.35	.18
90	1.10	1.06	1.04	1.03	1.02	1.01	.97	.84	.72	.53	.34	.17
95	1.10	1.07	1.04	1.03	1.02	1.00	.96	.82	.70	.51	.32	.17
100	1.11	1.07	1.05	1.04	1.02	1.00	.96	.81	.68	.50	.31	.16
Wave Parameter D:	1.5	2.2	3.4	6.1	8.8	13.7	24.4	54.8	85.6	152	342	1370

Table II

Theoretical Phase Correlation Coefficient

$R_s(\Delta L)$ for Longitudinal Separation of Receivers

Source-to-Receiver Distance L = 3000 km

Period T = 19.7 sec

Phase Velocity C = 3.641 $\frac{km}{sec}$

Wave Number K = 0.0876 km^{-1}

Separation ΔL(km)	Characteristic Dimension of Scatterers a (km)											
	300	250	200	150	125	100	75	50	40	30	20	10
0	1.00	1.00	1.00	1.00	1.00	1.00	1.00	1.00	1.00	1.00	1.00	.99
5	1.00	1.00	1.00	1.00	1.00	1.00	1.00	1.00	1.00	.99	.99	.91
10	1.00	1.00	1.00	1.00	1.00	1.00	1.00	1.00	1.00	.99	.96	.77
15	1.00	1.00	1.00	1.00	1.00	1.00	1.00	1.00	.99	.97	.92	.63
20	1.00	1.00	1.00	1.00	1.00	1.00	1.00	.99	.98	.96	.86	.52
25	1.00	1.00	1.00	1.00	1.00	1.00	1.00	.99	.97	.93	.80	.46
30	1.00	1.00	1.00	1.00	1.00	1.00	1.00	.98	.96	.91	.74	.41
35	1.00	1.00	1.00	1.00	1.00	1.00	.99	.97	.95	.88	.70	.38
40	1.00	1.00	1.00	1.00	1.00	1.00	.99	.97	.93	.85	.65	.35
45	1.00	1.00	1.00	1.00	1.00	.99	.99	.96	.92	.82	.61	.33
50	1.00	1.00	1.00	1.00	.99	.99	.99	.95	.90	.80	.58	.32
55	1.00	1.00	.99	.99	.99	.99	.98	.94	.89	.77	.55	.30
60	1.00	.99	.99	.99	.99	.99	.98	.93	.87	.74	.52	.29
65	.99	.99	.99	.99	.99	.99	.98	.92	.85	.72	.50	.28
70	.99	.99	.99	.99	.99	.99	.97	.91	.84	.69	.48	.27
75	.99	.99	.99	.99	.99	.99	.97	.90	.82	.67	.47	.26
80	.99	.99	.999	.99	.99	.98	.97	.89	.80	.65	.45	.25
85	.99	.99	.99	.99	.99	.98	.96	.88	.79	.63	.44	.25
90	.99	.99	.99	.99	.99	.98	.96	.87	.77	.61	.43	.24
95	.99	.99	.99	.99	.99	.98	.95	.86	.76	.60	.41	.24
100	.99	.99	.99	.99	.99	.98	.95	.85	.74	.58	.40	.23
Wave Parameter D:	1.5	2.2	3.4	6.1	8.8	13.7	24.4	54.8	85.6	152	342	1370

Table III

Theoretical Amplitude Correlation Coefficient

$R_b(\ell)$ for Transverse Separation of Receivers

Source-to-Receiver Distance L = 3000 km

Period T = 19.7 sec

Phase Velocity C = 3.641 $\frac{km}{sec}$

Wave Number K = 0.0876 km^{-1}

	Characteristic Dimension of Scatterers a (km)											
Separation ℓ(km)	300	250	200	150	125	100	75	50	40	30	20	10
0	1.01	1.01	1.01	1.01	1.01	1.01	1.01	1.00	1.00	1.00	1.00	.97
5	1.01	1.01	1.01	1.01	1.01	1.00	.99	.99	.99	.98	.96	.86
10	1.00	1.00	1.00	1.00	1.00	.99	.98	.96	.94	.91	.84	.60
15	1.00	1.00	.99	.99	.99	.98	.95	.91	.87	.80	.66	.29
20	.99	.99	.98	.98	.97	.95	.92	.84	.78	.67	.46	.05
25	.98	.98	.97	.96	.94	.92	.87	.76	.67	.52	.27	-.08
30	.97	.97	.95	.93	.91	.88	.81	.66	.55	.37	.11	-.11
35	.96	.95	.93	.91	.88	.84	.75	.56	.43	.23	-.01	-.08
40	.95	.93	.91	.88	.84	.79	.68	.46	.31	.12	-.08	-.06
45	.93	.91	.89	.84	.80	.73	.61	.36	.20	.02	-.11	-.05
50	.91	.89	.86	.80	.75	.68	.53	.26	.11	-.05	-.12	-.06
55	.89	.87	.83	.76	.71	.62	.45	.17	.03	-.10	-.11	-.05
60	.87	.84	.80	.72	.65	.55	.38	.09	-.04	-.12	-.10	-.05
65	.85	.82	.77	.68	.60	.49	.30	.02	-.09	-.14	-.10	-.05
70	.83	.79	.73	.63	.54	.42	.23	-.04	-.12	-.14	-.09	-.05
75	.80	.76	.69	.58	.49	.36	.16	-.09	-.15	-.14	-.09	-.05
80	.78	.73	.65	.53	.43	.30	.09	-.13	-.17	-.14	-.09	-.05
85	.75	.69	.61	.48	.37	.23	.03	-.16	-.18	-.14	-.09	-.05
90	.72	.66	.57	.43	.31	.17	-.03	-.18	-.18	-.13	-.09	-.05
95	.69	.62	.53	.37	.25	.11	-.08	-.20	-.18	-.13	-.09	-.05
100	.66	.59	.48	.32	.20	.05	-.12	-.21	-.18	-.13	-.09	-.05
Wave Parameter D:	1.5	2.2	3.4	6.1	8.8	13.7	24.4	54.8	85.6	152	342	1370

Table IV

Theoretical Phase Correlation Coefficient

$R_s(\ell)$ for Transverse Separation of Receivers

Source-to-Receiver Distance L = 3000 km

Period T = 19.7 sec

Phase Velocity C = 3.641 $\frac{km}{sec}$

Wave Number K = 0.0876 km^{-1}

Separation ℓ(km)	Characteristic Dimension of Scatterers a (km)											
	300	250	200	150	125	100	75	50	40	30	20	10
0	1.00	1.00	1.00	1.00	1.00	1.00	1.00	1.00	1.00	1.00	1.00	.97
5	1.00	1.00	1.00	1.00	1.00	1.00	1.00	1.00	.99	.98	.96	.88
10	1.00	1.00	1.00	1.00	.99	.99	.97	.94	.91	.84	.86	.36
15	1.00	1.00	1.00	1.00	.99	.99	.97	.94	.91	.84	.71	.36
20	1.00	1.00	.99	.99	.99	.98	.95	.89	.84	.74	.54	.14
25	1.00	.99	.99	.98	.98	.96	.92	.83	.76	.62	.38	.03
30	.99	.99	.99	.98	.96	.94	.89	.77	.67	.51	.25	.00
35	.99	.99	.98	.97	.95	.92	.86	.70	.58	.40	.15	.02
40	.99	.98	.97	.95	.93	.90	.82	.63	.50	.31	.10	.04
45	.98	.98	.97	.94	.92	.87	.77	.56	.42	.23	.07	.06
50	.98	.97	.96	.93	.90	.84	..73	.50	.35	.18	.06	.05
55	.97	.97	.95	.91	.88	.81	.69	.44	.29	.14	.06	.05
60	.97	.96	.94	.90	.85	.78	.64	.38	.24	.12	.06	.05
65	.96	.95	.93	.88	.83	.75	.60	.33	.20	.11	.07	.05
70	.96	.94	.92	.86	.81	.72	.55	.29	.18	.10	.07	.05
75	.95	.94	.91	.84	.78	.68	.51	.26	.16	.10	.08	.05
80	.95	.93	.90	.82	.76	.65	.47	.23	.14	.10	.08	.05
85	.94	.92	.88	.80	.73	.62	.44	.20	.13	.10	.08	.05
90	.93	.91	.87	.78	.71	.59	.40	.19	.13	.10	.08	.05
95	.92	.90	.86	.76	.68	.56	.37	.17	.13	.10	.08	.05
100	.92	.89	.84	.74	.65	.53	.35	.16	.13	.10	.07	.05
Wave Parameter D:	1.5	2.2	3.4	6.1	8.8	13.7	24.4	54.8	85.6	152	342	1370

Table V

Theoretical Amplitude Correlation Coefficient

$R_b(\ell)$ for Transverse Separation of Receivers

Source-to-Receiver Distance L = 9000 km

Period T = 19.7 sec

Phase Velocity C = 3.641 $\frac{km}{sec}$

Wave Number K = 0.0876 km^{-1}

Separation	Characteristic Dimension of Scatterers a (km)											
ℓ(km)	300	250	200	150	125	100	75	50	40	30	20	10
0	1.00	1.00	1.00	1.01	1.01	1.01	1.01	1.00	1.00	1.00	1.00	.98
5	1.00	1.00	1.00	1.01	1.01	1.00	1.00	.99	.99	.98	.96	.88
10	1.00	1.00	1.00	1.00	1.00	1.00	.99	.97	.95	.91	.84	.61
15	1.00	1.00	1.00	.99	.99	.98	.96	.92	.88	.81	.67	.30
20	.99	.99	.99	.98	.97	.96	.93	.85	.79	.68	.48	.07
25	.99	.98	.98	.97	.96	.93	.89	.78	.69	.54	.30	-.05
30	.98	.98	.97	.95	.93	.90	.84	.69	.58	.41	.14	-.08
35	.97	.97	.95	.93	.91	.86	.78	.60	.47	.28	.03	-.06
40	.96	.96	.94	.91	.88	.82	.72	.51	.36	.16	-.03	-.04
45	.95	.94	.92	.88	.84	.78	.66	.42	.26	.08	-.07	-.02
50	.94	.93	.90	.85	.81	.73	.59	.33	.17	.01	-.07	-.03
55	.93	.91	.88	.82	.77	.68	.53	.25	.10	-.04	-.07	-.03
60	.92	.90	.86	.79	.73	.62	.46	.17	.04	-.06	-.06	-.03
65	.90	.88	.84	.76	.68	.57	.39	.11	-.01	-.08	-.06	-.03
70	.89	.86	.81	.72	.64	.51	.33	.05	-.04	-.08	-.05	-.03
75	.87	.84	.79	.68	.59	.46	.27	.01	-.07	-.08	-.05	-.03
80	.86	.82	.76	.65	.55	.40	.21	-.03	-.09	-.08	-.05	-.03
85	.84	.80	.73	.61	.50	.35	.15	-.06	-.10	-.08	-.05	-.03
90	.82	.77	.70	.57	.46	.29	.10	-.08	-.10	-.08	-.05	-.03
95	.80	.75	.67	.53	.41	.24	.06	-.10	-.10	-.08	-.05	-.03
100	.78	.73	.64	.48	.36	.20	.02	-.11	-.10	-.08	-.05	-.03
Wave Parameter D:	4.6	6.6	10.3	18.3	26.3	41.1	73.1	164	257	457	1027	4110

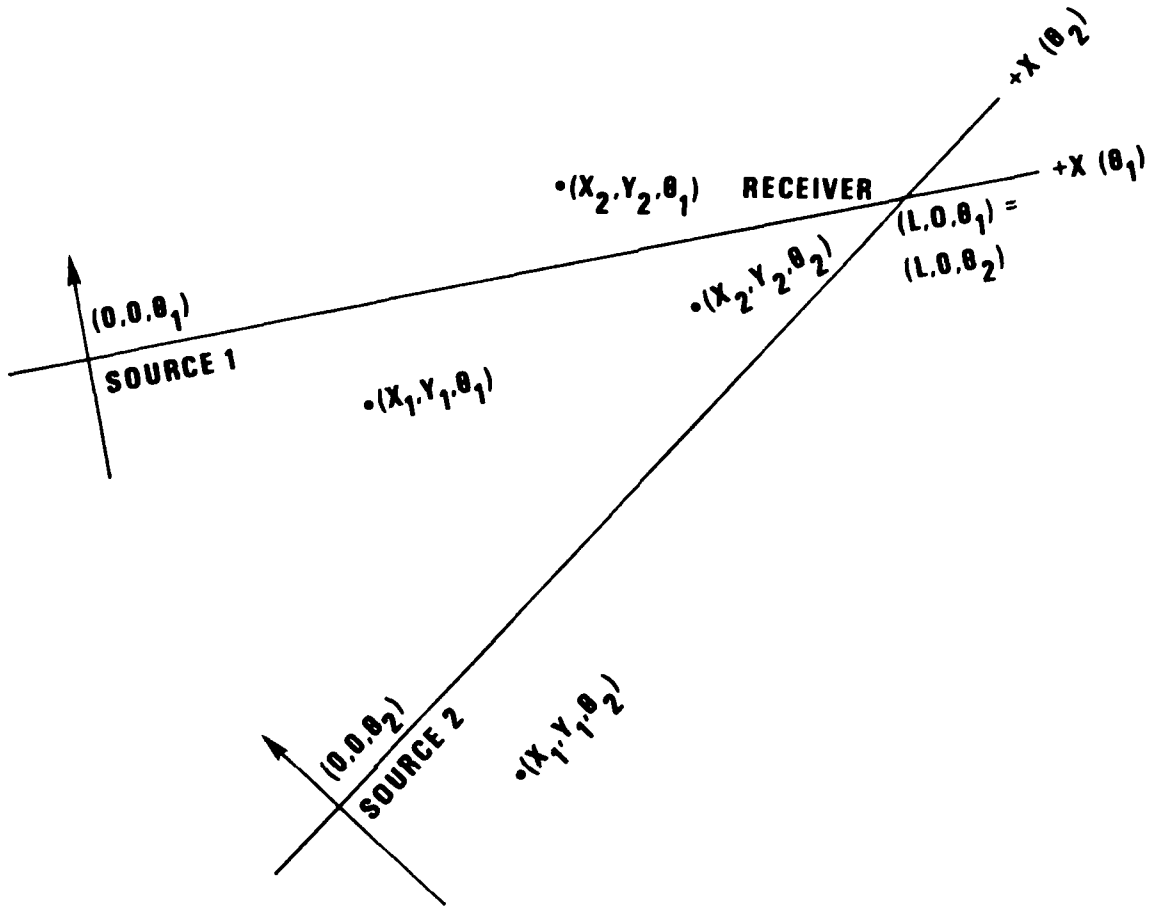

Figure 1. Geometry of the coordinate systems used for different souce and receiver pairs.

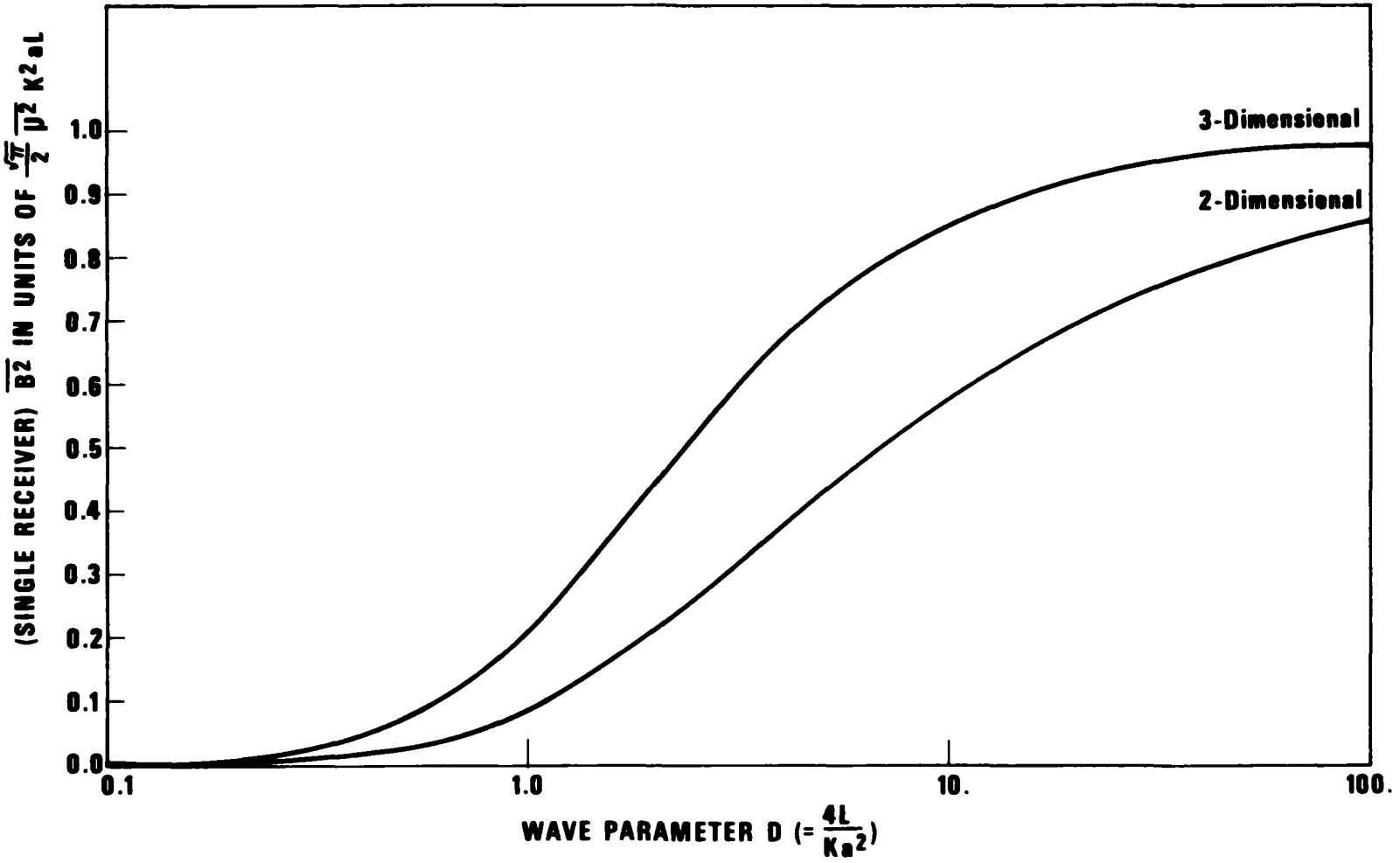

Figure 2. Theoretical logarithmic amplitude fluctuation as a function of wave parameter D.

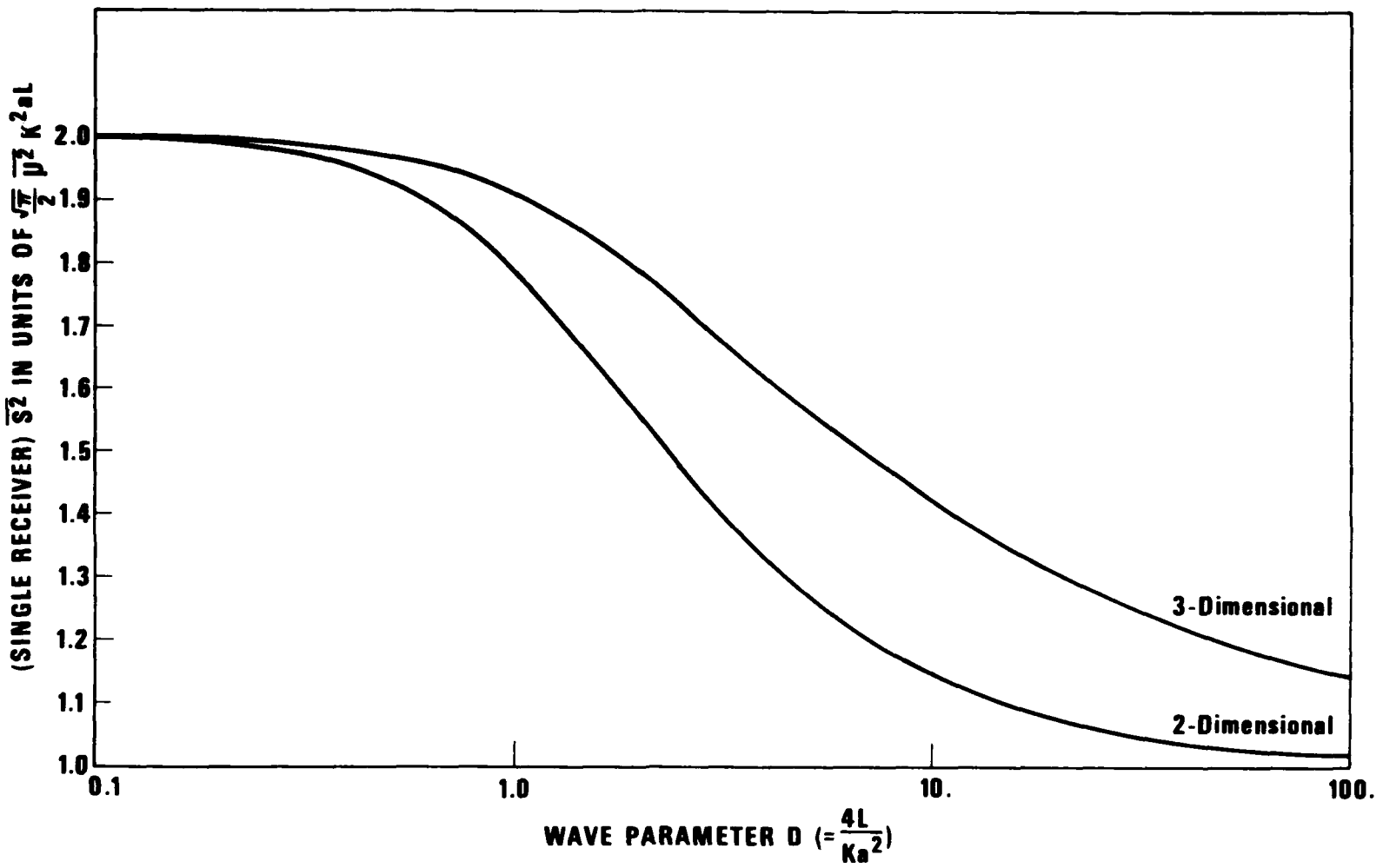

Figure 3. Theoretical phase fluctuations as a function of wave parameter D.

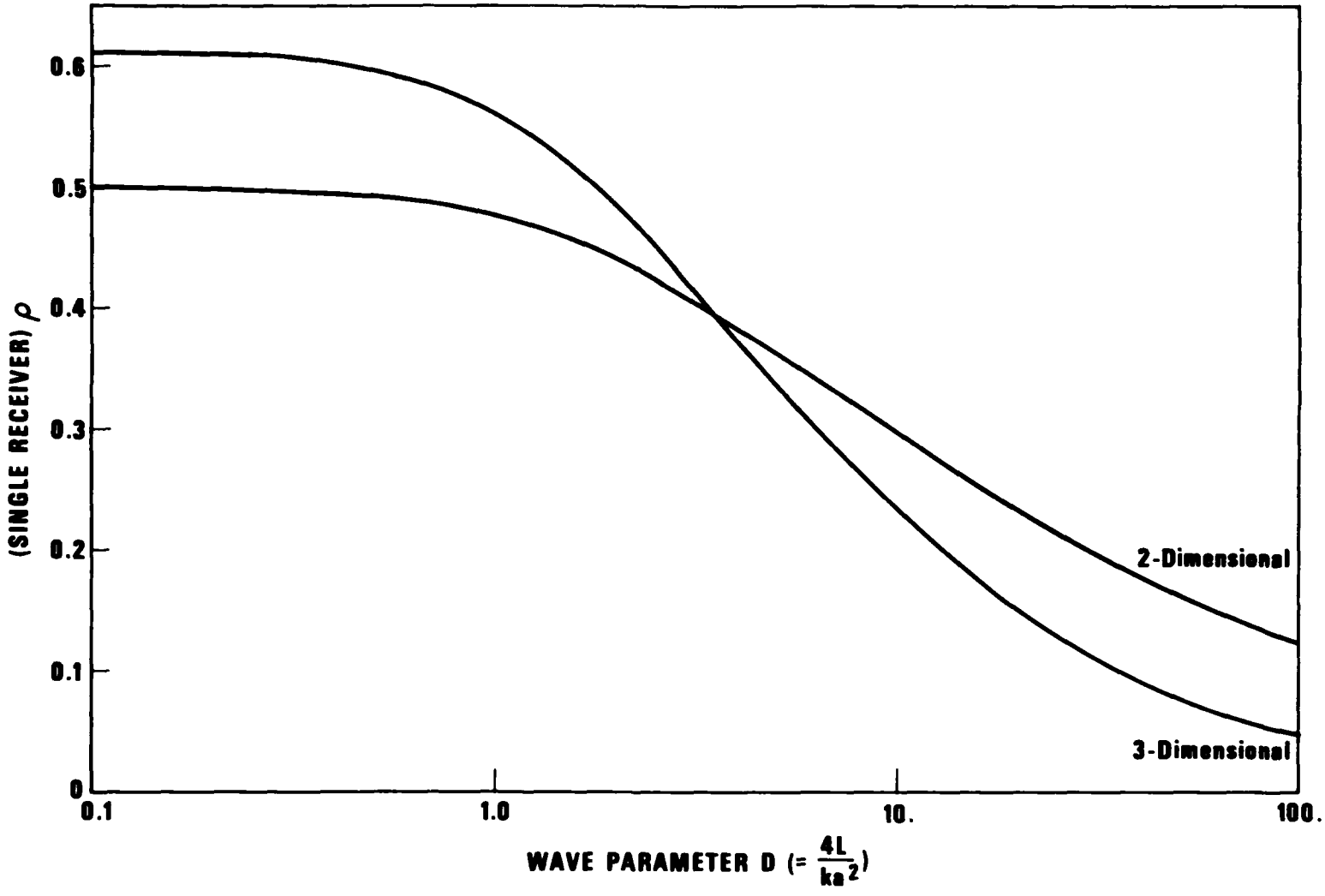

Figure 4. Theoretical correlation coefficient of logarithmic amplitude fluctuations and phase fluctuations (at a single receiver) as a function of wave parameter D.

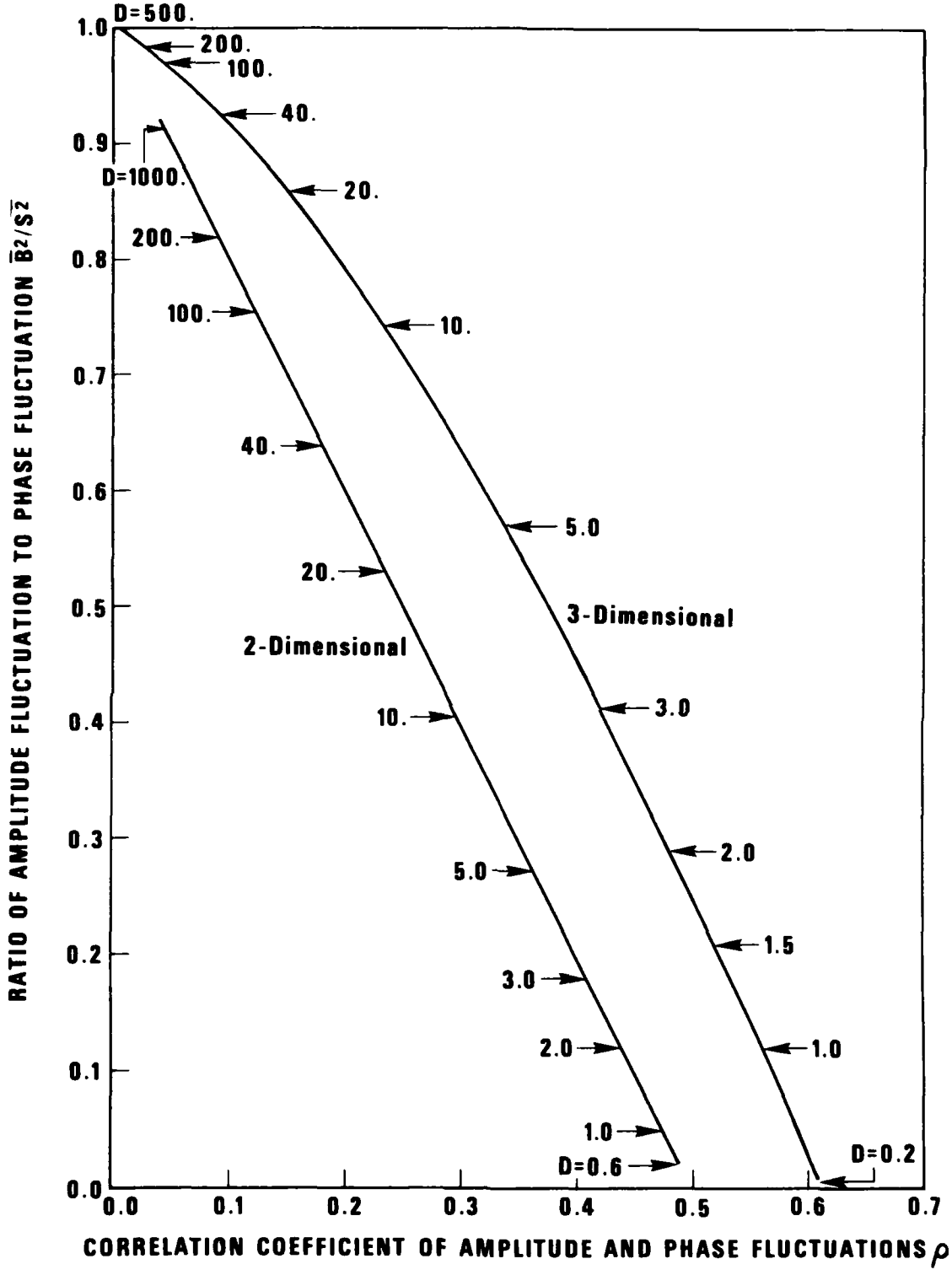

Figure 5. Theoretical values of $\frac{\overline{B^2}}{\overline{S^2}}$ and p for various values of the wave parameter D.

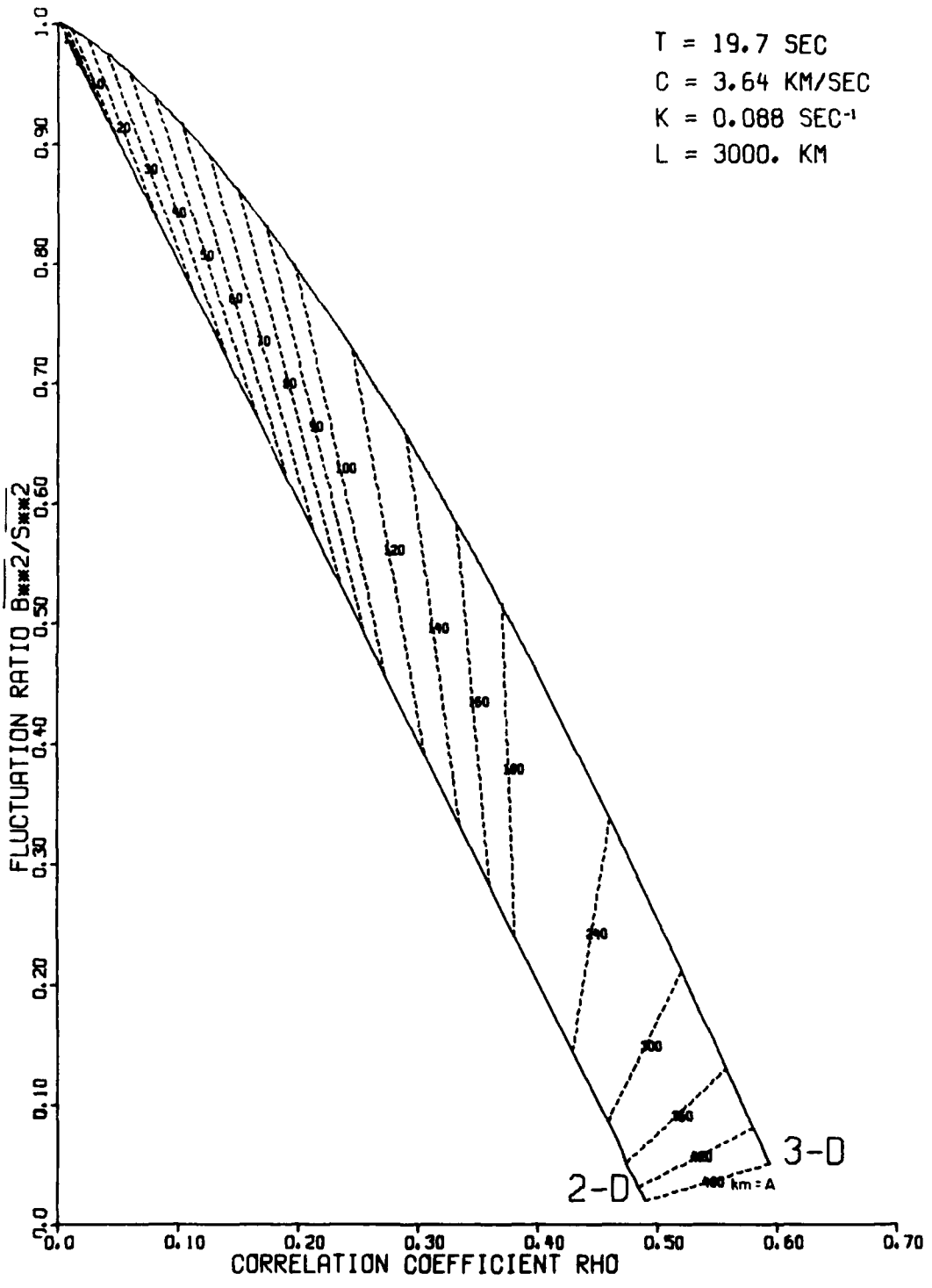

Figure 6. Theoretical values of $\frac{\overline{B^2}}{S^2}$ and p for various characteristic dimensions A of the random scatterers.

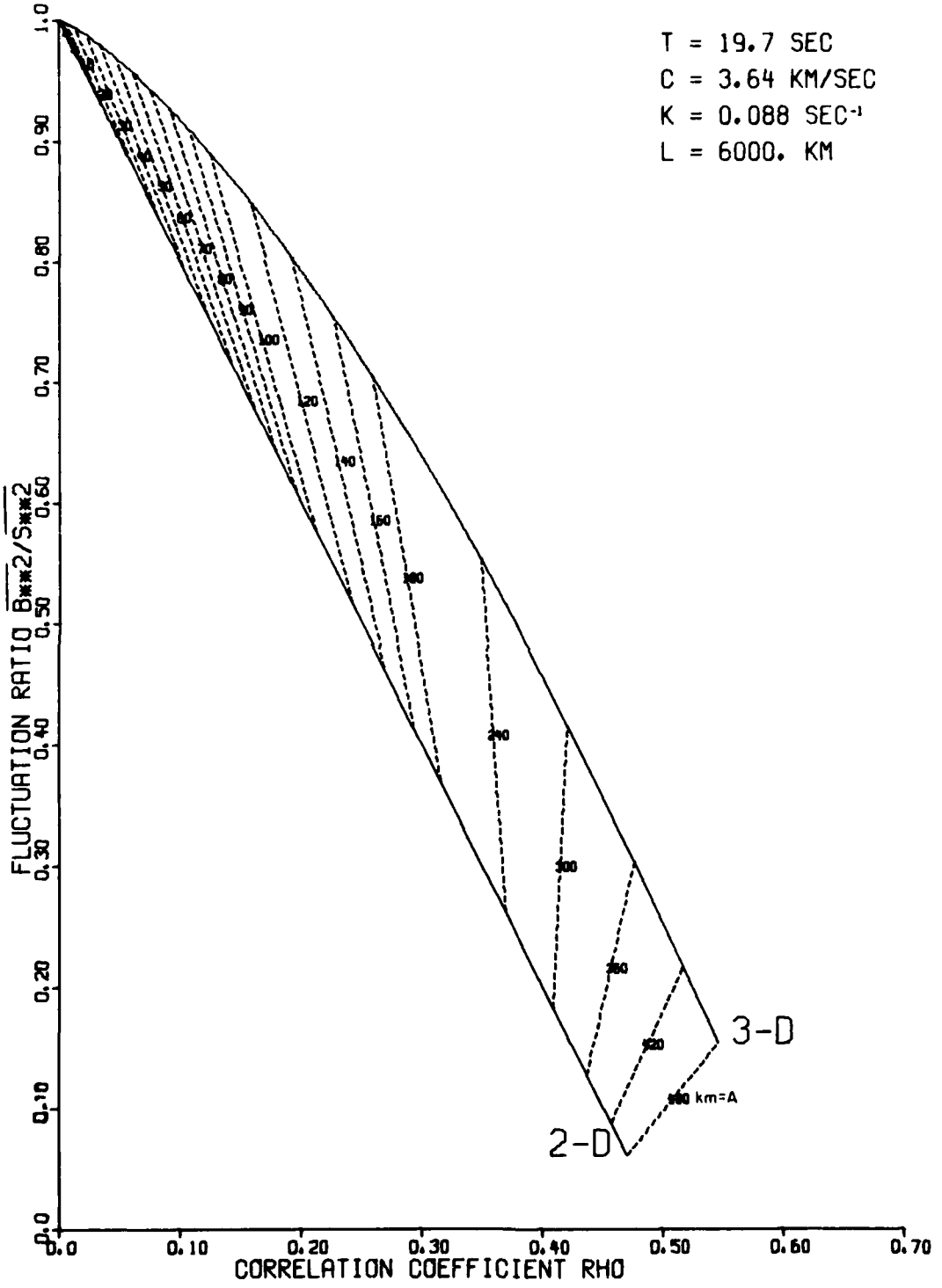

Figure 7. Theoretical values of $\frac{\overline{B^2}}{S^2}$ and p for various characteristic dimensions A of the random scatterers.

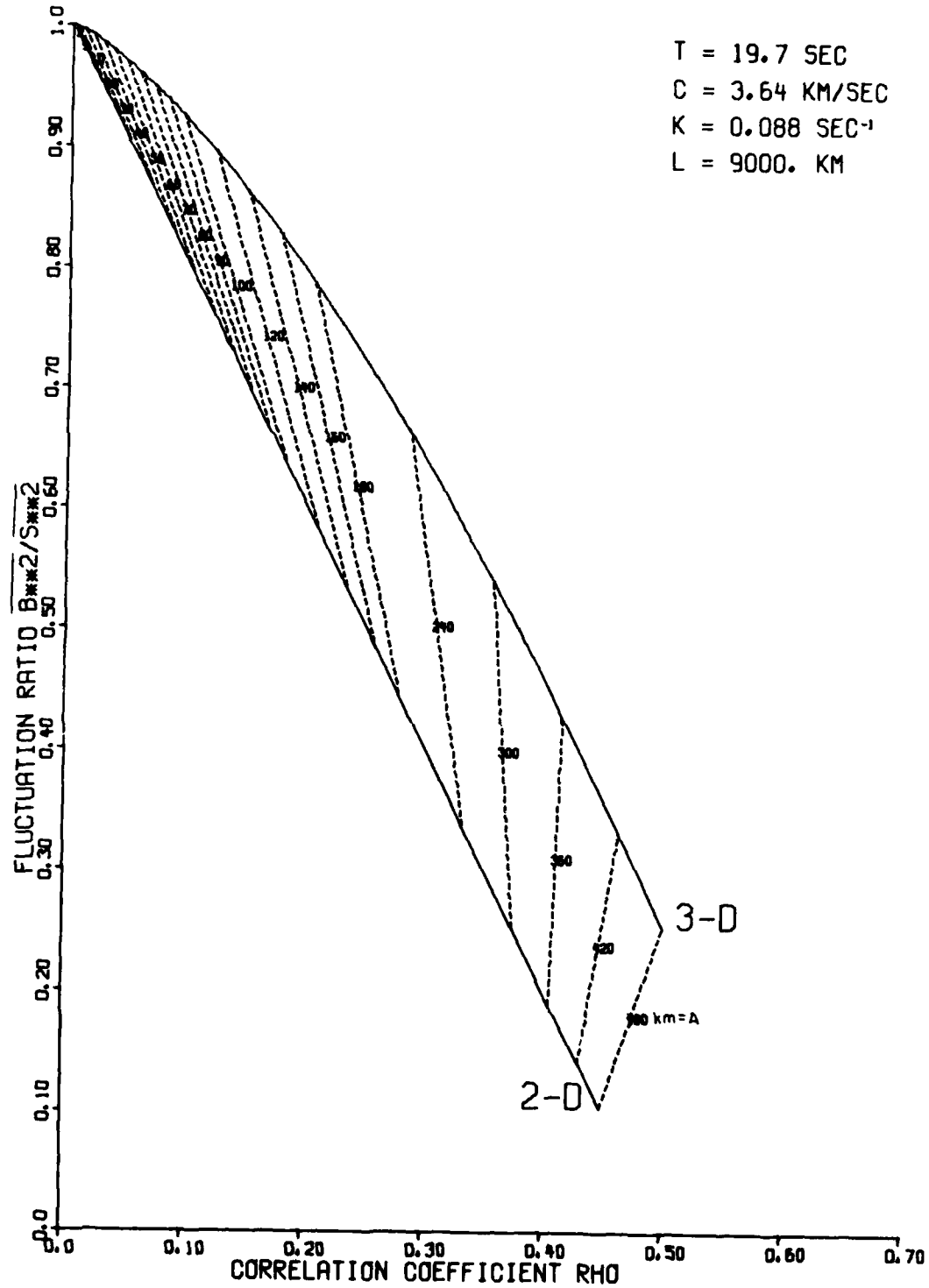

Figure 8. Theoretical values of $\frac{\overline{B^2}}{S^2}$ and p for various characteristic dimensions A of the random scatterers.

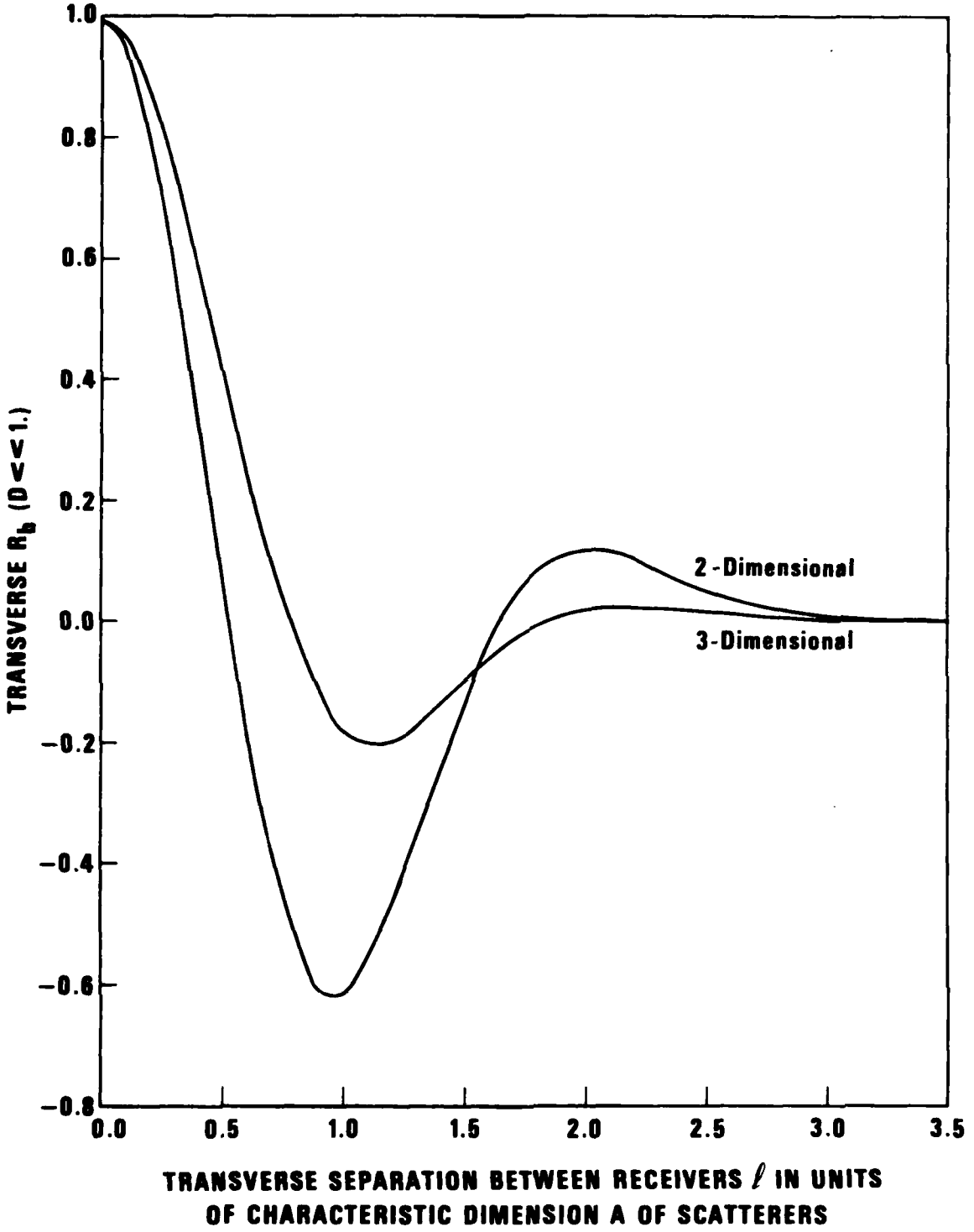

Figure 9. Theoretical transverse amplitude correlation coefficient $R_b(\ell)$ for case D<<1.

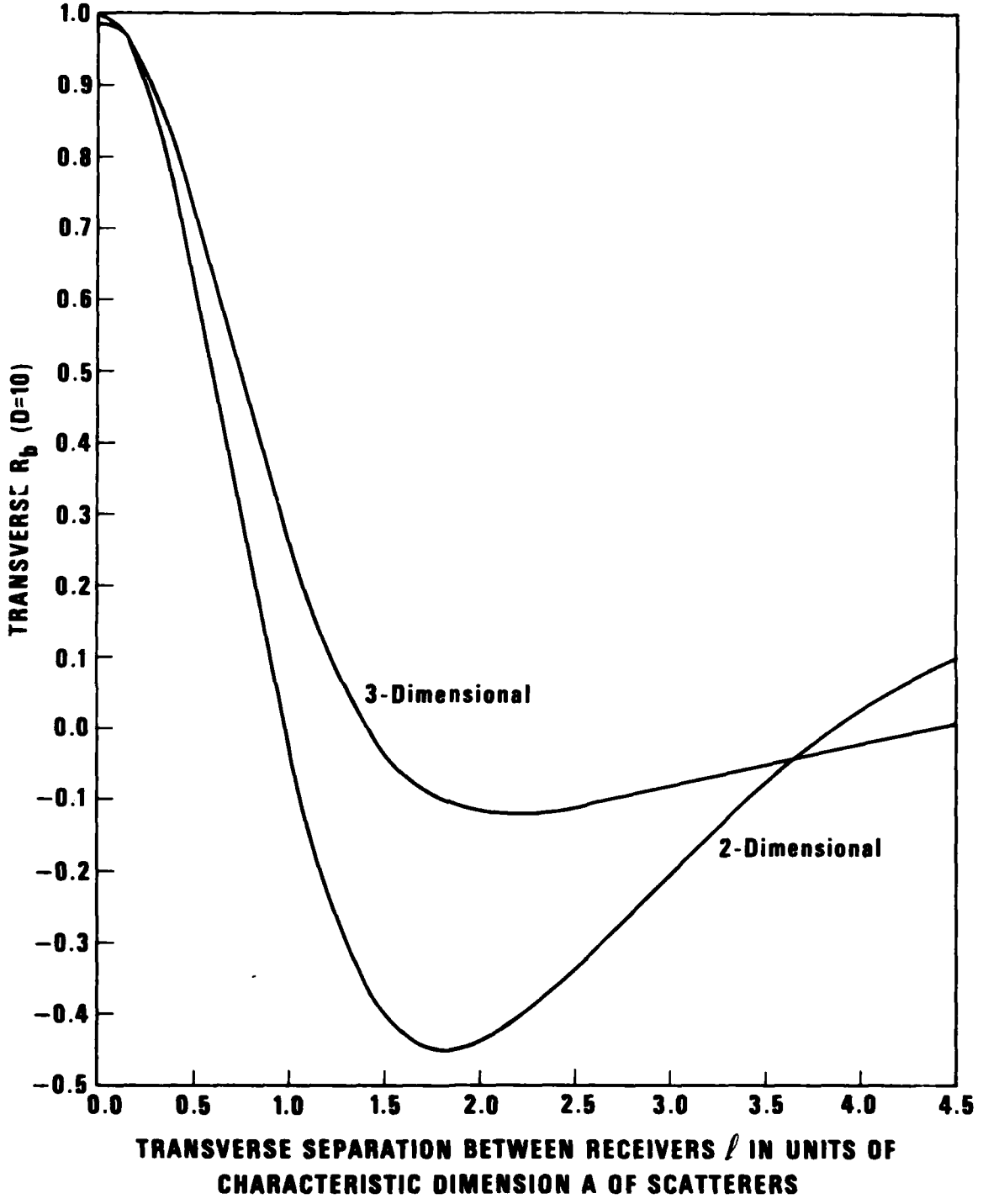

Figure 10. Theoretical transverse amplitude correlation coefficient $R_b(\ell)$ for case D = 10.

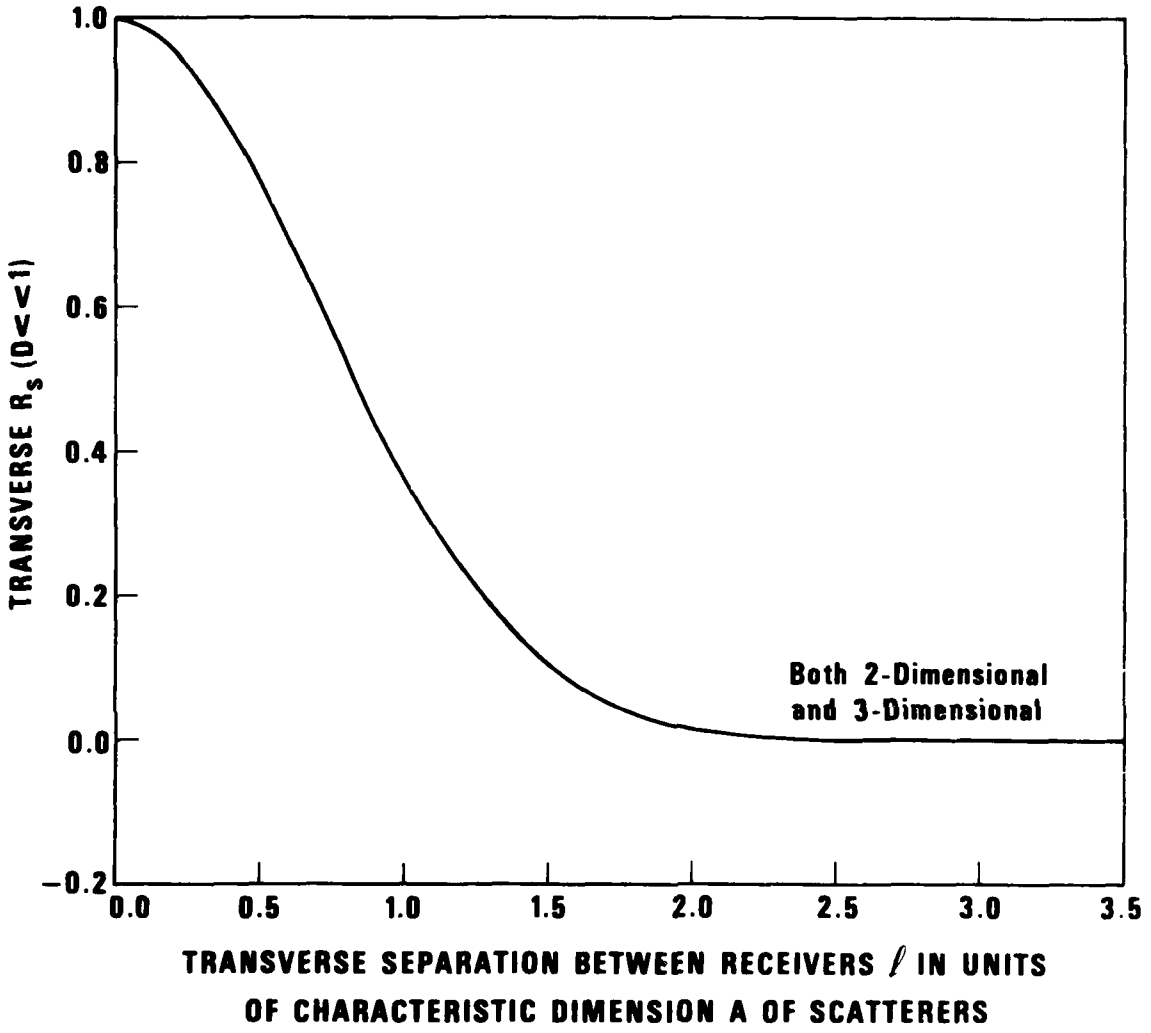

Figure 11. Theoretical transverse phase correlation coefficient $R_s(\ell)$ for case D<<1.

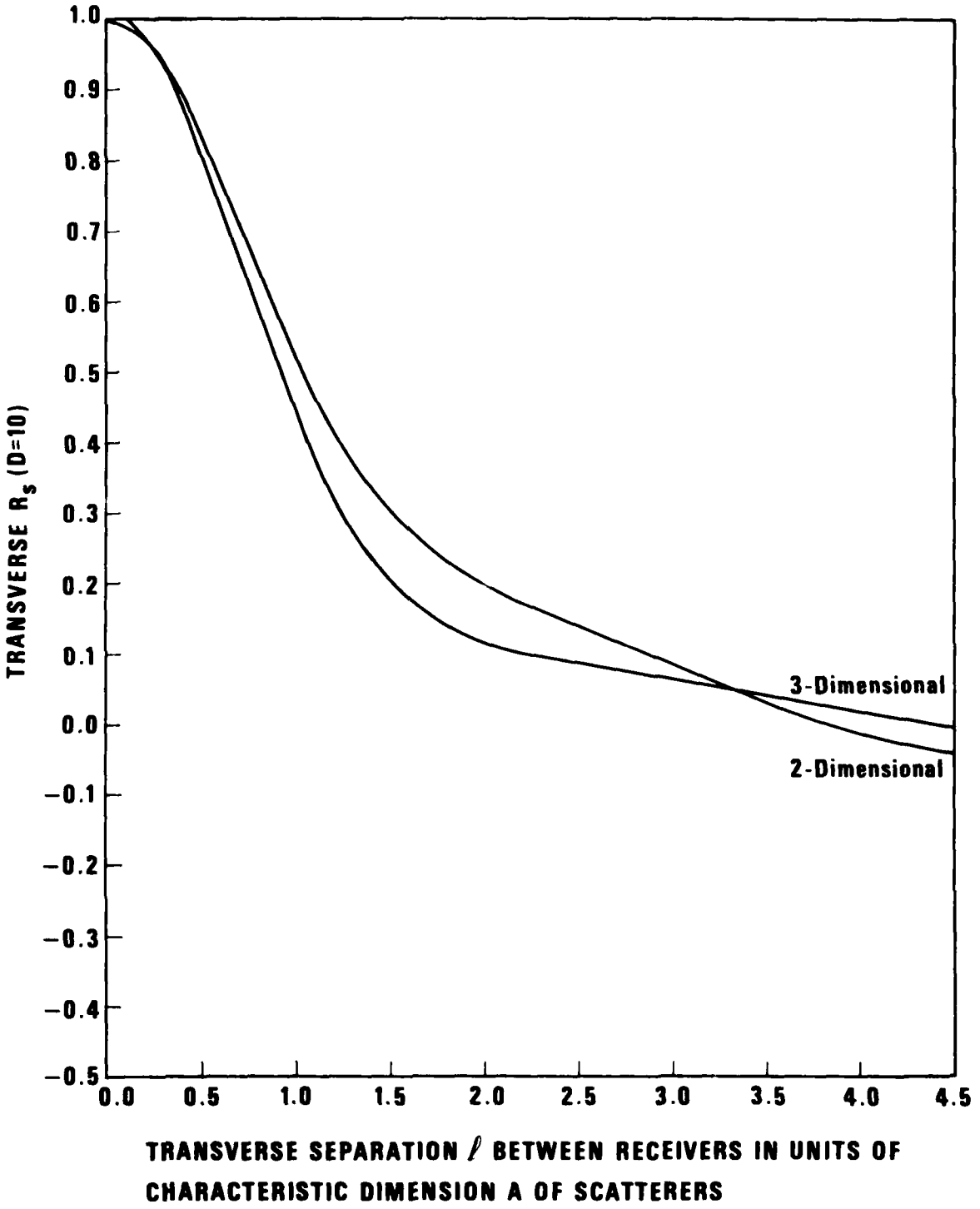

Figure 12. Theoretical transverse phase correlation coefficient $R_s(\ell)$ for case D = 10.

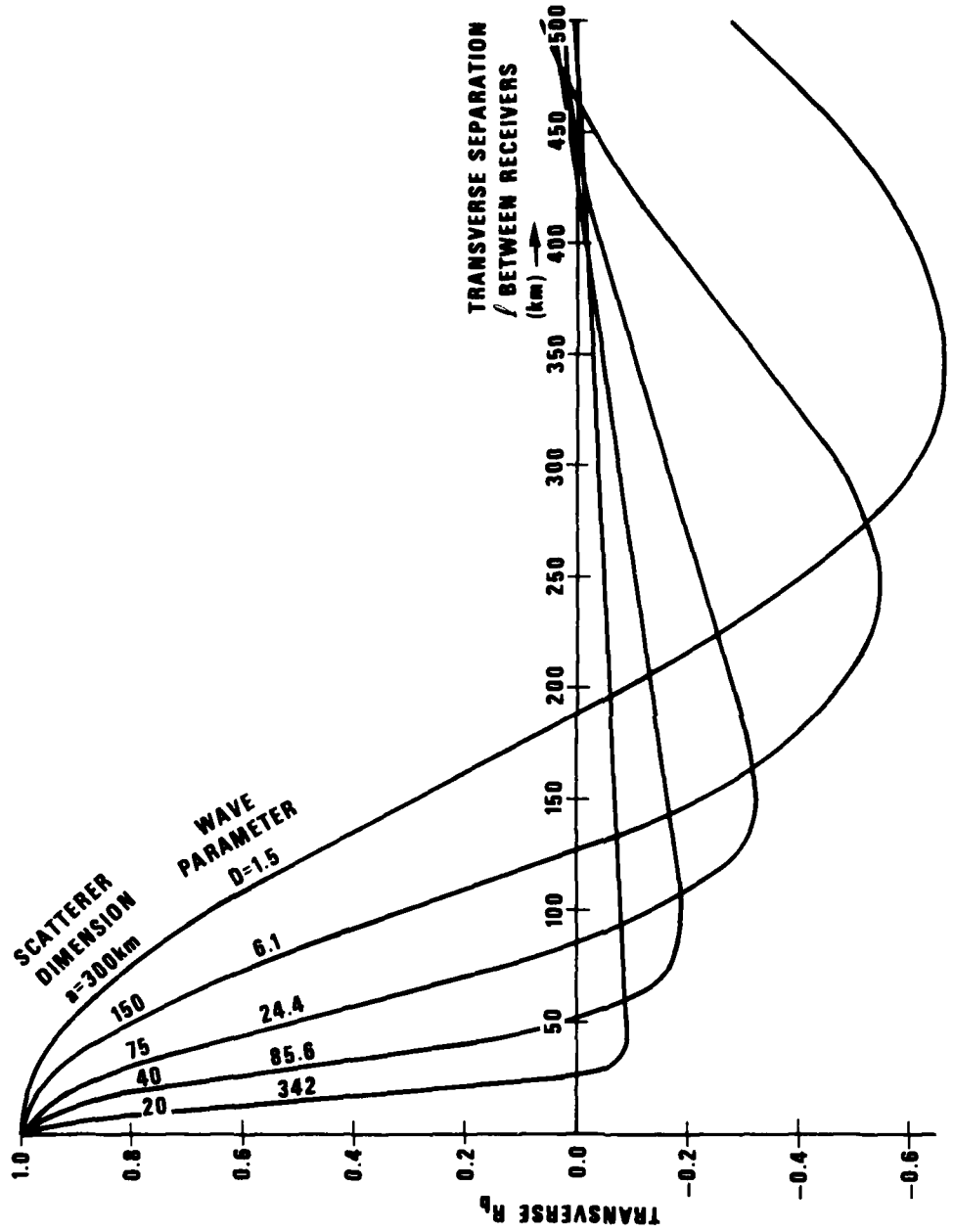

Figure 13. Theoretical transverse amplitude correlation coefficient $R_b(\ell)$
Source-to-receiver distance L = 3000 km
Period T = 19.7 sec
Phase velocity c = 3.641 $\frac{km}{sec}$
Wavenumber K = 0.0876 km^{-1}

APPENDIX II

EVALUATION OF CERTAIN INTEGRALS USED IN APPENDIX I

APPENDIX II

Evaluation of certain integrals used in Appendix I

In this appendix we evaluate three integrals involving the functions

$$A_1(\alpha,\beta) = \frac{1}{\sqrt{2\pi\alpha}} \sin\left(\frac{\beta^2}{2\alpha} + \frac{\pi}{4}\right) \tag{A.1}$$

and

$$A_2(\alpha,\beta) = \frac{1}{\sqrt{2\pi\alpha}} \cos\left(\frac{\beta^2}{2\alpha} + \frac{\pi}{4}\right) \tag{A.2}$$

which appear in the two-dimensional modification of Chernov's theory. The three integrals are

$$I_{A_1,A_1} \equiv \int_{-\infty}^{\infty} A_1(\alpha_1,\gamma_1+y)\, A_1(\alpha_2,\gamma_2+y)\, dy \tag{A.3}$$

$$I_{A_2,A_2} \equiv \int_{-\infty}^{\infty} A_2(\alpha_1,\gamma_1+y)\, A_2(\alpha_2,\gamma_2+y)\, dy \tag{A.4}$$

and

$$I_{A_1,A_2} \equiv \int_{-\infty}^{\infty} A_1(\alpha_1,\gamma_1+y)\, A_2(\alpha_2,\gamma_2+y)\, dy. \tag{A.5}$$

It follows from the definition (A.1) that

$$\begin{aligned} I_{A_1,A_1} &= \frac{1}{2\pi\sqrt{\alpha_1\alpha_2}} \int_{-\infty}^{\infty} \frac{e^{i\theta_1} - e^{-i\theta_1}}{2i} \cdot \frac{e^{i\theta_2} - e^{-i\theta_2}}{2i}\, dy \\ &= \frac{-1}{8\pi\sqrt{\alpha_1\alpha_2}} \int_{-\infty}^{\infty} \left[e^{i(\theta_1+\theta_2)} - e^{i(\theta_1-\theta_2)} - e^{i(\theta_2-\theta_1)} + e^{i(-\theta_1-\theta_2)} \right] dy \\ &= \frac{-1}{4\pi\sqrt{\alpha_1\alpha_2}} \left[\mathrm{Re} \int_{-\infty}^{\infty} e^{i(\theta_1+\theta_2)}\, dy - \mathrm{Re} \int_{-\infty}^{\infty} e^{i(\theta_1-\theta_2)}\, dy \right]. \end{aligned} \tag{A.6}$$

where we have made the substitutions

$$\theta_1 = \frac{(\gamma_1+y)^2}{2\alpha_1} + \frac{\pi}{4} \tag{A.7}$$

and

$$\theta_2 = \frac{(y_2+y)^2}{2\alpha_2} + \frac{\pi}{4} . \tag{A.8}$$

In order to evaluate the two integrals appearing in (A.6), we make use of the identity

$$\begin{aligned} \mathrm{Re}\int_{-\infty}^{\infty} e^{i(ay^2+by+c)}\,dy &= \mathrm{Re}\left\{e^{i\left(c-\frac{b^2}{4a}\right)}\int_{-\infty}^{\infty} e^{i\left(\sqrt{a}\,y+\frac{b}{2\sqrt{a}}\right)^2} dy\right\} \quad \text{iff } a>0 \\ &= \mathrm{Re}\left\{e^{i\left(c-\frac{b^2}{4a}\right)}\int_{-\infty}^{\infty} e^{i\xi^2}\frac{1}{\sqrt{a}}\,d\xi\right\} \\ &= \mathrm{Re}\left\{e^{i\left(c-\frac{b^2}{4a}\right)}\sqrt{\frac{\pi}{a}}\;e^{i\frac{\pi}{4}}\right\} \\ &= \sqrt{\frac{\pi}{a}}\cos\left(c-\frac{b^2}{4a}+\frac{\pi}{4}\right) \qquad \text{[iff } a>0\text{]} . \end{aligned} \tag{A.9}$$

The expressions appearing in the exponents in (A.6) are

$$\theta_1+\theta_2 = \frac{1}{2}\left[y^2\left(\frac{1}{\alpha_1}+\frac{1}{\alpha_2}\right)+y\left(\frac{2y_1}{\alpha_1}+\frac{2y_2}{\alpha_2}\right)+\frac{y_1^2}{\alpha_1}+\frac{y_2^2}{\alpha_2}\right]+\frac{\pi}{2} \tag{A.10}$$

and

$$\theta_1-\theta_2 = \frac{1}{2}\left[y^2\left(\frac{1}{\alpha_1}-\frac{1}{\alpha_2}\right)+y\left(\frac{2y_1}{\alpha_1}-\frac{2y_2}{\alpha_2}\right)+\frac{y_1^2}{\alpha_1}-\frac{y_2^2}{\alpha_2}\right], \tag{A.11}$$

so we may evaluate the first integral in (A.6) by substituting

$$a = \frac{\alpha_1+\alpha_2}{2\alpha_1\alpha_2} \tag{A.12}$$

$$b = \frac{\alpha_1 y_2+\alpha_2 y_1}{\alpha_1\alpha_2} \tag{A.13}$$

$$c = \frac{\alpha_1 y_2^2+\alpha_2 y_1^2}{2\alpha_1\alpha_2}+\frac{\pi}{2} \tag{A.14}$$

into (A.9). It follows from the definitions (A.12)-(A.14) that

$$c-\frac{b^2}{4a}+\frac{\pi}{4} = \frac{(y_1-y)^2}{2(\alpha_1+\alpha_2)}+\frac{3\pi}{4} , \tag{A.15}$$

so we have

$$\mathrm{Re}\int_{-\infty}^{\infty} e^{i(\theta_1+\theta_2)}\,dy = \sqrt{\frac{\pi}{a}}\cos 2\left(\frac{(y_1-y)^2}{2(\alpha_1+\alpha_2)}+\frac{3\pi}{4}\right)$$

$$= -\sqrt{\frac{2\pi\alpha_1\alpha_2}{\alpha_1+\alpha_2}}\sin\left(\frac{(y_1-y)^2}{2(\alpha_1+\alpha_2)}+\frac{\pi}{4}\right). \tag{A.16}$$

In order to evaluate the second integral in (A.6), we note that the restriction a > 0 was used in deriving (A.9), so we may substitute from (A.11) into that identity only if $\alpha_2 > \alpha_1$. We may treat the case $\alpha_1 > \alpha_2$, however, simply by noting that

$$\mathrm{Re}\int_{-\infty}^{\infty} e^{i(\theta_1-\theta_2)}\,dy = \mathrm{Re}\int_{-\infty}^{\infty} e^{i(\theta_2-\theta_1)}\,dy, \tag{A.17}$$

so we may treat both the cases $\alpha_2 > \alpha_1$ and $\alpha_1 > \alpha_2$ by substituting

$$a = \frac{|\alpha_1-\alpha_2|}{2\alpha_1\alpha_2} \tag{A.18}$$

$$b = \frac{|\alpha_1 y_2 - \alpha_2 y_1|}{\alpha_1\alpha_2} \tag{A.19}$$

$$c = \frac{|\alpha_1 y_2^2 - \alpha_2 y_1^2|}{2\alpha_1\alpha_2} \tag{A.20}$$

into (A.9). We find that

$$c - \frac{b^2}{4a} + \frac{\pi}{4} = \frac{-(y_1-y_2)^2}{2|\alpha_1-\alpha_2|} + \frac{\pi}{4} \tag{A.21}$$

and thus

$$\mathrm{Re}\int_{-\infty}^{\infty} e^{i(\theta_1-\theta_2)}\,dy = \sqrt{\frac{\pi}{a}}\cos 2\left(\frac{-(y_1-y_2)^2}{2|\alpha_1-\alpha_2|}+\frac{\pi}{4}\right)$$

$$= \sqrt{\frac{2\pi\alpha_1\alpha_2}{|\alpha_1-\alpha_2|}}\cos\left(\frac{(y_1-y_2)^2}{2|\alpha_1-\alpha_2|}-\frac{\pi}{4}\right)$$

$$= \sqrt{\frac{2\pi\alpha_1\alpha_2}{|\alpha_1-\alpha_2|}}\sin\left(\frac{(y_1-y_2)^2}{2|\alpha_1-\alpha_2|}+\frac{\pi}{4}\right). \tag{A.22}$$

Substituting (A.16) and (A.22) into (A.6), we derive as our first result

$$I_{A_1,A_1} = \frac{1}{2\sqrt{2\pi(\alpha_1+\alpha_2)}} \sin\left(\frac{(\gamma_1-\gamma_2)^2}{2(\alpha_1+\alpha_2)} + \frac{\pi}{4}\right) + \frac{1}{2\sqrt{2\pi|\alpha_1-\alpha_2|}} \sin\left(\frac{(\gamma_1-\gamma_2)^2}{2|\alpha_1-\alpha_2|} + \frac{\pi}{4}\right)$$

$$= \frac{1}{2}\left[A_1(\alpha_1+\alpha_2, \gamma_1-\gamma_2) + A_1(|\alpha_1-\alpha_2|, \gamma_1-\gamma_2)\right]. \tag{A.23}$$

We may use (A.16) and (A.22) to evaluate (A.4):

$$I_{A_2,A_2} = \frac{1}{2\pi\sqrt{\alpha_1\alpha_2}} \int_{-\infty}^{\infty} \frac{e^{i\theta_1} + e^{-i\theta_1}}{2} \cdot \frac{e^{i\theta_2} + e^{-i\theta_2}}{2}\, dy$$

$$= \frac{1}{8\pi\sqrt{\alpha_1\alpha_2}} \int_{-\infty}^{\infty} \left[e^{i(\theta_1+\theta_2)} + e^{i(\theta_1-\theta_2)} + e^{i(\theta_2-\theta_1)} + e^{i(-\theta_1-\theta_2)}\right] dy$$

$$= \frac{1}{4\pi\sqrt{\alpha_1\alpha_2}} \left[F_2 \int_{-\infty}^{\infty} e^{i(\theta_1+\theta_2)}\, dy + F_4 \int_{-\infty}^{\infty} e^{i(\theta_1-\theta_2)}\, dy\right]$$

$$= \frac{1}{2}\left[-A_1(\alpha_1+\alpha_2, \gamma_1-\gamma_2) + A_1(|\alpha_1-\alpha_2|, \gamma_1-\gamma_2)\right]. \tag{A.24}$$

For (A.5) we find

$$I_{A_1,A_2} = \frac{1}{2\pi\sqrt{\alpha_1\alpha_2}} \int_{-\infty}^{\infty} \frac{e^{i\theta_1} - e^{-i\theta_1}}{2i} \cdot \frac{e^{i\theta_2} - e^{-i\theta_2}}{2}\, dy$$

$$= \frac{1}{8\pi i\sqrt{\alpha_1\alpha_2}} \int_{-\infty}^{\infty} \left[e^{i(\theta_1+\theta_2)} + e^{i(\theta_1-\theta_2)} - e^{i(\theta_2-\theta_1)} - e^{i(-\theta_1-\theta_2)}\right] dy$$

$$= \frac{1}{4\pi\sqrt{\alpha_1\alpha_2}} \left[\mathrm{Im} \int_{-\infty}^{\infty} e^{i(\theta_1+\theta_2)}\, dy + \mathrm{Im} \int_{-\infty}^{\infty} e^{i(\theta_1-\theta_2)}\, dy\right]. \tag{A.25}$$

By inspection of (A.9) we may write

$$\mathrm{Im} \int_{-\infty}^{\infty} e^{i(ay^2+by+c)}\, dy = \sqrt{\frac{\pi}{a}} \sin\left(c - \frac{b^2}{4a} + \frac{\pi}{4}\right) \quad \text{iff } a > 0. \tag{A.26}$$

Our derivation proceeds as before, but now our treatment of the case $\alpha_1 > \alpha_2$ replaces (A.17) with the identity

$$\mathrm{Im} \int_{-\infty}^{\infty} e^{i(\theta_1-\theta_2)}\, dy = -\mathrm{Im} \int_{-\infty}^{\infty} e^{i(\theta_2-\theta_1)}\, dy, \tag{A.27}$$

and our final result is

$$I_{A_1,A_2} = \frac{1}{2}\left[A_2(\alpha_1+\alpha_2, \gamma_1-\gamma_2) \pm A_2(|\alpha_1-\alpha_2|, \gamma_1-\gamma_2)\right] \quad \text{(A.28)}$$

where the plus sign is to be used if $\alpha_2 > \alpha_1$, and where the minus sign is to be used if $\alpha_1 > \alpha_2$.